Critical Period for Murine Olfactory Map Formation

Thesis

Critical Period for Murine Olfactory Map Formation

Yunming Wu, B. Sc.

A thesis submitted in fulfillment of the requirement of the Open University

for the Degree of Doctor of Philosophy.

Stowers Institute for Medical Research

1000 E 50th street, Kansas City, Missouri, United States of America

an Affiliated Research Center of the Open University, United Kingdom.

2017 February 27th

Acknowledgement

I would like to thank my advisor, Dr. C. Ron Yu, for giving me the opportunity to conduct the research for my graduate study. I thank the entire Yu lab for their support. I would also like to give special thanks to the people who helped me with the work in this thesis: Dr. Limei Ma, Dr. Qiang Qiu, Dr. Sachiko Haga-Yamanaka, Ms. Andrea Moran, Ms. Ruohan Zhong, Ms. Hayley Sheerer, Ms. Vasha Dutell, Mr. Jose Lopez Hernandez and Mr. Kyle Duyck. I also thank Dr. Stavros Lomvardas for sharing the tet-LBR mice, cells from Neurog1-IRES-GFP and OMP-IRES-GFP animals, Dr. Gilad Barnea for sharing the antibodies against olfactory receptors, Dr. Sakano Hitoshi for sharing the antibodies against Kirrel2, Dr. Edward Callaway and Dr. Ian Wickersham for sharing the reagents for packaging the pseudotyped rabies virus. I also thank the Molecular Biology Facility, the Microscopy Center, the Cytometry Facility, and the Tissue Culture Core Laboratory of the Stowers Institute for Medical Research for their technical support.

This work is supported by the funding from the Stowers Institute for Medical Research to C. Ron Yu.

Part of the work has been published in the journals *Experimental Neurology* and *Science*. The related contents are cited in Chapter I and Chapter II.

Table of contents

Critical Period for Murine Olfactory Map Formation i

Acknowledgement ii

Table of contents iii

Table of figures xi

Abstract 1

1 Chapter I. Introduction 3

1.1 Organization of murine olfactory sensory system 4

1.1.1 Peripheral sensory organs 4

1.1.2 The olfactory bulb 7

1.1.3 The cortical areas of olfaction 11

1.2 Embryonic development of the OSNs and the OSN axons 11

1.2.1 Embryogenesis of OSNs 11

1.2.2 Embryonic development of OSN axons 13

1.3 Target independent models of OSN axon guidance 14

1.4 Contextual model of axon sorting 15

1.4.1 Establishment of OR identity 16

1.4.2 Contextual model of axon sorting 17

1.5 Activity dependent model of axon sorting 18

1.5.1 OR signaling 18

1.5.2 Neural activity is required for axon guidance 20

1.5.3 Activity dependent model of axon sorting 20

1.6 Axon guidance of the regenerated neurons 21

1.6.1 Regeneration of OSN 22

1.6.2 Challenge of axon guidance in the context of continuous regeneration 22

1.7 Critical period mechanism of neural circuit formation 23

1.8 Critical period of OSN axon guidance 24

2 Chapter II. Critical period in olfactory system 26

2.1 Introduction 26

2.2 Material and methods 26

2.2.1 Experimental Animals 26

2.2.2 In situ hybridization 27

2.2.3 Immunohistochemistry 27

2.2.4 DiI labeling of the mitral cells 28

2.2.5 Microscopy 28

2.2.6 In vivo Synapto-pHluorin imaging 29

2.3 Results 30

2.3.1 Genetic manipulation of the neural activity using Kir2.1 transgenic animal.....30
2.3.2 Activity deprivation during the postnatal development reveals a critical period.....33
2.3.3 Homotypic interaction between the olfactory sensory neurons.....37
2.3.4 The critical period is independent of neural activity.....39
2.3.5 Development of mitral cell dendrites.....41
2.4 Discussion.....43
2.4.1 Developmental switch of the axon guidance.....43
2.4.2 Activity independent perturbation is subject to the regulation by the critical period.....44
2.4.3 Sensory input independent pruning of the secondary neurons.....44
3 Chapter III. The settler neurons.....45
3.1 Introduction.....45
3.2 Material and method.....45
3.2.1 Animals.....45
3.2.2 Histology.....46
3.2.3 Imaging.....46
3.2.4 Adenovirus labeling.....47
3.2.5 CUBIC brain clearing.....47
3.2.6 Quantification of the lifespan of OSN.....47
3.3 Results.....49
3.3.1 Genetic labeling of the early and late neurons.....49

3.3.2 Axon dynamics of the early and late neurons 53

3.3.3 Genetic ablation of the early neurons 60

3.3.4 Neurogenesis and lifespan of the early and late neurons 64

3.3.5 Changes of the axon innervation in the glomeruli during weaning. 67

3.3.6 Extending the early neurons' lifespan through Bcl2 transgene promotes the axon exuberance growth. 70

3.3.7 Extending exuberant axons leads to deficient convergence 71

3.4 Discussion 74

3.4.1 The settler neurons 74

3.4.2 The role of settler neurons in the formation of the olfactory map during critical period 74

3.4.3 The dynamics of OSN axons during postnatal development 75

3.4.4 Development of synaptic connectivity during critical period 76

4 Chapter IV. Transcriptome analysis of the olfactory sensory neurons during the critical period 77

4.1 Introduction 77

4.2 Material and method 77

4.2.1 Animals 77

4.2.2 RNA sample preparation 78

4.2.3 Sequence processing 78

4.2.4 PCA analysis 78

4.2.5 ANOVA analysis 78

4.2.6 Hierarchical clustering analysis 79

4.2.7 GO term analysis 79

4.2.8 In situ hybridization 79

4.3 Results 80

4.3.1 Transcriptome profile of the olfactory epithelium during postnatal development 80

4.3.2 Genes differentially expressed during critical period 86

4.3.3 Identification of regulatory motifs in the genes differentially expressed during the critical period 93

4.3.4 Identification of GPCRs specifically expressed during critical period 97

4.3.5 Olfactory receptors are dynamically expressed during the critical period 101

4.3.6 Transcriptome change under activity deprivation 107

4.3.7 New cell markers label the constant changing cell populations 111

4.3.8 Gland specific markers 113

4.3.9 Novel cGMP cyclase 115

4.4 Discussion 117

4.4.1 Transcriptome change reveals a genetic program under the critical period 117

4.4.2 Transcriptome analyses reveals the change of cell identity in OSNs during the critical period 117

5 Chapter V. Wnt signaling and the critical period 119

5.1 Introduction 119

5.1.1 Wnt signaling 120

5.1.2 Wnt signaling and the axon guidance 121

5.1.3 Interaction between Wnt receptors 121

5.2 Material and method 122

5.2.1 Animals 122

5.2.2 Transgenesis 122

5.2.3 Immunohistochemistry 123

5.2.4 Cloning and vector construction 123

5.2.5 Imaging of histological samples 123

5.2.6 RNA-seq analysis 123

5.2.7 Whole mount imaging of the glomeruli 124

5.2.8 FRET 124

5.2.9 Surface expression test 124

5.3 Results 125

5.3.1 Frizzleds expression during the critical period 125

5.3.2 Genetic manipulation of Frizzled 1 and Frizzled 2 129

5.3.3 Ectopic expression of Frizzled 1 promotes exuberant axon projection 131

5.3.4 Turning off ectopic expression of frizzled 1 causes precocious closure of the critical period 133

5.3.5 Knockout of Frizzled 1 postpones the closure of the critical period 139

5.3.6 Frizzled receptors interact with olfactory receptors 145

5.4 Discussion....151

5.4.1 Fzd1 induces axon outgrowth....151

5.4.2 Down regulation of the Fzd1 triggers the closure of the critical period....151

5.4.3 Coupling between Frizzled and ORs as a potential mechanism for fine tuning of the OR signaling....152

5.4.4 Fzd1 and Fzd2 are not redundant in regulating the critical period....154

6 Chapter VI. Development of the next generation genetic screening methods in mammals. 155

6.1 Introduction....155

6.1.1 Genetic methods to visualize mRNA and proteins in vivo.....156

6.1.2 Genomic editing using CRISPR system....157

6.1.3 Brain clearing and imaging techniques....158

6.2 Material and method....159

6.2.1 Animals....159

6.2.2 Transgenesis....159

6.2.3 Adenovirus production....159

6.2.4 Cloning....160

6.2.5 CUBIC....160

6.2.6 SeeDB....160

6.2.7 DiI tracing....160

6.3 Results....161

6.3.1 High throughput knockout using adenovirus carrying CRISPR/Cas9 161

6.3.2 High through-put connectivity profiling using next generation brain imaging techniques 167

6.3.3 High throughput RNA detection using CRISPR/C2c2 system 173

6.3.4 High through-put ectopic gene activation using CRISPR/SAM 175

6.4 Discussion. 178

7 Reference 185

Table of figures

Figure 1.1.2-1 Illustration of the cell types and their morphologies in the olfactory bulb. 10

Figure 1.5.1-1 Illustration of olfactory receptor signaling.....19

Figure 2.3.1-1 Deprivation of the spontaneous activity using Kir2.1 mouse. 32

Figure 2.3.2-1 A systematic analysis of three receptor types in the Kir2.1 animal after the reversal of the neural activity deprivation. 35

Figure 2.3.2-2 Quantification of the results from the experiment in figure 2.3.2-1. 36

Figure 2.3.3-1 Homotypic interaction directs axon guidance during early development. 38

Figure 2.3.4-1 Axon rewiring is independent of activity deprivation.....40

Figure 2.3.5-1 The development of mitral cells following sensory neuron activity deprivation. 42

Figure 3.3.1-1 Schematic illustration of the lifespan tracing experiment using OMP-TetTag transgene. 50

Figure 3.3.1-2 OMP-TetTag transgene only labels existing neurons. 51

Figure 3.3.1-3 OMP-TetTag consistantly labels mOSNs through postnatal development. 52

Figure 3.3.2-1 OSN axons project exuberantly during critical period.....54

Figure 3.3.2-2 Exuberant axon growth is promoted during the critical period.....55

Figure 3.3.2-3 OSN axons traverse multiple glomeruli during the critical period. 56

Figure 3.3.2-4 OSN axons visualized in an intact olfactory bulb. 59

Figure 3.3.3-1 Eliminating the early neurons decreases axon exuberant growth. 62

Figure 3.3.3-2 Early neurons are required for the single glomerulus projection. 63

Figure 3.3.4-1 Analysis of the lifespan of the OSNs generated at various stages. 66

Figure 3.3.5-1 Axon pruning during the weaning week. 69

Figure 4.3.1-1 An overview of the transcriptome analysis. 82

Figure 4.3.1-2 Expression of the cell marker genes in the transcriptome. 85

Figure 4.3.2-1 Expression profile of the differentially expressed genes in the OE-seq. 87

Figure 4.3.2-2 Gene ontology term analysis. 92

Figure 4.3.3-1 Motif analysis of the critical period genes 95

Figure 4.3.4-1 Identification of potential GPCRs expressed during the critical period. 99

Figure 4.3.5-1 Expression profile of the olfactory receptors during postnatal development. 102

Figure 4.3.5-2 The spatial and temporal dynamics of the olfactory receptors. 105

Figure 4.3.5-3 The olfactory receptors expressed early are located in the center of the air duct. 106

Figure 4.3.6-1 Transcriptome changes under neural activity deprivation 108

Figure 4.3.6-2 The activity dependent genes revealed by the Kir2.1 transgenic mice. 109

Figure 4.3.6-3 Interferon pathway genes are upregulated in the Kir2.1 animals. 110

Figure 4.3.7-1 Representative images of six cell markers. 112

Figure 4.3.8-1 The gland specific genes. 114

Figure 4.3.9-1 Expression profiles of nine guanylate cyclases detected in the OE-seq. 116

Figure 5.3.1-1 The expression patterns of Fzd1 and Fzd2 during the critical period. 126

Figure 5.3.1-2 The expression of Fzd1 and Fzd2 during the critical period, continued. 128

Figure 5.3.2-1 Overexpression of Fzd1 and Fzd2 through tetracycline trans-activation system. 130

Figure 5.3.3-1 Ectopic expression of Fzd1 promotes the axon exuberant growth. 132

Figure 5.3.4-1 Manipulating Fzd1 expression using tet-Fzd1 transgene.....135

Figure 5.3.4-32 Down-regulation of Fzd1 before the closure of the critical period results in precautious closure. 138

Figure 5.3.5-1 Axon projection in the absence of Fzd1 and Fzd2.....141

Figure 5.3.6-1 FRET analysis of the OR-Frizzled interaction.....148

Figure 5.3.6-2 Association analysis with receptor transporter protein. 150

Figure 6.3.1-1 Design of the high throughput knockout vector AV136.....162

Figure 6.3.1-2 Validation of the adenovirus mediated genome editing in vitro and in vivo. 164

Figure 6.3.1-3 Genomic editing of endogenous locus using adenovirus mediated CRISPR.....166

Figure 6.3.2-1 The Thy1-eYFP-H line mouse cleared by CUBIC. 169

Figure 6.3.2-2 Visualization of axon guidance molecules over the whole olfactory bulb using CUBIC. 170

Figure 6.3.2-3 Visualizing the entire olfactory pathway using CUBIC immunohistochemistry.....171

Figure 6.3.2-4 Neurons visualized by SeeDB. 172

Figure 6.3.3-1 CRISPR/C2c2 labeled and amplified RNA tracking (CLARNT).....174

Figure 6.3.4-1 Schematic illustration of the adenovirus mediated CRISPR/SAM system.....176

Figure 6.3.4-2 tet-SAM animal and AV160. 177

Abstract

Formation of neural circuits in the brain is sensitive to deprivation of neural activity during the critical period. In the last few decades, the critical period has been studied extensively. These studies are primarily focused on the development of receptive fields in the cortex. Mechanisms regulating the connection between sensory neurons and their central targets during the critical period remain unknown.

In this study, together with other members of the Yu lab, I performed a series of experiments in mice to perturb the projection pattern of olfactory sensory neurons (OSNs) during postnatal development. I observed a critical period during the formation of the olfactory circuit. Neurons generated during and after the critical period adopted different mechanisms in axon targeting. The early-born neurons were able to form converging projection into single glomerulus *de novo*. They also possessed the ability to correct mis-targeted axons. The late born neurons relied on existing axon tracks to target the correct glomeruli. Through genetic chronicle tracing experiments, I was able to demonstrate that early born neurons had a shorter life span, a faster turnover rate, and an increased axon projection plasticity compared to the late born neurons. Because of these unique characteristics, I defined the early born OSNs as “settler neurons”. Genetic ablation of settler neurons resulted in a disrupted axon projection pattern. Transgenic expression of Bcl2, an anti-apoptotic gene, in the OSNs extended the life span of the settler neurons beyond the critical period. The existence of the settler neurons after the critical period promoted the axon exuberant growth. It also affected the OSNs’ axon projection pattern. Transcriptome analysis revealed a genetic switch during the critical period. Different sets of transcription regulators, axon guidance molecules, and signaling molecules were expressed between the settler neurons and the OSNs born afterwards. I identified a G protein coupled receptor, Frizzled 1 (Fzd1), as a critical regulator of the critical period in the olfactory system. Ectopic expression of Fzd1 after the closure of the critical period enabled OSN axons to grow exuberantly and caused mis-targeting phenotype. Removing Frizzled 1 postponed the closure of the critical period. Finally, I showed that

Fzd1 was physically associated with olfactory receptors (ORs). This interaction provided a molecular basis for Fzd1 to influence OSN's axon guidance.

1 Chapter I. Introduction

The brain receives and processes information from both the external and internal worlds. It coordinates the sensory and intellectual activities, creates internal representations of the environment, and produces memories, enables one to learn and dictate individual's behavior. Information in the brain is carried by the neurons, the functional unit of the nervous system, through the spatial and temporal patterns of the neural activity. Neurons form massive and organized connectivity - the neural circuit that determines the outcome of neural computation in the brain. The degree of complexity of the connectivity is a direct measurement of the computation capacity of the system and is highly correlated with the intelligence of the organisms (Jerison, 2012). A crucial stage of brain development is the early postnatal period, when the neural system starts to encounter myriad environmental stimuli that eventually shape the brain circuit. In all the sensory systems, following the initial rapid growth, the ability of building new connectivity is greatly reduced in the adult stage. How does the nervous system make this drastic change during postnatal development? To address this question, I will employ the murine olfactory sensory neuron as a model and focus on how the OSNs form their connections during the postnatal period.

The murine olfactory system forms highly specific connections. Odorants are detected by the ORs expressed by the OSNs (Buck and Axel, 1991). One OSN only expresses one olfactory receptor from a repertoire of ~1000 OR genes (Malnic et al., 1999; Serizawa et al., 2000). The OSNs in the nasal cavity project their axons to the olfactory bulb (OB), the primary brain center for olfaction. OSNs expressing the same receptor type converge into the same glomeruli at stereotypic positions in the olfactory bulb (Mombaerts et al., 1996), whereas neurons expressing different receptor types project into different glomeruli. Thus, a topographic map defined by the OR identity is formed in the OB. This map is called the "olfactory map" (Mori et al., 2006), the structural basis for the sensory perception of smell.

This specific axon projection pattern offers great advantages to study circuit formation. First, OR identity can be adopted as a genetic readout to address the specificity of connection. Second, the stereotypy in the axon projection makes it possible to observe any alterations in the system. Third, OSNs are being regenerated through the animal's life span. The regenerative capacity makes it possible to study how the neurons maintain specific connectivity after the circuit is fully developed or under damage. Lastly, the olfactory sensory neurons also share the properties of other types of neurons. Understanding the system can provide insight to the general circuit formation mechanism in the neural system.

In this chapter, I briefly review the study of the circuit connectivity in the olfactory system and current questions in the field.

1.1 Organization of murine olfactory sensory system

1.1.1 Peripheral sensory organs

There are four major olfactory sensory organs: the Gruenenberg ganglion (GG) (Breer and Fleischer, 2010), the main olfactory epithelium (MOE, OE for olfactory epithelium), the vomeronasal organ (VNO) and the septal organ of Masera (SO) (Rodolfo-Masera, 1943). All four organs are located in the nasal cavity (Figure 1.1.1-1). Neurons in MOE, GG, and SO project their axons to the main olfactory bulb (MOB), whereas neurons in VNO project their axons to the accessory olfactory bulb (AOB). This study focuses on the main olfactory system that consists of MOE and MOB.

The main olfactory epithelium is a pseudostratified epithelium. In addition to the olfactory sensory neurons, there are also other types of cells in the olfactory epithelium. The neurons in the olfactory epithelium are constantly regenerated. Two types of stem cells, globose basal cells (GBCs) and

horizontal basal cells (HBCs), are located at the basal layer of the epithelium. Cells between the stem cells and the mature neurons are the transitional cell types, including transient amplifying cells (TACs), intermediate progenitor cells (INPs) and immature olfactory sensory neurons (iOSNs). Besides OSNs and the cells deriving them, there are two other cell types. The gland cells are sparsely distributed in the OE. Cells on the apical surface of the OE are the sustentacular cells. They are a type of protective supporting cells (Yu and Wu, 2017).

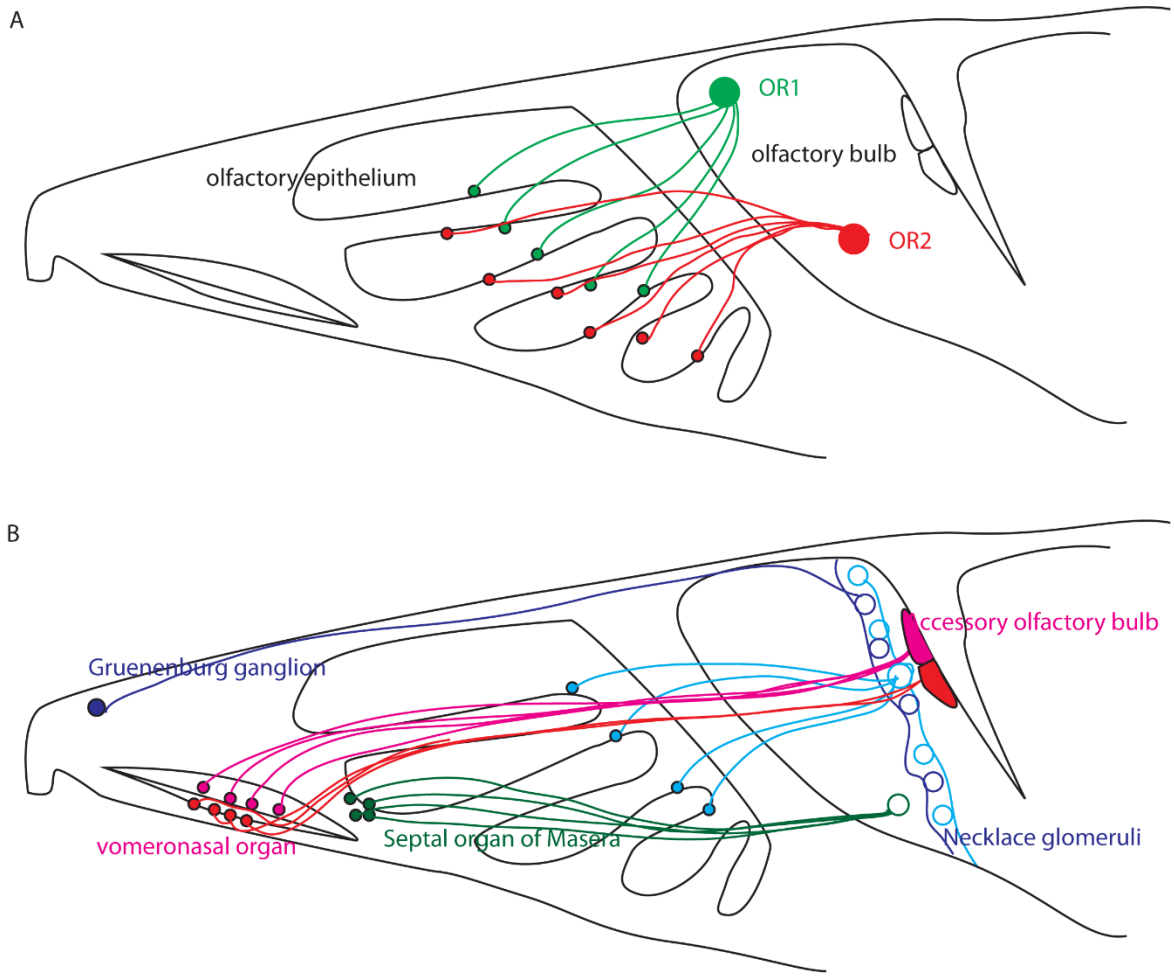

Figure 1.1.1 1 Illustration of the Olfactory map

(A) The cell bodies of olfactory sensory neurons (colored circles) are located in the olfactory epithelium. Neurons expressing the same receptor type (green) project to the same glomerulus in the olfactory bulb. Neurons expressing another receptor type (red) project to a different glomerulus.

(B) The projection of other types of neurons in the peripheral olfactory system. GC-D cells (light blue) project to a ring-like structure, called the necklace glomeruli. The Gruenenburg ganglion cells (dark blue) project to a different ring in the necklace glomeruli area. The V1R expressing neurons in VNO (pink) project to the anterior accessory olfactory bulb. The V2R expressing neurons in VNO (red) project to the posterior accessory olfactory bulb. The sensory neurons in septum organ (green) project to the glomeruli in the ventral olfactory bulb.

Odorants are detected by the olfactory receptors. The olfactory receptor gene family is the largest gene family in mammals. There are about 1000 functional OR genes and about 300 pseudogenes in mice (Zhang et al., 2004). Each OSN only expresses one olfactory receptor type. Each OR is expressed exclusively from one of the two alleles. Neurons expressing a specific receptor type are located sparsely within a defined zone in the olfactory epithelium (Ressler et al., 1993) (see also Figure 1.1.1-1, the pattern of green OSNs and red OSNs). After exiting the OE, OSN axons make a sharp nighty degree turn to cross the cribriform bone to enter the brain. OSN axons are sorted inside the axon bundles according to the OR identity before reaching the OB. Axons of the same OR type from different bundles start to converge when they reach the OB. Finally, all the neurons expressing the same receptor type converge into the same glomeruli. This seemingly challenging task is conducted faithfully during the development and maintained throughout the life span of the animals with new OSNs continuously integrated into the circuit. It is very rare to observe projection errors, such as mis-targeted axons into other glomeruli, even in the aged mice (Richard et al., 2010).

1.1.2 The olfactory bulb

The olfactory bulb is the first brain center for processing odorant information. The types of cells in the olfactory bulb are illustrated in Figure 1.1.2-1. The OSN axons (Figure 1.1.2-1A) make contact with mitral cells and tuft cells (M/T cells for short, Figure 1.1.2-1B, C, K) inside the glomeruli. M/T cells are glutamatergic projection neurons. They extend long-range projection to the piriform cortex and other cortical areas (Igarashi et al., 2012; Sosulski et al., 2011). They can be marked by the molecular marker Pcdh21 (also known as Cdhr1) (Nagai et al., 2005) and transcription factor Tbr1 (Mitsui et al., 2011). One mature mitral cell only connects to one glomerulus in the adult animal. This one mitral cell-one glomerulus connectivity also preserves the spatial pattern of the OSN projection map by passing the information from a specific glomerulus to the corresponding mitral cells. There are many inhibitory interneuron types in the OB. The majority of them are granule cells (Figure 1.1.2-1E, N). These granule

cells are generated in the subventricular zone (SVZ). The neurogenesis of granule cells is continuous throughout the animal's life span (Alvarez-Buylla and Garcıa-Verdugo, 2002). The periglomerular cells, also known as PG cells, form dendrites around the OSNs' axons in the glomeruli (Figure 1.1.2-1D, M). They are a mixture of different cell types that can be distinguished by molecular markers, such as TH (tyrosine hydroxylase, markers for dopaminergic neurons) and calcium binding proteins Calretinin and Calbindin D28K (labels a subtype of GABAergic neurons). Additionally, the inhibitory neurons in the olfactory bulb express different types of molecular markers, such as pavalbumin (Figure 1.1.2-1H, O). There are also neurons, whose cell bodies reside in other parts of the brain that project into the olfactory bulb. For example, glutamatergic projection from piriform cortex terminates at the granule cell layer (Figure 1.1.2-1G). Serotoninergic projection from Raphe nuclei (Figure 1.1.2-1F, L) terminates in the glomerular layer. Cholinergic projection from horizontal diagonal band (HDB, a posterior thalamic nucleus) projects into both glomerular and external plexiform layers (Figure 1.1.2-1G). These centrifugal projections may involve in the top-down control of the odorant response.

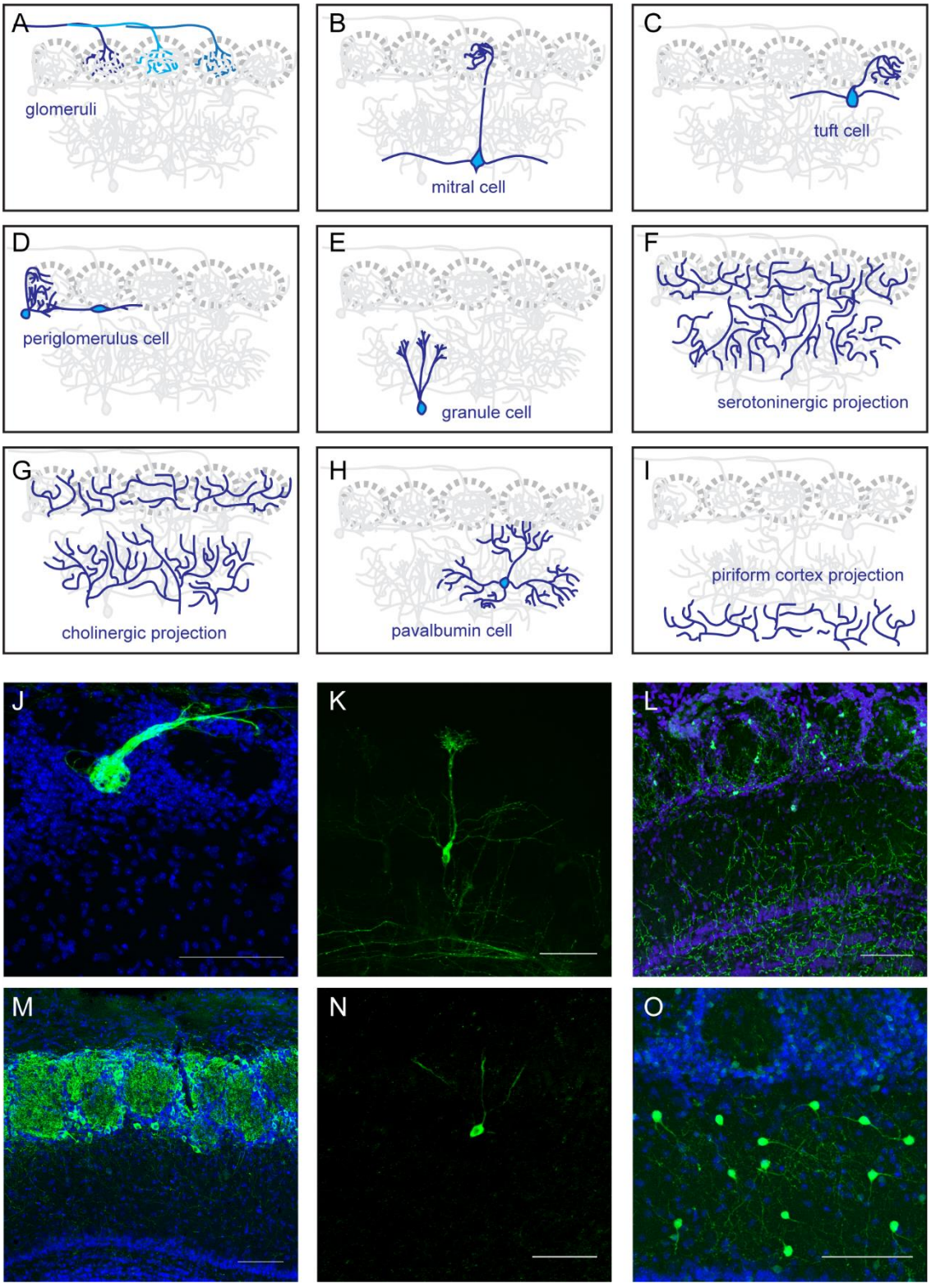
A
glomeruli
B
mitral cell
C
tuft cell
D
periglomerulus cell
E
granule cell
F
serotoninergic projection
G
cholinergic projection
H
pavalbumin cell
I
piriform cortex projection
J
K
L
M
N
O

Figure 1.1.2-1 Illustration of the cell types and their morphologies in the olfactory bulb.

(A) Illustration of the OSN axons. The OSN axons project into the glomeruli. Different receptor types project into different glomeruli (colored with various levels of blue).

(B) Illustration of mitral cells. Mitral cells are glutamatergic excitatory projection neurons in the olfactory bulb. The mature mitral cells form a single primary dendrite connecting with a single glomerulus. They have multiple secondary dendrites extending laterally. Their axons project to the piriform cortex.

(C) Illustration of tuft cells. Tuft cells are another type of excitatory projection neurons in the olfactory bulb. They are different from the mitral cells by their cell bodies' positions. Their cell bodies are normally located at the upper part of external plexiform layer.

(D) Illustration of periglomerular cells. Periglomerular cells are a mixture of different cell types. They are mostly GABAergic local interneurons. Their dendrites direct towards the glomeruli and form synapses in the glomeruli.

(E) Illustration of granule cells. Granule cells are a large population of GABAergic interneurons located below the M/T cells layer. They form dendro-dendritic synapses onto mitral cells' secondary dendrites and mediate inhibition through this connection.

(F) Illustration of serotonin projection from the Raphe nuclei into the olfactory bulb.

(G) Illustration of cholinergic fibers. Cholinergic fibers are projections from horizontal diagonal band (HDB). This type of projection is seen over the entire olfactory bulb.

(H) Illustration of Parvalbumin positive interneurons. Parvalbumin positive interneurons are one type of GABAergic interneurons in the EPL.

(I) Illustration of centrifugal projection from piriform cortex.

(J) Immunostaining of GFP showing one M71 glomerulus from a M71-IRES-GFP transgenic animal.

(K) Representative image of a mitral cell labeled with DiI from the lateral olfactory tract (LOT).

(L) Immunostaining of serotoninergic fibers in the olfactory bulb using anti-5HT antibody.

(M) Immunostaining of PG cells using anti-Tyrosine hydroxylase antibody.

(N) Representative image of a granule cell visualized by electrophoresis of biotin.

(O) Immunostaining of Parvalbumin positive cells in the OB using anti-Parvalbumin antibody.

Scale bar: 100 μm. The DAPI counter staining is shown in blue color in the images.

1.1.3 The cortical areas of olfaction

The mitral and tuft cells project their axons to a broad area along the ventral brain. It is not well understood how their projection patterns are organized. There are several lines of evidence suggesting that their axon projection patterns do not have spatial stereotypy as the sensory neurons. Calcium imaging study by Stettler and colleagues indicates that odorants activate a random set of cells in the piriform cortex. There is no stereotypy for the activation of a given odorant or the similar types of chemicals (Stettler and Axel, 2009). Axon projections from mitral cells have been traced both physically and genetically. In these tracing experiments, axons from the mitral cells connected with a defined glomerulus project to almost the entire ventral brain. The projections from different glomeruli intermingle with each other (Igarashi et al., 2012; Sosulski et al., 2011). Retrogradely traced mitral cells from different regions of cortex also intermingle with each other (Miyamichi et al., 2011).

These lines of evidence suggest that the piriform cortex may be an associative cortex, where the neurons activated by an odorant is assigned through experience rather than genetic mechanisms. Alternatively, a spatial pattern in the cortex exists at molecular level that is yet to be discovered.

1.2 Embryonic development of the OSNs and the OSN axons

1.2.1 Embryogenesis of OSNs

The development of the olfactory map consists of multiple steps: neurogenesis of the OSNs, establishment of single receptor expression, axon outgrowth, sorting of the axons according to their receptor types, and the formation of the glomeruli.

During embryogenesis, the olfactory epithelium develops from the olfactory placode. It is an area in the cranial non-neural ectoderm. The invagination of the olfactory pit starts as early as E9.5. The earliest OSNs reaching the OB are called pioneering neurons (Whitlock and Westerfield, 1998). Upon genesis of the earliest OSNs, some cells that express olfactory marker protein (OMP, a gene specifically expressed by olfactory sensory neurons and widely used as a molecular marker for mOSNs) and olfactory receptors migrate together with the outgrowing axons from the pioneering neurons. These migration cells may contain the "guidepost" cells that help guide the initial axon growth towards the telencephalon (Treloar et al., 2010). The development of pioneering neuron axons precedes the development of the OB. Their axons reach the telencephalon at E11.5. The transcriptional control of the olfactory placode development is not well understood compared to that of other sensory pits. There are some transcription factors identified in the chick studies, including Pax5, Sox2, Dlx5 (Treloar et al., 2010).

Two populations of stem cells reside in the basal layer of OE: the horizontal basal cells and the globose basal cells. During embryogenesis, the GBCs are actively self-renewing and give rise to transit-amplifying cells (TAC) that express the marker Mash1 (also known as Ascl1, a transcription factor) (Guillemot et al., 1993). Another population of TACs expressing Nestin is also observed in a sub-region of the OE (Murdoch and Roskams, 2008). Both TACs give rise to INPs. The INPs express the molecular marker Neurog1, and Neurod1 (Cau et al., 2002; Packard et al., 2011). The INPs give rise to OSNs. iOSNs express growth cone marker GAP43 and G protein subunits Gng8 (Ryba and Tirindelli, 1995). Mature OSNs (mOSNs) express OMP. The iOSNs already develop the axon structures that can be visualized through GAP43 staining and Gγ8-tTA transgene. In another word, the axon outgrowth happens before the OSNs respond to odor stimulation.

1.2.2 Embryonic development of OSN axons

During embryonic development, the first OMP positive OSNs are seen at E9.5, marking the start point of axon growth (Treloar et al., 2010). The first axon arrives at the forebrain at E11. The development of the olfactory bulb starts after the arrival of the pioneering axons, indicating that the formation of OB may be induced by the pioneering axons (Gong and Shipley, 1995). Upon arrival, the olfactory nerves restrict in a region outside the olfactory bulb, the olfactory nerve layer, (ONL for short) until the glomerulogenesis. Glomerulogenesis starts around E15 (Treloar et al., 2010). The glomeruli organization is not well defined at the end of embryonic stage. The axons project to a coarse area, around which the final glomerulus will be further refined (Potter et al., 2001). Many projection errors can be seen at this stage (Royal and Key, 1999). Refinement of the glomerulus structure occurs postnatally (Zou et al., 2004).

Several molecular cues have been identified to be involved during embryonic axon growth. These include transcription factors, such as Arx, Gli3, Fez, Klf, Dlx5, Six1, Emx2, and molecules involved in cell signaling pathways, such as Wnt, Fgf, retinoic acid, Cxcr4, and Igf (McIntyre et al., 2010; Paschaki et al., 2013; Scolnick et al., 2008a; Treloar et al., 2010). The regulation of axon growth may not be completely cell autonomous, because some of the cues are expressed outside OSNs. Mutations in most of these genes lead to nerve growth defect, but OSN maturation and neuronal fate commitment are not affected, suggesting that the axon growth and the neurogenesis of OSNs are two separated processes.

In term of axon growth, the OSNs are not a homogenous population. During the pioneering neuron axon outgrowth, a group of cells migrate together with the axons, including the cells expressing GnRH (Schwanzel-Fukuda and Pfaff, 1989), olfactory ensheathing cells (Valverde et al., 1992), and the hypothesized “guide post cells” (cells expressing OMP and ORs during embryonic development that migrate along with axons) (Conzelmann et al., 2002). The causal relationship between the migrating cells and the pioneering axons is not established.

In summary, the axon growth during embryonic stage precedes the development of the target, the olfactory bulb, suggesting a target independent mechanism. Both cell-autonomous and non-autonomous guidance cues may be involved in the initial axon growth. The process requires signaling from multiple pathways, as well as transcription level regulation. OSNs generated at different embryonic stages do not share the same axon guidance mechanism. The glomerulus structure is not fully developed when the animal is born. The axons of the same receptor type project to a coarse area around the position of the final glomerulus, which is defined as "proto-glomerulus". The formation of well-defined, mature glomerulus structure requires critical steps after birth. The axons of the same receptor type further converge into a single glomerulus during postnatal development. The following discussion will be focusing on this process.

1.3 Target independent models of OSN axon guidance

A well-described axon guidance model is the chemotaxis model, initially proposed by Santiago Ramón y Cajal in 1890s. In this model, the target derives attractant and guide the axons through the attractant's gradient. It was not until 1990, that the first axon guidance molecule netrin was identified (Hedgecock et al., 1990). The first mammalian homolog of netrin was identified in 1994 (Serafini et al., 1994) and many others guidance molecules were discover in the years followed(Tessier-Lavigne and Goodman, 1996). From these studies, we now know that both attractive and repulsive cues can be secreted by the cells in the target areas. The chemotaxis cues form a gradient. The axons expressing the receptors could follow these gradients to locate the target.

In the olfactory system, the axon growth during embryonic stage appears to follow the chemotaxis model. Previous studies have identified some axon guidance molecules following the chemotaxis theory. Axon guidance molecule gradient has been observed in both the dorsal-ventral (D-V) axis and the anterior-posterior (A-P) axis. The axons targeting alone D-V axis appear to grow in parallel with

the locations of their cell bodies. Robo2/Slit1, Nrp2/Sema3F ligand-receptor pairs and their gradients have been identified to be involved in the D-V axis formation (Cho et al., 2007; Nguyen-Ba-Charvet et al., 2008; Norlin et al., 2001; Takeuchi et al., 2010). Nrp1/PlxnA1 signaling gradient has been identified for the A-P axis (Imai et al., 2009). The D-V and A-P coordinates specify a general area for the axons to project to. Within A-P and D-V axes defined zones, specific receptor type shows a local permutation (relevant position of a given glomeruli on the olfactory bulb) by up to a few hundred microns, even within the same animal (Zapiec and Mombaerts, 2016). The level of this variability can't be reconciled by a target-derived guidance cue gradient. The local sorting of axons may require additional mechanisms.

In contrast to axon growth during the embryonic stage, development of the glomeruli map is largely target-independent. Most evidence support this claim. Early studies with olfactory bulbectomy have shown that the OSN axons converge into glomerulus-like structures in the cortex in the absence of the OB (Graziadei et al., 1978). Modern genetic studies demonstrate that genetic ablation of the postsynaptic cells, including M/T cells (using Tbr1 knockout), and GABAergic interneurons (using Dlx1 and Dlx2 double mutant), does not alter the olfactory map (Bulfone et al., 1998). Another genetic mutation in the Gli3 gene (also call *extratoes* mouse), which eliminates the formation of the olfactory bulb, does not alter the coalescence of the OSN axons (St John et al., 2003). Ocam, an axon guidance molecule exclusively expressed in the ventral olfactory sensory neurons, is hypothesized to mediate the topographic organization because of its spatial expression pattern. However, knocking out Ocam does not alter the axon projection of OSNs (Walz et al., 2006). In addition, the OSN axons are pre-sorted within the axon bundles before reaching the glomeruli (Imai et al., 2009).

1.4 Contextual model of axon sorting

Is OR directly involved in OSN axon guidance? In 2004, Mombaerts and colleagues proposed the contextual model that incorporates ORs as axon guidance cues (Feinstein and Mombaerts, 2004). In this model, a hypothesized complex associated with ORs mediates the axon guidance of OSN at the

axon terminals. Here, I will first review how OR identity is established and then discuss how the OR identity can guide the axons in this model.

1.4.1 Establishment of OR identity

How is single receptor type expression achieved by the OSNs? Given the fact that one cell only expresses one receptor type in an allelic occlusive manner, there must be a mechanism to specifically regulate the olfactory receptor choice. The stable expression of receptors requires coupling the signals from the expressed receptor (Dalton et al., 2013). When one receptor is expressed without activating the downstream signaling, the neuron switches to a second OR (Lyons et al., 2013). On the other hand, the expression of a functional receptor also inhibits the expression from other loci (Lyons et al., 2013). Therefore, it has been hypothesized that an activity-dependent epigenetic mechanism is involved to secure the single receptor choice (Magklara et al., 2011). Lomvardas and colleagues have elucidated this epigenetic process through a series of experiment (Clowney et al., 2012; Dalton et al., 2013; Lyons et al., 2013; Magklara et al., 2011). First, during the maturation of the OSN, chromatin silencing blankets the OR loci (Magklara et al., 2011). OR rich genomic loci are condensed into a few heterochromatic loci in the nucleus. This nuclear topology change is mediated by the down regulation of lamin B receptor (LBR) (Clowney et al., 2012). Second, in iOSNs, transient expression of LSD-1, a histone demethylase desilences the OR loci and allows the initial expression of OR (Lyons et al., 2013). The initial expression of OR in iOSNs is not stable. Expression of multiple ORs in one iOSN has been observed (Hanchate et al., 2015; Tan et al., 2015). When the expression of ORs accumulates at ER, it generates unfolded protein response through PKR-like ER kinase (PERK). The ER stress is followed with phosphorylation of the translation initiation factor Eif2a and results in the selective translation of ATF5. ATF5 is a transcription factor that promotes the expression of adenylate cyclase (Adcy3, ACIII). Adcy3 downregulates LSD1 to stabilize the receptor choice (Dalton and Lomvardas, 2015). Adcy3 is coupled with OR signaling and maintains the feedback signal from the functional OR. In addition, ORs are controlled by enhancer elements in *cis*. These kinds of enhancers have been discovered, including H element(Serizawa et al., 2003), P element (Khan et al., 2011) and the “Greek islands”, such as

"Sfaktiria" and "Ikaria" (Markenscoff-Papadimitriou et al., 2014). It is not clear how the cells make initial choice of which receptor type to be expressed. Since a conserved set of ORs always expresses from the same zone of the epithelium, these enhancers apparently are involved in determine the receptor choice between different zones. Indeed, disruption of the enhancer interaction by knocking out BPTF (bromo and PDH-finger transcription factor) disrupts the single receptor expression in the OSN (Markenscoff-Papadimitriou et al., 2014).

1.4.2 Contextual model of axon sorting

The involvement of ORs in OSN axon guidance was first proposed in 1996 (Mombaerts et al., 1996). Both transcripts of ORs and OR proteins are detected at the axon terminal (Barnea et al., 2004), indicating that the ORs may play a role in the axon targeting. Direct evidence along this line of study emerges from the OR swapping experiment. For most of ORs, replacing the coding sequence of an endogenous receptor with another results in the convergence into an ectopic glomerulus (Wang et al., 1998). There is one exception, where replacing the M71 with M72 receptor results in the glomerulus of the switched receptor type (Feinstein and Mombaerts, 2004). Small changes, in the extreme case, a single nucleotide mutation in the coding sequence, also leads to ectopic glomeruli (Feinstein and Mombaerts, 2004). These results indicate that the ORs determine the convergence of the axons. In the contextual model, Mombaerts and colleagues hypothesize that the OSN axons target themselves instead of a target in the OB (Feinstein and Mombaerts, 2004). More importantly, the model indicates that the OR is necessary, but not sufficient in mediating the sorting process. First, olfactory receptors don't possess immunoglobulin-like domains that cell adhesion molecules have (Hall et al., 2004). Their extracellular domains are short compared to other GPCRs that response to protein ligand (Katada et al., 2005). From the predicted structures, the ligand binding occurs within the center area surrounded by seven transmembrane domains, leaving little space for interaction with any potential protein ligand that could serve as adhesion ligand. Second, swapping receptor types do not always lead the axons to the corresponding glomerulus position. Additional molecules, such as MHC peptide and receptor transporter proteins could be associated with ORs and mediate the interaction between the axons.

1.5 Activity dependent model of axon sorting

An alternative model is the activity dependent model. In theory, neural activity provides a single dimension of an infinite level of variations. When the neural activity level is used as a label, it could be particularly beneficial for the OSNs, as the OSNs are sorted by more than 1000 receptor types.

1.5.1 OR signaling

Olfactory receptors are G protein coupled receptors. The neural activity in the OSNs is generated through cAMP signaling activated by the G protein, mostly Golf (Reed, 1992). The signaling components identified in the pathway are Gnas (Gs), Gnal (Golf), Adcy3 (ACIII), and Cnga2. Deletions of these molecules result in anosmia (Belluscio et al., 1998; Brunet et al., 1996; Wong et al., 2000). The current model of action potential generation in the OSN is as follows: The binding of the odorant causes the dissociation of the G protein alpha unit, G alpha olf (G_{olf}). Golf activates the adenylate cyclase Adcy3. Activation of Adcy3 results in an increase of cAMP level and opens the cyclic nucleotide gated channel Cnga2, leading to depolarization.

Gs is another G protein alpha subunit that is also expressed by the OSNs (Jones et al., 1990). However, in the G_{olf} knockout, the existence of Gs doesn't rescue the signaling, suggesting that it is not sufficient to mediate odor detection. The expression of Gs is also earlier than that of G_{olf} during the OSN development. Knockout of Gs results in the disruption of OSN axon guidance (Nakashima et al., 2013), at least for a subset of receptor types (Movahedi et al., 2016). It is likely that Gs mediates signaling in the iOSNs, or the spontaneous activity in the mOSNs when the odorant is not present through the CREB pathway (Figure 1.5.1-1).

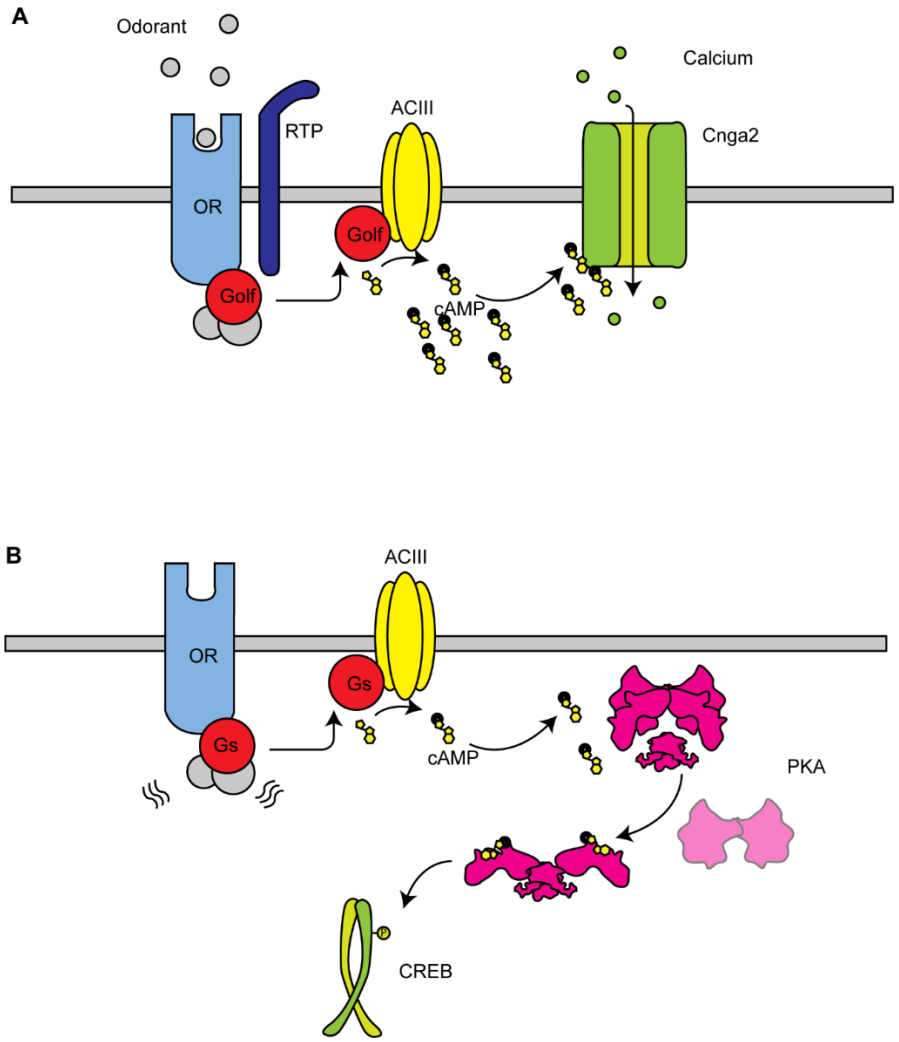

Figure 1.5.1-1 Illustration of olfactory receptor signaling

(A) Signaling in mOSNs. Odorants are detected by olfactory receptors (light blue). Olfactory receptors are coupled to Golf (red). When the olfactory receptor is activated, G protein alpha unit Golf dissociates from the complex and triggers the activation of ACIII (yellow). The cAMP level is subsequently increased, causing the Cnga2 channel (green) to open.

(B) Signaling in iOSNs. Most of the signaling molecules expressed by mOSN are not expressed in the iOSNs. ORs are expressed at a lower level. The Gs can potentially couple to the ORs without binding of the ligand. The activation of ACIII produces a lower level of cAMPs from the Gs than from the Golf, which is not sufficient to fire action potential, but instead activates the cAMP dependent protein kinase (PKA). PKA phosphorylates cAMP response element-binding protein (CREB) to activate downstream gene expression.

1.5.2 Neural activity is required for axon guidance

There are two types of neural activities, the odorant induced activity and the spontaneous activity. Ligand dependent activity is induced by the odorant through the signaling transduction described in 1.5.1. The OSNs also fire action potentials in the absence of odorant, which is defined as spontaneous activity (Yu et al., 2004). Little is known about what molecules are regulating spontaneous activity. Different ORs have different spontaneous activity pattern, which suggests that the OR itself can regulate the spontaneous activity pattern (Connelly et al., 2013). These two types of activities are distinct in their roles in axon guidance. Deletions of the signaling molecules in the ligand dependent signaling including Cnga2 and G_{olf} do not affect the axon projection (Belluscio et al., 1998; Brunet et al., 1996; Nakashima et al., 2013). The unilateral naris occlusion (UNO) blocks odorant from contacting the epithelium but doesn't alter the axon projection (Cummings and Belluscio, 2010). UNO also delays the refinement of single glomerulus convergence during the postnatal development (Zou et al., 2004). In contrast, the deletions of Adcy3 or Gs cause the OSNs unable to enter the OB (Nakashima et al., 2013). The ectopic expression of potassium inward rectifier channel, Kir2.1, which blocks the spontaneous activity, results in a disrupted map, suggesting that the spontaneous activity is required for the axon targeting (Yu et al., 2004). In summary, both types of neural activity are involved in the axon guidance of OSNs, but their roles are different.

1.5.3 Activity dependent model of axon sorting

Sakano and colleagues have proposed an activity dependent model, which states that neural activity of ORs drives the axons to separate (Mori and Sakano, 2011; Sakano, 2010; Serizawa et al., 2006). In the activity dependent model, the precise axon targeting requires two steps. First, around early postnatal stages, a coarse map is developed by specifying A-P and D-V axis. The D-V axis projection occurs based on the anatomical locations of the cell bodies in the OE. The A-P axis projection requires the cAMP signals from OSNs. The difference in OR signaling results in different levels of cAMP. Thus, downstream transcription of axon guidance molecules, such as Sema2A and Nrp1, are differentially

expressed, which results in the separation of axons of different OR types. In the second stage, axon projection is further refined by neural activity through CNG channels. A different class of axon guidance molecules, such as Kirrels and ephrins, are expressed according to the neural activity level. The differential expression of these molecules refines the projection pattern into stringent single receptor type. The activity dependent model agrees with the previous model in that the axon targeting relies on axon-axon interactions. But the structure of OR is not the determinant of the sorting. The activity differences derived from different OR types are the driving force for the sorting.

Even though the activity dependent model could explain many of the observations, it is likely to be incomplete. For example, G_{olf} knockout doesn't alter the convergence, even though the expression levels of the sorting molecules are changed (Nakashima et al., 2013). Transgenic expression of Kir2.1, which suppresses action potential and alters the expression of Kirrel2 and Kirrel3, however, dramatically affects the convergence (Nakashima et al., 2013; Yu et al., 2004). The Gs knockout, which only affects the A-P axis position determining molecules, also affects the convergence. A more recent study using Nrp1 conditional knockout animal also showed the A-P axis location doesn't change for a different receptor type, M71. Neural activities from different receptor types, or the cAMP signals, are likely to be very noisy because of the constant spontaneous firing from the OSNs and the unpredictable odorant environment. However, the sorting of axons is very reliable. Additional signaling may be involved in the axon guidance of OSNs.

1.6 Axon guidance of the regenerated neurons

OSNs are unique in that they are the only sensory neurons that regenerate throughout the life span. Neurons generated at different stages of the animal's life encounter different environment. For example, the turbinate between the OE and OB is highly calcified at the adult stage, but is not fully developed at the postnatal stage. The peripheral sensory neurons are subject to damage in adult animals. Although OSNs are being renewed constantly through the lifespan, the OSN axons maintain stringent singular projection. The olfactory map formation should be studied under the context of

regeneration in order to understand how neurons generated at different stages can keep targeting the same glomerulus.

1.6.1 Regeneration of OSN

OSNs maintain a continuous regeneration capacity through the animal's life span. Two populations of stem cells have been identified in the olfactory epithelium, the horizontal basal cells (HBCs), and the globose basal cells (GBCs). Both are located in the basal layer, right above the basal lamina.

Most of the GBCs are mitotically active (Beites et al., 2005; Chen et al., 2014; Huard and Schwob, 1995). Under normal condition, these GBCs are responsible for the generation of most cells types in the OE, including sustentacular cells, OSNs, as well as the Bowman's gland. Some of the GBCs are mitotically quiescent and express cyclin-dependent kinase inhibitor p27Kirp1 (Jang et al., 2014). Mild damage, such as axonomy and bulbectomy, damage the axons and leave the cell body intact. The GBCs are activated under these conditions (Yu and Wu, 2017).

HBCs are mitotically quiescent under normal circumstances and are not normally activated without extensive damage of the OE. Chemical ablation using zinc sulfate, dichlobenil, or methyl bromide gas can cause drastic damage to the OE. This type of severe damage triggers the activation of HBCs. Upon severe damage, HBCs differentiate into GBCs, OSNs, as well as other cell types (Brann et al., 2015; Schwob et al., 1995).

1.6.2 Challenge of axon guidance in the context of continuous regeneration

OSN axon guidance highly relies on the olfactory receptor. However, there are more than 1000 receptor types. The regulation of the expression requires activity from Adcy3, which is activated by the odorant. The odorant environment is different at different time and space for an animal. It is unlikely all the

receptors are expressed equally during the lifespan of the animal. In another word, the axon guidance mediated by the receptor is also a dynamic process. How is the map maintained under this dynamic condition? Since neural activities and ORs being expressed are different depending on the odorant encountered at different time and space, the regulation of the axon guidance must also be coordinated to the changing neural activity through development and at different environment. Molecules independent of ORs could be involved at the stage where the circuit connection is mature and requires consistency in the targeting.

1.7 Critical period mechanism of neural circuit formation

The requirement of neural activity during circuit development is not unique to the olfactory system. As early as in the late 1930s, people were aware of this requirement. For example, children with cataracts who are not treated at early ages have a permanent deficiency in vision (Lewis and Maurer, 2005). The learning of language requires early experience (Johnson and Newport, 1989). Feral children have permanently impaired ability to learn languages and social skills (Scovel, 1988). Activity dependent circuit development is most extensively studied in the visual system. A well-known study is the formation of ocular dominance column by David Hubel and Torsten Wiesel around the 1960s. They found that the cells in the primary visual cortex responded predominantly towards only one of the two eyes. Cells with similar ocular bias are found in the same columns, which are termed the ocular dominance columns. They found the development of ocular dominant column is dependent on the activities from eyes. Blocking neural activity by suturing one eye results in a shift in the dominance and permanently changes the column arrangement in the visual cortex (Hubel and Wiesel, 1959, 1962). The system is highly sensitive to activity deprivation during a restricted time window during the postnatal development, called the “critical period”. In the adult stage, even a prolonged monocular deprivation, as long as two years, doesn’t alter the columns (Hubel and Wiesel, 1970). The study reveals two key concepts of neural circuit development. First, neural activity is required for the formation of a specific neural circuit. Second, neurons are sensitive to activity deprivation during the critical period. Alteration in the activity pattern during the critical period permanently changes the circuit.

In the past three decades, the critical period has been studied extensively. Detailed reviews are written (Hensch, 2004, 2005). To briefly summarize the findings, neuronal circuits are shaped by experience during the critical period. The neurons form coarse projections before the onset of the critical period. During the critical period, the synaptic connectivity is refined by the pattern of neural activity. The change in the response field of the circuit is coupled to the local interneurons' maturation. After the critical period, perineuronal net acts as a physical barrier to prevent further reorganization of the circuit. This process is controlled by proteolytic modulation of the extracellular matrix.

1.8 Critical period of OSN axon guidance

Does the regenerating olfactory system also exhibit a critical period for circuit formation? This is an interesting question in the context of regeneration. The OSNs have continuous regeneration capacity throughout the animal's lifespan. However, the singular projection pattern of the olfactory map is always maintained. It is likely that neurons, even generated at the adult stage, maintain a capacity to target the correct glomeruli. In a previous study, Constanzo and colleagues severed the nerves of OSNs through the cribriform plate of the ethmoid bone. They observed that the newly generated OSNs expressing the P2 receptor no longer projected to the original single glomerulus (Costanzo, 2000). This experiment indicates that the neurons generated at adult do not have the capacity to target the correct glomeruli. However, the surgical ablation leaves scars, which prevents the axons from reaching the target. Therefore, a genetic approach is preferred to better verify this observation. Gogos and colleagues have done another ablation experiment through genetically engineering the OSN to express the diphtheria toxin A (DTA). In this experiment, only a subset of OSNs expressing a given receptor were ablated (Gogos et al., 2000). The newly generated P2 neurons were still able to target the single glomerulus. A major difference between the experiment is how the neurons are being ablated. The genetic ablation experiment leaves about 20% of the neurons intact. These results imply that the neurons generated at different stages may have different axon targeting capacity. The neurons generated at the adult stage may require additional factors from the existing neurons to target the

correct glomerulus. There might be a critical period in the olfactory system to regulate the axon projection development.

If such a critical period exists in the OSNs, it will be beneficial for understanding many things. A couple of questions that can be address using the olfactory system are as follows: How do the sensory neurons develop connectivity during the critical period? How do the sensory neurons maintain the connectivity after the critical period? What is the molecular and cellular mechanism for the sensory neurons' circuit development? How do the regenerated neurons connect the circuit after the critical period under damage? Will we be able to apply these pieces of knowledge to treat human neural degenerative diseases? In my Ph. D. study, I explored the critical period using the olfactory system to address these questions.

2 Chapter II. Critical period in olfactory system

2.1 Introduction

The development of the neural system requires both intrinsic factors and extrinsic factors. One major extrinsic factors are the environmental stimuli, which eventually transform into neural activity. The existence of the critical period is observed in almost all the sensory systems, such as visual, auditory (Kral, 2013), and somatosensory system (Erzurumlu and Gaspar, 2012), but it remains unclear if a critical period exists for the development of the olfactory system. An early study used unilateral nasal occlusion (UNO) surgery to block the sensory input to the OSNs. This study shows that activity is involved in the circuit development (Brunjes, 1994). However, UNO doesn't completely block the odorant because the two nasal cavities are connected. In a later study, using the transgenic animal expressing potassium inward rectifier channel Kir2.1 (Kir2.1 animal) to block the action potential, it is shown that, the spontaneous activity, rather than the odorant triggered activity is critical for the olfactory map formation (Yu et al., 2004). Using the Kir2.1 animal, it is possible to deprive the neural activity at any desired time during the postnatal development. In this study, I sought to investigate the critical period in the olfactory system using the Kir2.1 animal.

2.2 Material and methods

2.2.1 Experimental Animals

The tetO-Kir2.1-IRES-tauLacZ, OMP-IRES-tTA, OMP-SpH, M72-IRES-tauGFP, M71-IRES-tauGFP, (Jackson laboratory, stock number 009136, 017754, 004946, , 006678, and 006676, respectively) and the P2-IRES-GFP, MOR28-IRES-GFP, tetO-LBR-IRES-GFP, tetO-M71-IRES-tauLacZ and Gγ8-tTA mice were described previously (Clowney et al., 2012; Fleischmann et al., 2008; Nguyen et al., 2007; Treloar et al., 2002). All animals were maintained in Lab Animal Services Facility of Stowers Institute

with a 14:10 light cycle, and provided with food and water ad libitum. Experimental protocols were approved by the Institutional Animal Care and Use Committee at Stowers Institute and in compliance with the NIH Guide for Care and Use of Animals.

2.2.2 In situ hybridization

In situ hybridization was performed according to a published protocol (Ishii et al., 2004). The Kir2.1 probe was designed and synthesized in a previous study (Yu et al., 2004). The coding region of Kir2.1 was cloned from the mouse olfactory brain cDNA and cloned into pGEM-T vector (Promega A3600). The sense and antisense probes were transcribed using the DIG labeling kit from Roche (Catalog#: 11175025910). The olfactory epithelium was dissected from the Kir2.1 and control animal, embedded in O. C. T. (Sakura Tek 4583), snap froze in liquid nitrogen vapor, and stored under -80C until use. 16um sections were made using Leica cryostat. The hybridization was carried out under 60C overnight. After the hybridization, the slides were incubated with anti-DIG fab fragment conjugated with AP (Roche 11093274910) and visualized using NBT/BCIP (Promega S3771)

2.2.3 Immunohistochemistry

Immunohistochemistry was carried out according to published protocols (Ma et al., 2014). The olfactory bulb was stained using free-floating protocol. The animals were transcardially perfused with 10mL PBS and followed with 10mL 4% PFA in PBS. The olfactory bulb was dissected and post-fixed in 4% PFA in PBS at 4C overnight. After the fixation, the samples were sectioned using a vibratome (Leica VT1000), stained with primary antibody in PBST for overnight at room temperature, washed with PBST 5 minutes for 3 times, stained with secondary antibody and DAPI in PBST for overnight at room temperature, and mounted in VECTASHIELDS mounting media (Vector Labs H-1400) for imaging.

The olfactory epithelia were stained using cryo-sections. After the fixation, the samples were de-calcified in 0.5M EDTA at 4C overnight, dehydrated in 30% sucrose at 4C overnight, embedded in O. C. T., snap frozen in liquid nitrogen vapor, and stored in -80C until use. The sections were made the same way as in 2.2.2, and stained the same way as the free-floating protocol.

Primary antibodies were chicken anti-GFP (Abcam ab13970-100), rabbit anti-GFP (Invitrogen A-6455), mouse anti-beta-galactosidase (Promega Z3788), mouse anti-Kir2.1 (UC Davis/NIH NeuroMab Facility). Secondary antibodies were donkey anti-chicken DyLight488, donkey anti-mouise-Cy3 (Jackson ImmunoResearch), donkey anti-rabbit Alexa488, donkey anti-mouse Alexa 488 and 568 (Invitrogen). Antibodies were used at 1:500 or 1:1000 dilution for overnight staining at 4C. Sections were counter stained with DAPI and mounted in VECTASHIELDS mounting media (Vector Labs).

2.2.4 DiI labeling of the mitral cells

DiI labeling was carried out as described previously (Lin et al., 2000). Dissected brains were fixed in 4% PFA for 24 hours at 4C, then embedded in 4% low melting point agarose (Promega V2111). A coronal cut in the brain was made to expose the lateral olfactory tract where DiI crystals (ThermoFisher D282) were sparsely placed. A drop of agarose was applied to secure the DiI crystals in place. The tissues were kept in PBS at 37C for one week to allow the migration of DiI along the axons. Horizontal sections of 150 μm were made prior to imaging.

2.2.5 Microscopy

All images were acquired with Axiovert microscope (for chromogenic staining) or LSM-510 confocal system (Zeiss).

2.2.6 In vivo Synapto-pHluorin imaging

Live animal imaging was performed as previously described (Bozza et al., 2004). Mice were anesthetized with intraperitoneal injection of urethane (Sigma-Aldrich, 2 mg/g of body weight) and the bone above the dorsal olfactory bulb was gently thinned with electric dental tools. Odorants were fresh prepared at 10^{-3}, 10^{-2}, 10^{-1} dilution in mineral oil and delivered through the olfactometer. Odors were delivered 100 ml/min before merging with the carrier air and the total flow rate was maintained at 400ml/min. Synapto-pHluorin responses were acquired by Olympus BX60WI microscope with 4X (0.28 NA) objectives (Olympus) at a sample rate of 8.3 Hz Odor delivery was controlled by an automated olfactometer with custom written software developed in the National Instrument Labview programming environment as described previously (Qiu et al., 2014).

2.3 Results

2.3.1 Genetic manipulation of the neural activity using Kir2.1 transgenic animal

In order to deprive the neural activity, I used the Kir2.1 transgenic mouse by mating the OMP-IRES-tTA mouse and the tetO-Kir2.1-IRES-tauLacZ mouse into a compound transgene. OSNs in the Kir2.1 animal express potassium inward rectifier channel Kir2.1 under the control of tTA from the OMP promoter. Doxycycline can bind to the tTA and prevent Kir2.1 expression from the tetO-Kir2.1-IRES-tauLacZ allele. By feeding the animal doxycycline, the effect of activity deprivation can be removed at different time points (Figure 2.3.1-1).

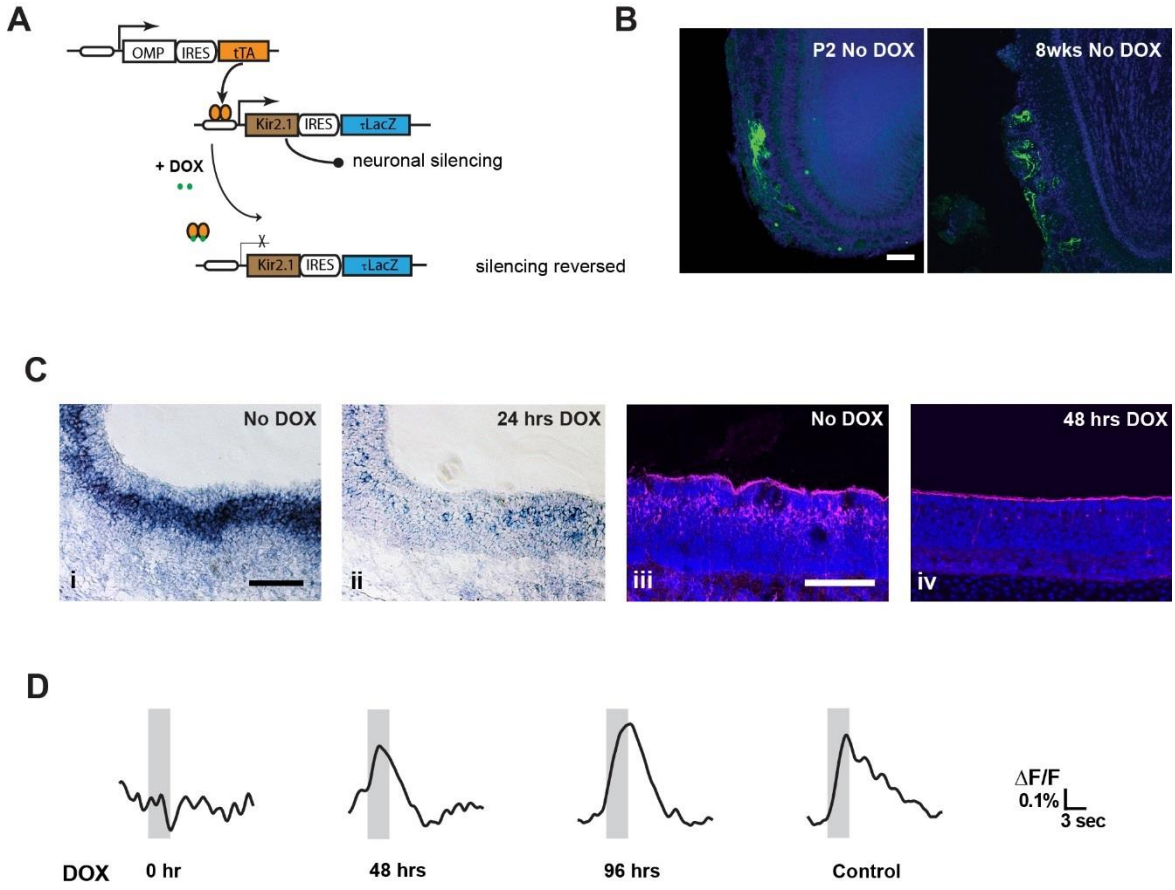
A
OMP
IRES
tTA
Kir2.1
IRES
τLacZ
neuronal silencing
+ DOX
Kir2.1
IRES
τLacZ
silencing reversed
B
P2 No DOX
8wks No DOX
C
No DOX
24 hrs DOX
No DOX
48 hrs DOX
i
ii
iii
iv
D
ΔF/F
0.1%
3 sec
DOX
0 hr
48 hrs
96 hrs
Control

Figure 2.3.1-1 Deprivation of the spontaneous activity using Kir2.1 mouse.

(A) Illustration of the Kir2.1 mouse. The OMP promoter drives the expression of tTA (yellow). tTA binds to the tetO promoter, and activates the Kir2.1 (brown) expression together with a marker tauLacZ (blue). The expression of Kir2.1 results in the neuronal activity silencing. When the animal is given doxycycline (DOX), tTA is inhibited by DOX. Kir2.1 is no longer expressed. As a result, DOX will reverse the activity silencing.

(B) The axon projection of the P2 neurons in the Kir2.1 animal. The P2 axons (green) are examined at postnatal day 2 (P2, left) and 8 weeks (right) without DOX treatment. P2 axons project to multiple glomeruli.

(C) *In situ* hybridization detection of Kir2.1 transcripts using a DIG labeled ribonucleic acid probe (blue colored signal), at P0 without DOX treatment (i) and P1 with 24 hours DOX treatment (ii). Immunohistochemistry detection of Kir2.1 protein using an antibody (red signal) at P0 without DOX treatment (iii) and P2 with 48 hours DOX treatment (iv). (i) and (ii) shows a dramatic decreased in the level of Kir2.1 transcript after 24 hours. (iii) and (iv) shows a decrease of protein level after DOX treatment. Kir2.1 protein is not detectable after 48 hours.

(D) Restoration of neural activities after DOX treatment in the Kir2.1 animal. Activities are detected through synapto-PHluorin (sPH) imaging. Kir2.1 animal carrying sPH is given DOX at P7. The dorsal olfactory bulb response stimulated with methyl-butyrate is imaged at P7 (0 hr), P9 (48 hrs), and P11 (96 hrs). The control animal without Kir2.1 is imaged at P11. The shaded boxes indicate when the odor is delivered. Recording traces indicate fluorescence change normalized to basal fluorescence before the odor is given.

To test the efficiency of the genetic manipulation, I performed in situ hybridization and immunohistochemistry to detect the Kir2.1 transcript and protein. After given doxycycline at P3, both the transcript and the protein level start to decrease instantly. The mRNA is diminished from the majority of the cells after 24 hours. After 48 hours, the mRNA is completely removed from all cells. The protein is eliminated between 48-72 hours. Functional imaging using Synapto-pHluorin shows the odorant response is restored after 72 hours after doxycycline administration (Figure 2.3.1-1). These results indicate it takes two to three days for the transgene to be shut down by doxycycline.

2.3.2 Activity deprivation during the postnatal development reveals a critical period

Next, we investigated whether the OSNs are sensitive to the activity deprivation during a specific time window. We performed time course doxycycline treatment to the Kir2.1 animal at P0, P3, P5, P7, P10, P14, P21 (postnatal day 0, 3, 5,7, 10, 14, 21, respectively). For animals given doxycycline at P0, the disrupted glomeruli projection pattern was restored into single projection pattern at the adult stage (Figure 2.3.2-1). However, for the animals given doxycycline at P21, the glomeruli projection pattern remained disrupted at the adult stage (Figure 2.3.2-1). Statistically, the number of ectopic glomeruli started to show a significant difference at P5 (Figure 2.3.2-2). Disrupted projection pattern persisted for at least a year. Different receptor types, including MOR28 (Olfr1507), M72 (Olfr160) and P2 (Olfr17) followed the same curve (Figure 2.3.2-2), even though their target glomeruli were on different parts of the olfactory bulb. OSNs are regenerated during the animal's life span. The restoration of the disrupted axon projection pattern of those P0 to P5 doxycycline treated mice indicates that the neurons existing at this period are able to reroute the axons when the activity is restored. In another word, the neurons generated during this period can target the correct glomerulus *de novo*. This evidence suggests that a critical period exists in the olfactory sensory neurons. Since the doxycycline takes about two days to shut down the transgene, the timing of this period is from P0 to P7. On the contrary, the neurons generated after critical period appear to recapitulate the existing projection pattern. That is to say, if the

projection is single at P7, they will keep projecting to the single glomerulus. If the projection is multiple at P7, they maintain the multiple-projection pattern instead.

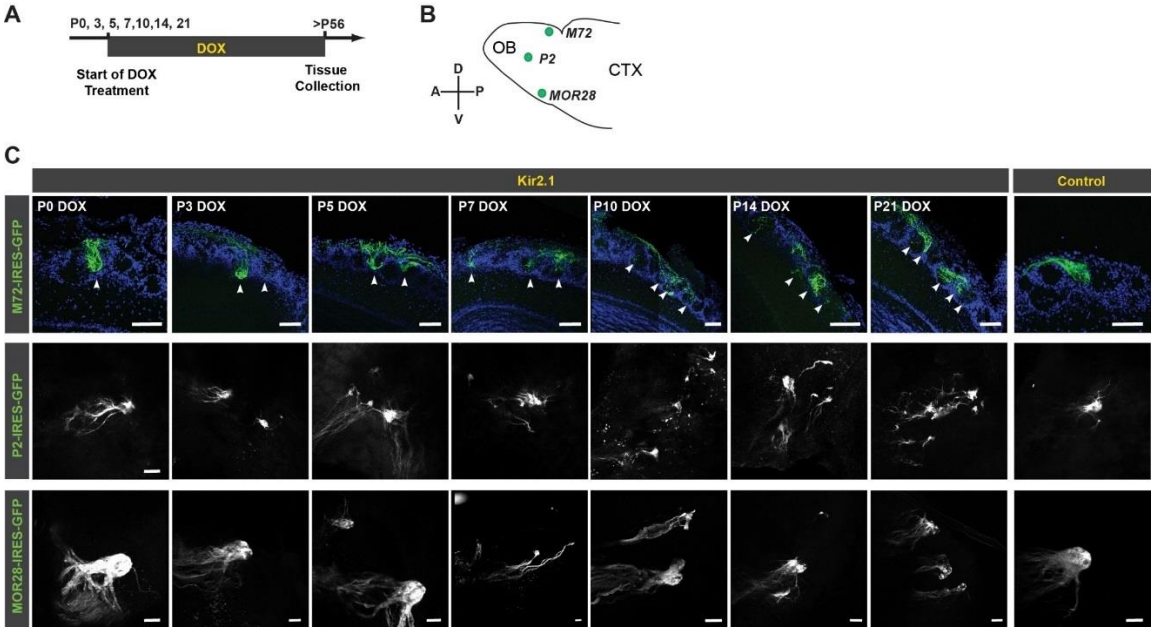

Figure 2.3.2-1 A systematic analysis of three receptor types in the Kir2.1 animal after the reversal of the neural activity deprivation.

(A) The schematic of the experiment design. The Kir2.1 animal is fostered to DOX treated mom at P0, P3, P5, P7, P10, P14, P21. The glomeruli projection is observed after 56 days of DOX treatment.

(B) The illustration of the glomerulus positions on the OB.

(C) Representative images from the experiment. Panel Kir2.1 shows the images from Kir2.1 animal. Panel Control shows the images from the littermate control animals. The samples from the M72-IRES-GFP animals are sectioned and stained with antibodies against GFP (green). The sections are counter stained with DAPI (blue). Samples from P2-IRES-GFP animals and MOR28-IRES-GFP animals are imaged with whole-mount preparation. The GFP signal is shown in gray scale. Scale bar: 100 μm.

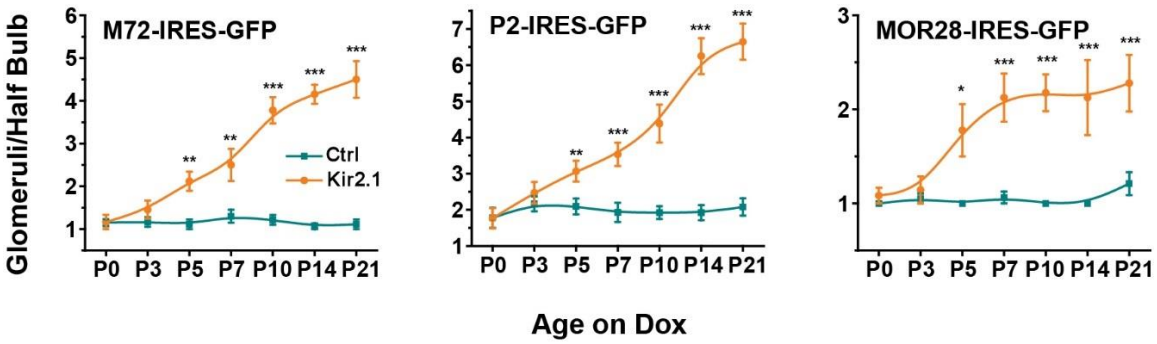

Figure 2.3.2-2 Quantification of the results from the experiment in figure 2.3.2-1.

The number of GFP positive glomeruli per half olfactory bulb is quantified for each receptor type and plotted against the age when the animal is given DOX. 6-18 half bulb are counted for each condition. The results from Kir2.1 animals are labeled yellow. The results from the control animals are labeled green. Stars indicate the P-value in the t-test between Kir2.1 and control animal. *: 0.05; **: 0.01; ***: 0.001.

2.3.3 Homotypic interaction between the olfactory sensory neurons

OSNs always target the glomeruli with the same receptor type. As discussed in the previous chapter, the genetic ablation experiment using P2 promoter driven DTA transgene suggests the existing axon tracts could guide the later generated axons through homotypic interaction within the same receptor type. To test the hypothesize, we used the OMP-IRES-tTA; tetO-M71-IRES-tauLacZ animal (M71 animal for short) (Fleischmann et al., 2008). In this compound strain, a particular olfactory receptor, M71(also known as Olfr151) is expressed in all the olfactory sensory neurons under the control of tTA, which is expressed under the OMP promoter. If the homotypic interaction exists during the critical period, the neurons expressing M71 from the endogenous allele will be guided to ectopic glomeruli which contain transgenic M71.

We performed the same time course doxycycline treatment to this animal as we did with the Kir2.1 animal. Consistent with our hypothesis, neurons expressing M71 from the endogenous allele projected to multiple glomeruli containing transgenic M71. However, OSNs with different olfactory receptors, M72 and MOR28, were not affected in the transgene and projected perfectly into the same glomerulus (Figure 2.3.3-1). This result indicates homotypic attraction from only the same receptor type is involved in the mistargeting of M71 animal. When the animals are given DOX, the disrupted projection could be restored at the early stages (P0). The restoration followed the same trend as we observed in Kir2.1 animal (Figure 2.3.3-1). This indicated the homotypic interaction from the existing axons could guide the axons generated at a later stage. This result also demonstrates that homotypic interaction is sufficient to redirect axon routing before P7, but not after.

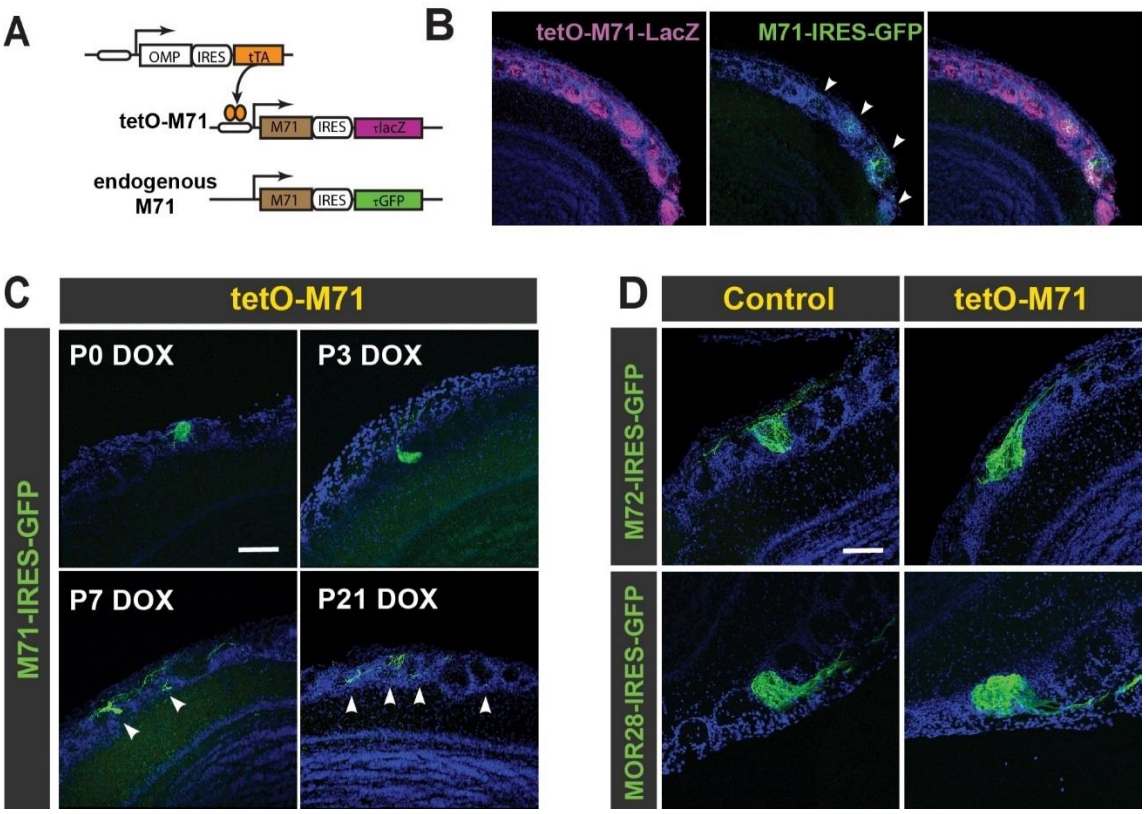

Figure 2.3.3-1 Homotypic interaction directs axon guidance during early development.

(A) The schematic illustration of the M71 transgenic animal. The OMP promoter drives the expression of M71 together with a marker tauLacZ. The expression can be inhibited by DOX treatment. Endogenous M71 is expressed together with marker GFP.

(B) A representative image of the axons expressing M71 from the endogenous locus in the M71 animal. The axons expressing M71 from the tetO-M71-IRES-tauLacZ allele are stained with antibodies against LacZ (red). The axons expressing M71 from the endogenous locus are stained with antibodies against GFP (green). These axons project to multiple glomeruli (white arrow).

(C) Representative images showing the axons expressing M71 from the endogenous locus at adult stage after the animal is treated with DOX at different time points (P0, P3, P7, P21).

(D) Representative images showing the axons expressing M72 or MOR28 in the M71 animals and their littermate control animals. These axons project to a single glomerulus.

2.3.4 The critical period is independent of neural activity

The time courses of the glomeruli restoration in M71 animal and Kir2.1 animal experiment are very similar. Even though two different genetic mechanisms drive the disruption in the two transgenes, the neurons are able to correct the multi-projection pattern as long as the transgene is stopped before P5. We are curious to see 1) if there is an invariant closure time of the critical period, which is defined as the neurons lose the ability to target the correct glomerulus, and 2) whether the timing of the closure is independent of the transgenic manipulation. We used a third transgenic mouse, OMP-IRES-tTA; tetO-LBR-IRES-tauGFP animal (LBR animal, Lbr is the gene name for lamin-B receptor) (Clowney et al., 2012). This compound transgenic mouse also has a disrupted glomeruli projection by overexpression LBR, which de-activates the epigenetic mechanism that secures the single receptor expression in the olfactory sensory neuron (Lyons et al., 2013). As a result of multiple receptor types being expressed in the same neuron, the identity of the cell is compromised. That eventually misleads the axon into the convergence with other receptor types (Clowney et al., 2012). We performed exactly the same experiment as done with the M71 and Kir2.1 animal. The same observation was seen again. When the LBR expression was shut down before P5, the disrupted projection pattern was restored at the adult stage (Figure 2.3.4-1). The time is also the same with the other two transgenes. That is to say, there is an intrinsic switch of axon guidance mechanism around P7. The timing of the switch is independent of whether the projection is formed properly.

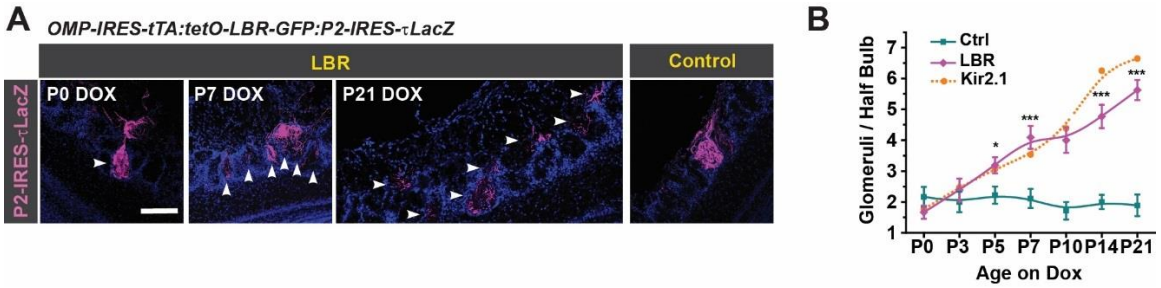

Figure 2.3.4-1 Axon rewiring is independent of activity deprivation.

(A) Representative images showing the P2 axons in the LBR and control animals treated with DOX at different time points (P0, P7, P21). The LBR and control animals are given DOX at the indicated time points. The P2 neurons are stained by antibody staining against LacZ(red). The sections are counterstained with DAPI (blue). Scale bar: 100 µm. White arrow: P2 innervated glomeruli.

(B) Quantification of the time course DOX treatment experiment in the LBR animals. The number of P2 innervated glomeruli per half olfactory bulb is plotted in red. Dashed yellow line indicates the data from figure 2-2-3 using Kir2.1 animals. The two curves follow similar trend. Stars indicate the P-value in student t-test. *: <0.05. **: <0.01. ***: <0.001.

2.3.5 Development of mitral cell dendrites

In the classic study of the critical period in the visual system, neurons receiving input from the sensory neurons, such as those in the lateral geniculate nucleus (LGN), and the primary visual cortex V1, are dramatically affected by sensory deprivation during the critical period. In order to know whether the same principle applies to the olfactory system, we performed mitral cell labeling in the olfactory bulb from the Kir2.1 animal at different development stages between P0 to P7. The mitral cells initially have multiple primary dendrites. Only one of the primary dendrites will remain connected to the glomerulus after P7. In this experiment, I didn't observe any obvious difference in the M/T cells between Kir2.1 and control animals (Figure 2.3.5-1). The timing of pruning is also not affected (Figure 2.3.5-1). That is to say, dendritic pruning of secondary projection neurons is not affected following the neural activity deprivation in the sensory neurons. However, whether activity deprivation within the M/T cells themselves will affect their dendritic pruning requires more experiments.

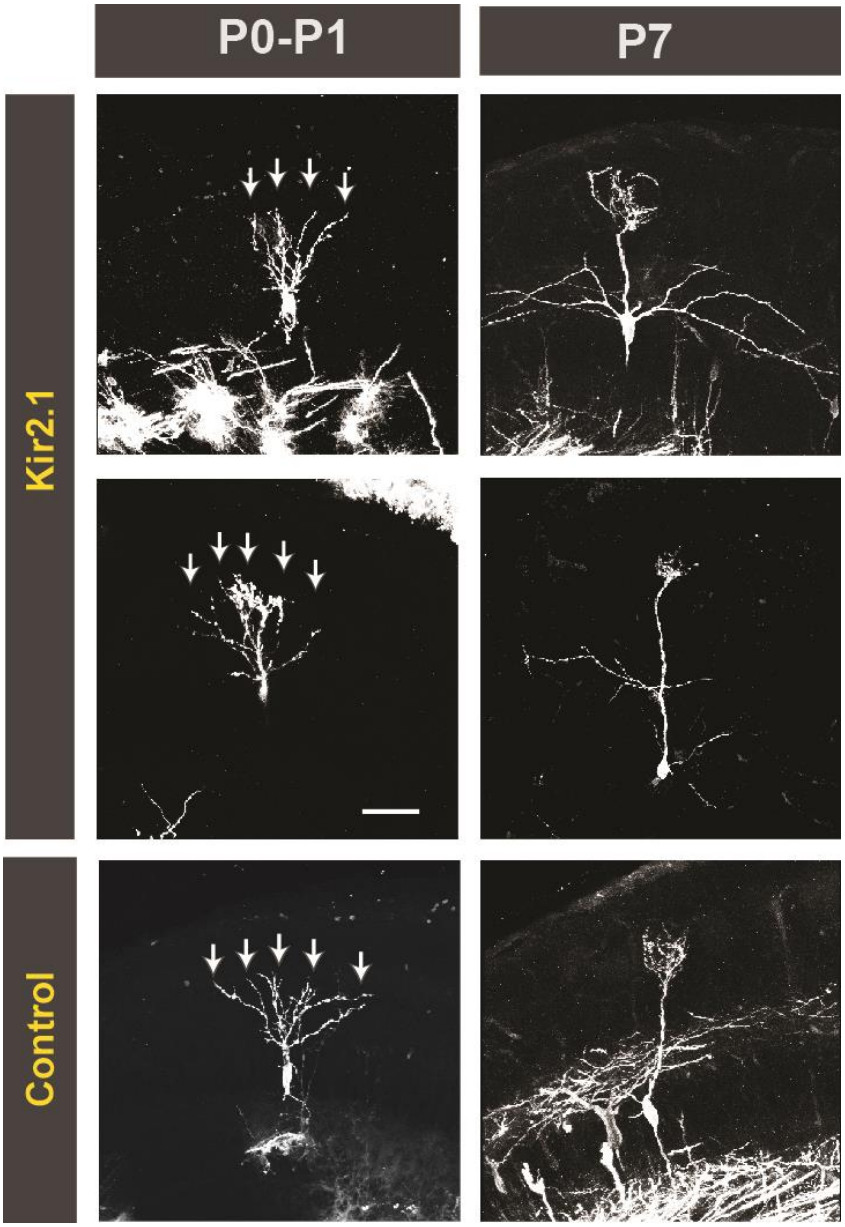

Figure 2.3.5-1 The development of mitral cells following sensory neuron activity deprivation.

Representative images showing the mitral cells labeled by DiI in the Kir2.1 and control animals. At P0-P1, the mitral cells have multiple primary dendrites. At P7, the dendrites are pruned. Only one primary dendrite remains connected with a single glomerulus. There is no obvious difference between Kir2.1 and control animals. Scale bar: 100 μm.

2.4 Discussion

2.4.1 Developmental switch of the axon guidance

Our experiment showed that the OSN axons target the glomeruli through different mechanisms during the postnatal development. There is a critical period for the circuit formation. Neurons generated during the critical period target the glomerulus *de novo*. When the projection pattern is disrupted, they are able to repair the circuit. The neurons generated afterward require the existence of the early neurons for correct targeting. The olfactory map is imprinted during the critical period. The late generated neurons follow the existing projection pattern. There is a developmental switch at the closure of the critical period. Different sets of axon guidance molecules may be expressed before and after the critical period. The early and late neurons may adopt different sets of axon guidance molecules for glomeruli targeting.

This developmental switch could explain the previous inconsistency in the ablation experiment. When the neurons are ablated during the adult stage after the critical period is closed (Costanzo, 2000), the neurons are no longer able to project back to the original glomerulus. However, in the ablation of P2 expressing neurons (Gogos et al., 2000), a small number of P2 expressing neurons (10%-20%) leave a track for the later generated P2 neurons to follow. Therefore, there is no disruption of the P2 projection after the new neurons are regenerated. The tet-M71 time course on DOX experiment supports this hypothesis. After M71 expression from the transgenic allele is shut down, the neurons expressing M71 from the endogenous allele could serve as a track for the late generated neurons to follow. After the critical period, Neurons expressing M71 from the endogenous allele could not reroute the axons. As the late generated axons keep following the existing M71 track, the multiple-projection pattern is maintained to the adult stage.

2.4.2 Activity independent perturbation is subject to the regulation by the critical period

In our experiment, we have used three methods to disrupt the axon projection pattern, Kir2.1, LBR and M71 transgenes. The latter two methods disrupt axon projection without silencing the neurons. Regardless of the transgene being used, the time course of restoration is consistent. Only between P0 to P7, the neurons can repair the disrupted projection pattern. This implies that the closure time of the critical period is independent of the interrogation method. In the study of the ocular dominance column critical period, activity deprivation is often used to decide the timing of critical period. Our study showed that the timing of critical period is independently regulated. There is an intrinsic genetic program determining the timing of closure.

2.4.3 Sensory input independent pruning of the secondary neurons

In contrast to the neurons in the visual system, M/T cells' dendritic development is not affected by the sensory neurons' activity deprivation. In this study, neither the timeline of pruning or the final morphology of the mitral cell is affected. This result also implies the pruning of M/T cell dendrites is independent of their presynaptic partner. It is not clear how the neural activity within the mitral cells and the postsynaptic neurons will affect the pruning. The future experiment requires activity silencing from the mitral cells and the piriform projection neurons.

3 Chapter III. The settler neurons

3.1 Introduction

In the previous chapter, we conducted the neural activity deprivation experiment using Kir2.1 animal and identified a critical period. We found neurons born at different postnatal stages adopted different mechanisms for axon targeting. Cells generated during the critical period were able to restore the disrupted projection pattern when the neural activity was restored. In contrast, the cells born after the critical period relied on the existing projection pattern to target the glomeruli. To unveil differences in cellular and molecular properties that distinguish the two population, it is necessary to label them by when they are generated. In this study, we used the OMP-IRES-tTA; tetO-tTA*-tauLacZ mouse (OMP-TetTag mouse) to genetically pulse-chase the neurons to study how the two population integrate into the circuit during the critical period.

3.2 Material and method

3.2.1 Animals

TetTag (tetO-tTA*-tau-LacZ allele), tetO-DTA and OMP-IRES-tTA mice (the Jackson laboratory, stock number 008344, 008468, and 017754, respectively) were described previously (Reijmers et al., 2007) and mated to create OMP-TetTag mice (OMP-IRES-tTA; tetO-tTA*-tau-LacZ). All animals were maintained in Lab Animal Services Facility of Stowers Institute with a 14:10 light cycle, and provided with food and water *ad libitum*. Doxycycline (DOX) treatment was performed by either weaning the pups onto DOX diet or by fostering the pups to CD1 moms fed with DOX diet at least 48

hours earlier. Experimental protocols were approved by the Institutional Animal Care and Use Committee at Stowers Institute and in compliance with the NIH Guide for Care and Use of Animals.

3.2.2 Histology

Animals were fully anesthetized with Urethane (2mg/g body weight) and perfused intracardially with 10mL 1X PBS and 10mL 4% PFA. The olfactory epithelia and brain were dissected and post fixed in 4% PFA overnight at 4℃. Coronal sectioning of the olfactory bulbs was performed on a Leica Vibratome system at 50 µm thickness. The olfactory epithelia were decalcified with 0.5M EDTA and treated with 30% sucrose at 4°C overnight, then embedded in Tissue-Tek O.C.T. (Sakura). Coronal sectioning of the nose was performed with a cryostat (Leica microsystem) at 16 µm thickness. Immunofluorescent staining was performed by incubating the sections with primary antibodies in PBST overnight at 4℃, washing 3 times with PBST, and incubating with secondary antibodies in PBST overnight at 4℃. Primary antibodies used in the study were: mouse anti-β-gal (Promega Z3788, 1:1000 dilution), goat anti-OMP (Waco 544-10001, 1:500 dilution), rabbit anti-RFP (MBL PM005, 1:1000 dilution) and rabbit anti-GFP (Abcam ab290, 1:1000 dilution). Secondary antibodies used were: donkey anti-mouse Alexa 594, donkey anti-goat 488, donkey anti-rabbit 488, and donkey anti-rabbit 594 from Life Technologies. DAPI (Life Technologies) and secondary antibodies are used at 1:1000 dilution.

3.2.3 Imaging

Olfactory bulb sections were imaged on Zeiss 700 and Zeiss 510 system. Olfactory epithelium sections were imaged using Ultraview Spinning disk confocal microscope (Perkin Elmer). Images were acquired using 20X lens and 40X lens (Zeiss).

Measurements were performed using FIJI ImageJ. To quantify lacZ+ axons in the olfactory bulb, z-stack images were projected into a single plane. Signals were threshold using the “Triangle” method to

produce a binary image. EPL and Glomeruli areas were defined by DAPI staining. Resulting lacZ+ pixels within EPL were quantified by “Analyze particles…” function.

3.2.4 Adenovirus labeling

The AV5-CMV-EGFP and AV5-CMV-RFP were constructed according to published protocol by recombining pADTrack-CMV (addgene 16405) and RedTrackCMV (addgene 50957) with ADeasy-1 in the ADeasier-1 cells (Luo et al., 2007). The virus stock was titrated to 10^7 infectious particles/mL. P0-P7 CD1 pups were anesthetized on ice. 10uL of stock virus was injected into the nose using a 30G syringe. The animals were then recovered and returned to the mom. P7 to P21 CD1 pups were anesthetized with isoflurane. The virus was delivered by letting the animal to inhale the solution. Histology analysis was performed at the indicated time points after viral labeling.

3.2.5 CUBIC brain clearing

The CUBIC clearing is performed according to the published protocol (Susaki et al., 2015). The immunostainings against GFP and RFP were performed after reagent 1 treatment to improve the visualization of individual axon. After CUBIC, the samples were embedded in a customized mounting media, Y-mount. The recipe for Y-mount is: 215g H2O, 35g Porcine gelatin, 250g sucrose, 2.5g n-propyl-gallate. Y-mount is a reversible gel, which is melt into liquid phase under 50℃, and solidified at 4℃. The use of Y-mount helps to prevent movement in liquid phase mounting media such as oil and glycerol during the imaging. The images were taken using LSM-700 system with single photon excitation.

3.2.6 Quantification of the lifespan of OSN

To quantify lacZ+ neurons in the olfactory epithelia, we made coronal tissue sections at the posterior position along the A-P axis of the olfactory epithelia and quantified the number of cells labeled. Images

were stitched together using “Grid/Collection Stitching” in FIJI. Only cells with intact nuclei, clear cell bodies and intact dendrites were counted. To quantify the number of labeled OSNs consistently, we only counted lacZ+ cells that included the cell body, the dendrite as well as clear nuclear staining. The density of the cells was normalized to adjust for the growth expansion of the neuroepithelia during development (Weiler and Farbman, 1997). All neurons from the section were counted and then used to calculate the density of cells. During postnatal development, the nasal tissue undergoes expansion in all three dimensions. The changes in width and height of the section were quantified from the section. Changes along A-P axis were measured using littermate control animals. The changes along all three axes were multiplied and divided to that of P3 to generate the expansion factor. The number of cells per mm^3 was normalized to that of a P3 mouse by multiplying the expansion factors.

3.3 Results

3.3.1 Genetic labeling of the early and late neurons

In the OMP-TetTag animal, the doxycycline insensitive form of tTA, tTA*, is expressed from the Tet-Tag allele. This allele is controlled by a bi-cistronic tetO allele, which also expresses LacZ. Expression of tTA from the OMP promoter activates this allele. Once the animal is given doxycycline, neurons that have already expressed tTA from the OMP allele will keep expressing the marker LacZ, because the tTA* is not sensitive to DOX and can activate its own allele. In contrast, the newly generated neurons will not express LacZ, because the tTA* is never expressed (see Figure 3.3.1-1).

To test the efficiency of method, I performed *in utero* doxycycline treatment to the OMP-TetTag animal. No LacZ signal could be detected after the animal is born, indicating no leakage expression of the marker (Figure 3.3.1-3B). This result shows the doxycycline successfully suppressed expression from the Tet-Tag allele.

In the next control experiment, animals were raised without doxycycline to P7. At P7, the animals were fed with DOX and injected with BrdU. BrdU is incorporated into the dividing cells and labels newborn neurons. After 7 days of doxycycline treatment, none of the LacZ positive neurons is BrdU positive (Figure 3.3.1-2). This mutually exclusive staining pattern indicates the method only labels the neurons generated before doxycycline treatment.

I co-stained the OMP together with LacZ using the animals without any doxycycline treatment. About 80% OMP positive neurons are labeled across the different time points I have tested (P3, P7, P14, P21, Figure 3.3.1-3). The neurons that are OMP positive, but not labeled by LacZ do not show any specific spatial localization (Figure 3.3.1-3), indicating a stochastic mosaicism in the labeling of the cells.

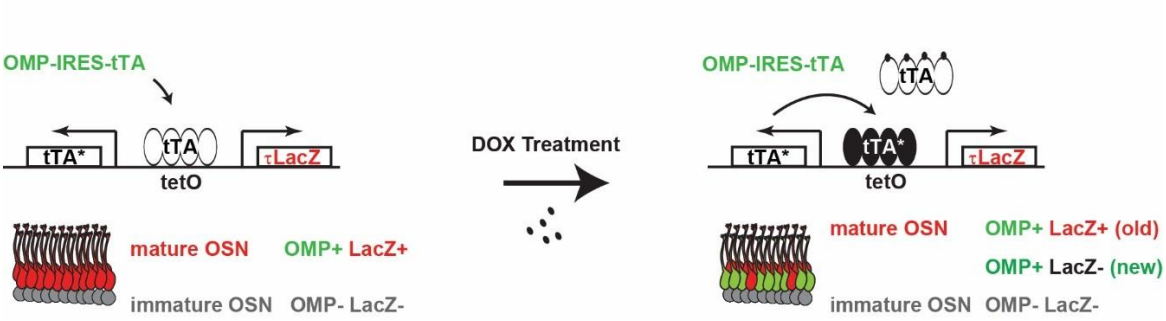

Figure 3.3.1-1 Schematic illustration of the lifespan tracing experiment using OMP-TetTag transgene.

OMP promoter drives the expression of tTA from the OMP-IRES-tTA allele. tTA activates the transcription from the tetO-tTA*-tauLacZ (Tet-Tag) allele. As a result, mOSNs are labeled by lacZ. After the animal is given DOX, tTA is inhibited. tTA* expressed from the tet-Tag allele continues to activate the Tet-Tag allele, forming a self-perpetuation loop and allows the neurons to be continuously labeled. Newly generated OSNs never express tTA*, and are not labeled by lacZ. As a result, only the existing neurons before the DOX is given are labeled by lacZ.

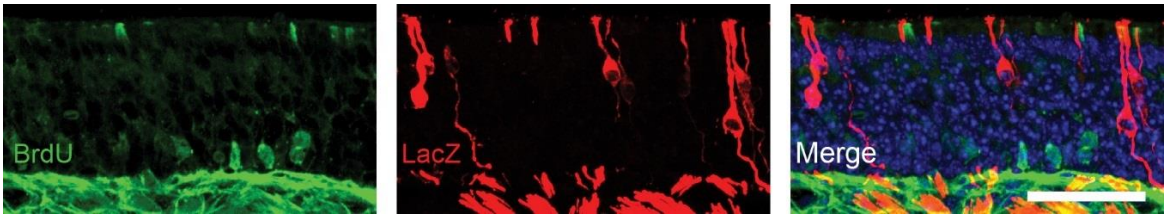

Figure 3.3.1-2 OMP-TetTag transgene only labels existing neurons.

The OMP-TetTag animal is given DOX and BrdU at P7. After 7 days, the olfactory epithelia sections are stained by BrdU and LacZ antibodies. The signals from BrdU (green) and LacZ (red) stainings are mutually exclusive. The sections are counter-stained with DAPI (blue). Scale bar: 100 μm.

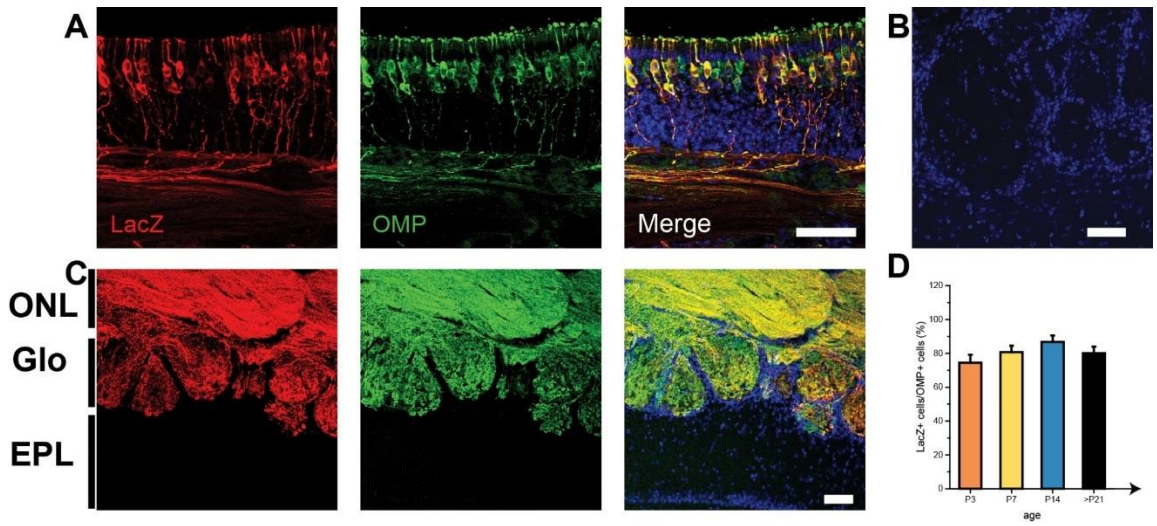

Figure 3.3.1-3 OMP-TetTag consistantly labels mOSNs through postnatal development.

(A) A double staining against LacZ (red) and OMP (green) of the olfactory epithelia from the OMP-TetTag animals.

(B) Representative olfactory bulb section of an adult OMP-TetTag animal, treated with DOX from embryonic stage E0, stained with LacZ antibody.

(C) A double staining against LacZ (red) and OMP (green) of the olfactory bulb from the OMP-TetTag animals.

(D) Quantification of the percentage of LacZ positive cells within the OMP positive cells at different ages. Scale bar: 50 µm.

3.3.2 Axon dynamics of the early and late neurons

The control experiment showed that the OMP-TetTag labeling can be used reliably to label the neurons generated before a defined time point. I then dissected the olfactory bulb of the OMP-TetTag animal at different time points around the critical period and stained against LacZ to study the axon projection. Strikingly, I observed axons projecting beyond the glomeruli, into the EPL layer, and sometimes into granule cell layer (Figure 3.3.2-1) between P0 to P7. The time course of this exuberant growth at the different areas of the olfactory bulb is different. Medial and lateral areas of the OB have earlier onset than the dorsal and ventral areas by about two days. Ventral axons are the most exuberant. Axons in posterior OB are more exuberant than anterior. The onset time of exuberant projection from posterior axons is also earlier than anterior. Axons from all regions showed a significant increase in the exuberant growth after P7. To confirm this observation, I also used adenovirus to label the axons. The same axon overgrowth was seen during the critical period (Figure 3.3.2-1), indicating that the exuberant axon growth is not generated by the OMP-TetTag transgene, but an intrinsic phenotype of the OSNs.

Considering the regeneration capacity of the olfactory sensory neurons, I think the exuberant axon growth may be unique to the neurons generated during the critical period. To test this hypothesis, I performed doxycycline treatment to the animals at P0 and P7. For the axons labeled at P0, there is an increase of exuberant growth at P7. This means the exuberant growth is not a result of the accumulation of newly arrived axons, but from the existing axons. It is likely that the existing axons extrude across the boundary of the glomerulus layer during the critical period. It is also very interesting that the P0 labeled axons are diminished after 14 days of doxycycline treatment. In contrast, a substantial number of axons labeled at P7 remains in the OB after 21 days of treatment (Figure 3.3.2-2). This indicates the stability of the axons from the late generated neurons is higher than that of P0 neurons.

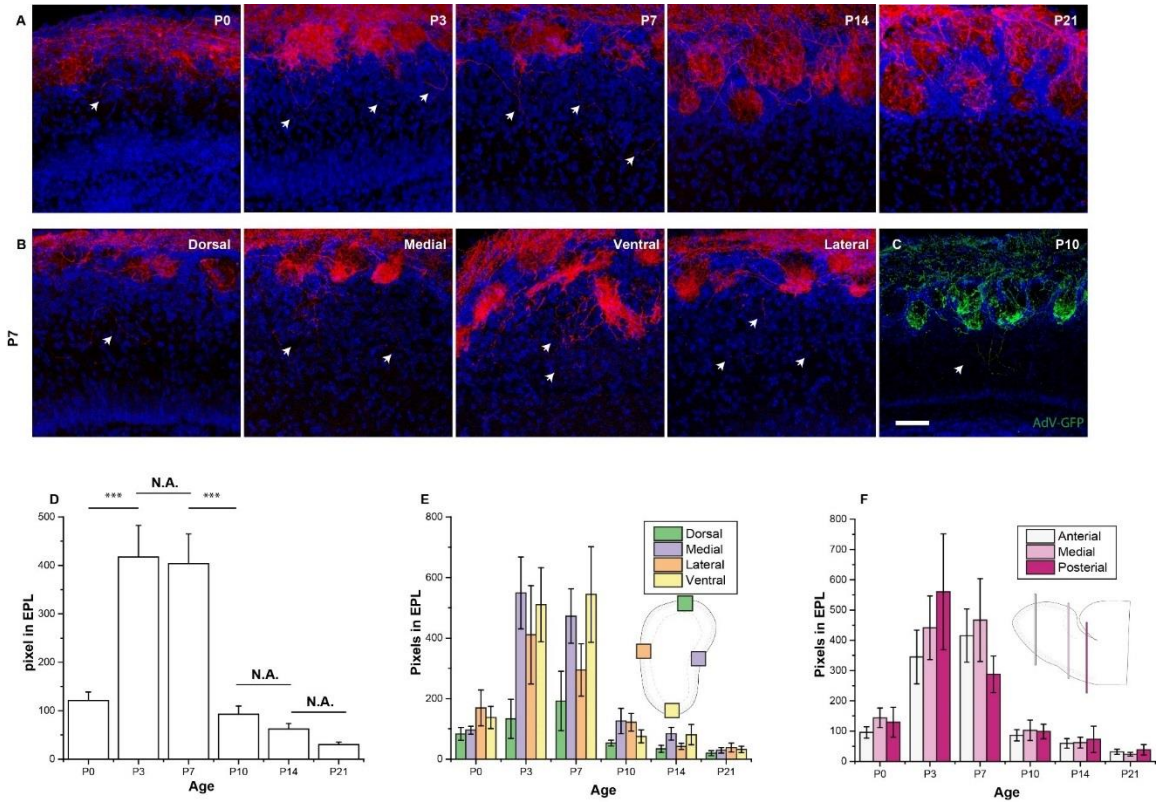

Figure 3.3.2-1 OSN axons project exuberantly during critical period.

(A) Representative images showing the OSN axons labeled by OMP-TetTag (lacZ, red) through postnatal development. White arrows indicate exuberant axons that protrude into EPL layer.

(B) Different olfactory bulb regions of the OMP-TetTag animals at P7.

(C) OSN axons labeled using adenovirus expressing GFP (green) at P0 and visualized at P10.

(D) Quantification of the exuberant axons during postnatal development. The LacZ positive pixels in the EPL layer are calculated for each time point as an indicator of exuberance.

(E) And F) The samples in D are separated by their positions on the olfactory bulb. An illustration of the positions is shown on the right side of each plot.

Scale bar: 50 μm. Star indicates the P-value from student t-test: *:<0.05. **:<0.01, ***:<0.001.

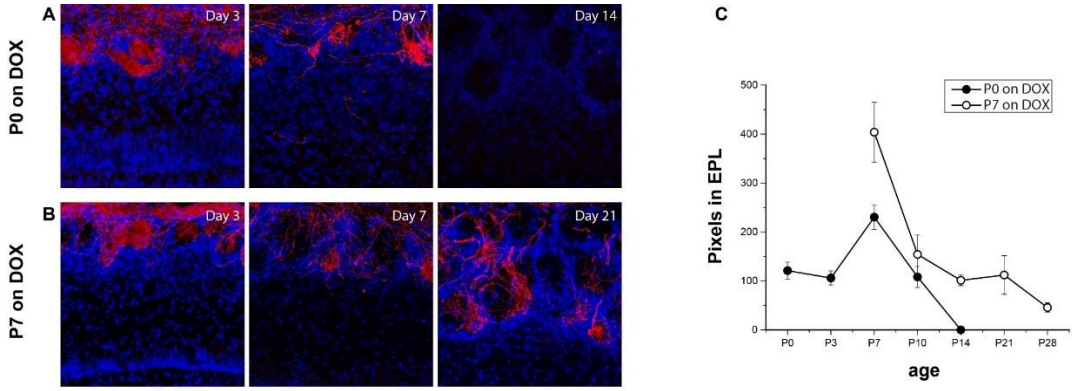

Figure 3.3.2-2 Exuberant axon growth is promoted during the critical period.

(A) Representative images from the OMP-TetTag animals treated with DOX at P0 for 3, 7 and 14 days.

(B) Representative images from the OMP-TetTag animals treated with DOX at P7 for 3, 7 and 21 days.

(C) Quantification of the exuberant axon growth using the LacZ positive pixels in the EPL layer. P0 labeled samples (black dots) show an increase of exuberance at P7. P7 labeled samples (empty dots) show a decrease of exuberance at P28.

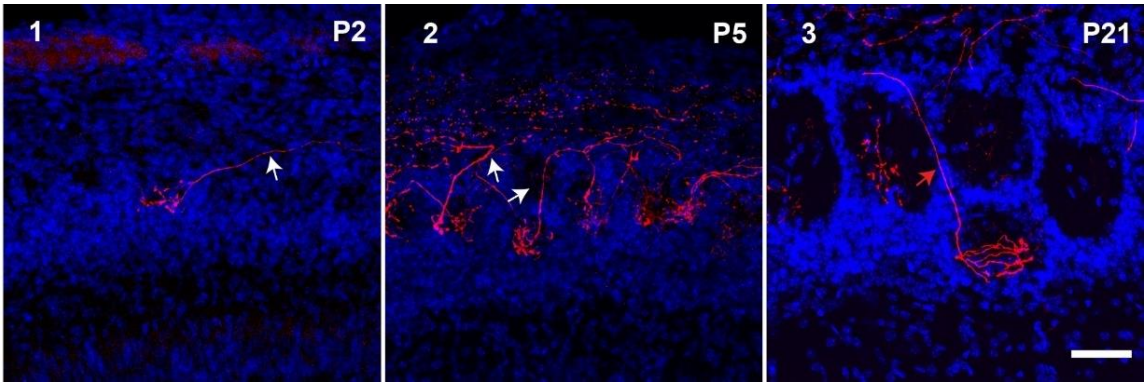

Figure 3.3.2-3 OSN axons traverse multiple glomeruli during the critical period.

OSN axons are labeled with adenovirus expressing RFP (red) at P0 and visualized at P2 (1), P5 (2), P21 (3). The axons at P2 and P5 can be seen going through other glomeruli (white arrow) before reaching the final glomerulus. The axons project directly into the final glomerulus (red arrow) at P21. Scale bar: 50 μm.

The extensive projection pattern of P0 labeled axons indicates that these axons have a higher plasticity than that of late neurons. I think the axons from the P0 neurons first project to a vicinity area with errors, then refine the target region by seeking the nearby axons of the same OR identity. I tested this hypothesis by labeling the axons using adenovirus. I found the axons generated at early stage cross the boundary of glomeruli (Figure 3.3.2-3).

Recent advances in the histology techniques, such as CLARITY, CUBIC, and 3DISCO, have allowed the visualization of the neuron's morphology with an intact tissue preparation. These new methods allow us to see the axon's trajectory over the entire olfactory bulb. To further analyze the number of glomeruli crossed by the axons, I performed CUBIC brain clearing and immunostaining of the axons labeled by adenovirus. After tracing individual axon's track, I found the axons of that labeled from P0 go through multiple glomeruli at P3 (Figure 3.3.2-4). The axons visualized at P21 (labeled at P5) showed a straight path towards the final target glomeruli without entering any extra glomeruli (Figure 3.3.2-4). Given that neurons generated during the critical period are nearly eliminated after 14 days, these axons seen at P21 are from the late neurons. Therefore, the evidence suggests the early neurons' axons are more plastic and able to cross the boundary of glomeruli.

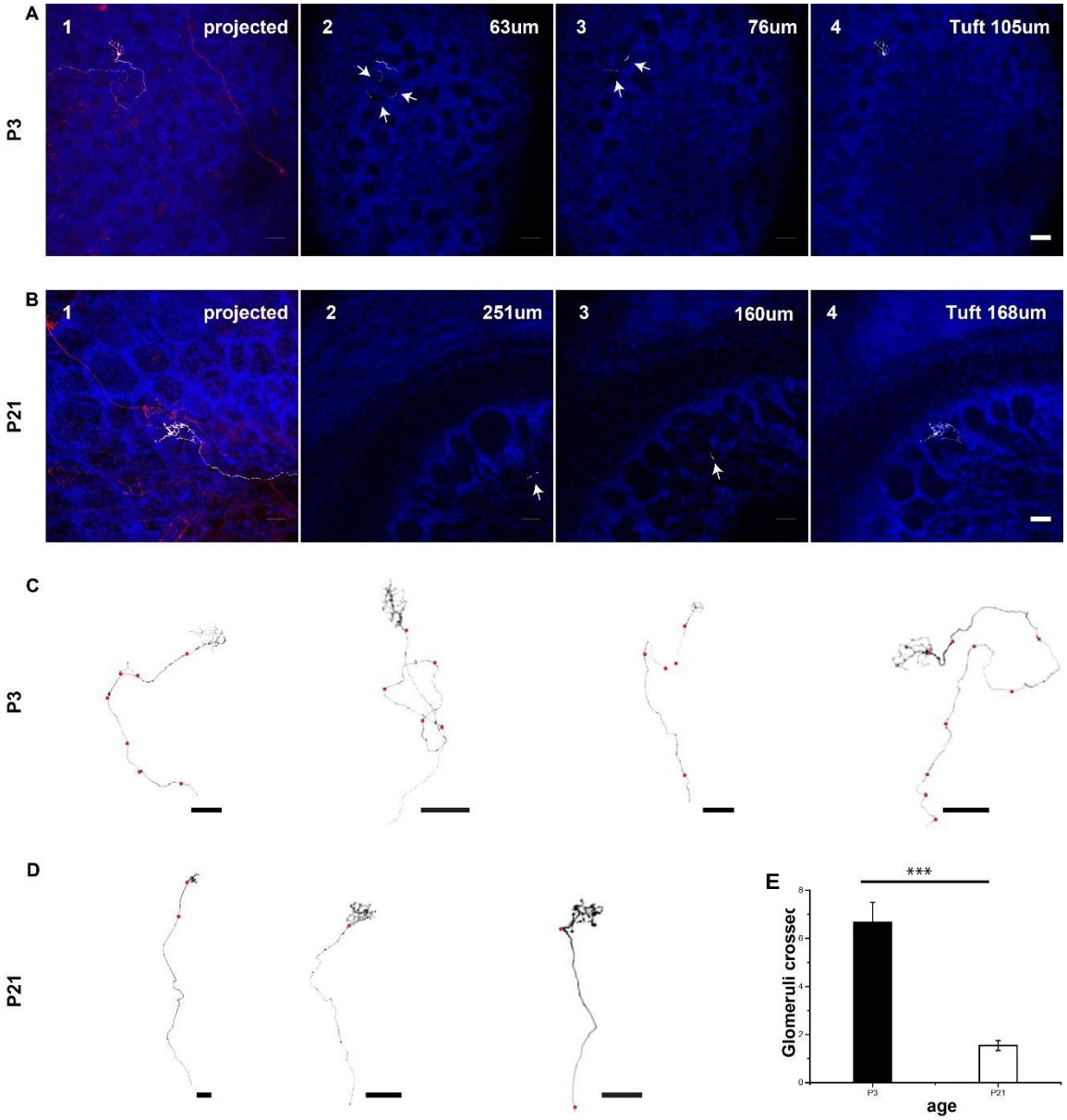
A
P3
1
projected
2
63um
3
76um
4
Tuft 105um
B
P21
1
projected
2
251um
3
160um
4
Tuft 168um
C
P3
D
P21
E
***
Glomeruli crosse
0
2
4
6
8
P3
P21
age

Figure 3.3.2-4 OSN axons visualized in an intact olfactory bulb.

The OSN axons are labeled by adenovirus expressing RFP (red) at P0 and P5, and visualized in an intact olfactory bulb cleared with CUBIC at P3 (A, C) and P21 (B, D).

(A) Representative images showing a traced axon at P3 (white). The Z-projected image is shown in (1). (2)-(4) show individual images at different depth.

(B) Representative images showing a traced axon at P21 (white). The Z-projected image is shown in (1). (2)-(4) show individual images at different depth.

(C) 4 example axon traces observed at P3.

(D) 3 example axon traces observed at P21.

(E) Quantification of the traced axons at P3 (black bar) and P21 (white bar). Y-axis shows the number of glomeruli crossed by the axon before reaching the final glomerulus.

Scale bar: 50 μm. ***: P-value in student t-test smaller than 0.001.

3.3.3 Genetic ablation of the early neurons

Next, I tested whether the exuberant growth is specific to the neurons generated during the critical period. I performed genetic ablation to eliminate these neurons using OMP-IRES-tTA; tetO-DTA animal (DTA animal). DTA is the recombinant diphtheria virus toxin A. In these animals, the expression of DTA is controlled by tTA and can be shut down by doxycycline (Figure 3.3.3-1). I applied doxycycline at P0 for the DTA animal. At P7, comparing to the control animals where the DTA is not expressed, the axons in the DTA animals showed much less exuberant growth (Figure 3.3.3-1). This confirmed that the exuberant axon growth is largely from the neurons generated between P0 to P3.

These histology analyses provide very strong evidence that the neurons generated during the critical period are highly plastic, and are responsible for the initial projection errors seen during the first postnatal week. I think their high level of plasticity accounts for the single glomerulus targeting ability. I tested this hypothesis by performing DTA ablation on the M71-IRES-GFP animals. When the animal was given DOX at P0, the single glomerulus projection was formed at the adult stage. However, when the animal was given DOX at P3 or later, multiple glomeruli were observed at the adult stage (Figure 3.3.3-2). This indicates that single glomerulus convergence cannot form properly without the early neurons.

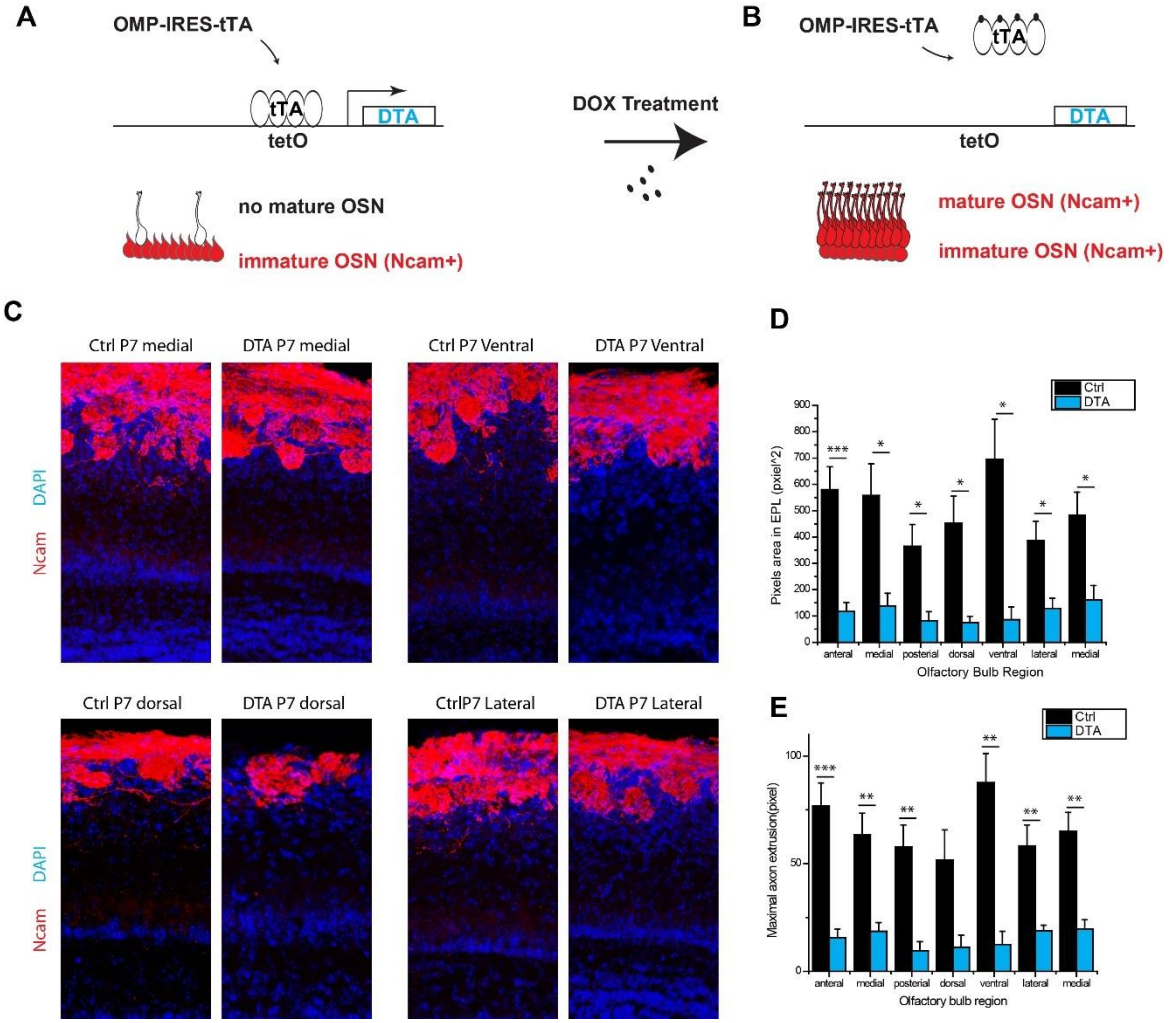
A
OMP-IRES-tTA
tTA
DTA
tetO
no mature OSN
immature OSN (Ncam+)
DOX Treatment
B
OMP-IRES-tTA
tTA
DTA
tetO
mature OSN (Ncam+)
immature OSN (Ncam+)
C
Ctrl P7 medial
DTA P7 medial
Ctrl P7 Ventral
DTA P7 Ventral
DAPI
Ncam
Ctrl P7 dorsal
DTA P7 dorsal
CtrlP7 Lateral
DTA P7 Lateral
D
Ctrl
DTA
Pixels area in EPL (pixel^2)
anteral
medial
posterial
dorsal
ventral
lateral
medial
Olfactory Bulb Region
E
Maximal axon extrusion(pixel)
Olfactory bulb region

Figure 3.3.3-1 Eliminating the early neurons decreases axon exuberant growth.

(A) Illustration of the tetO-DTA transgene. tTA is expressed from the OMP-IRES-tTA allele driven by the OMP promoter. tTA activates the expression of diphtheria toxin A (DTA, blue) from the tetO-tTA-IRES-tauLacZ allele. As a result, the mOSNs are ablated by DTA. The immature neurons can still be stained and detected by Ncam antibody (red, A).

(B) After the animal is given DOX, the DOX will inhibit tTA, resulting in the shutdown of DTA expression, which allows the mOSNs to be generated. Both mOSN and iOSN axons can be stained by the Ncam antibody (red, B).

(C) Representative images of the olfactory bulb from the DTA and control animals given DOX at P0 and visualized at P7. The OSN axons are stained with Ncam antibody (red). The section is counterstained with DAPI (blue).

(D) Quantification of the axon exuberant growth using Ncam signals in the EPL layer, comparing DTA (blue) and control (black) animal.

(E) Quantification of the axon exuberant growth using the maximal extrusion distance from the glomeruli layer, comparing DTA (blue) and control (black) animal.

Star indicates the p-value in student t-test. *:<0.05, **:<0.01, ***:<0.001.

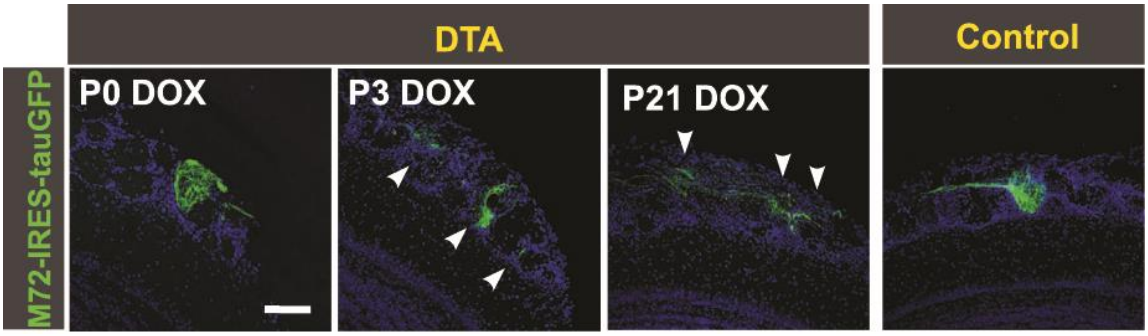

Figure 3.3.3-2 Early neurons are required for the single glomerulus projection.

DTA animals are given DOX at P0, P3, and P21. The glomerular projection of M72 neurons are observed after 7 weeks by staining against GFP (green). When DOX is given at P0, the axons project into a single glomerulus at adult. When DOX is given at P3 and P21, the axons project into multiple glomeruli (white arrow). Scale bar: 100 μm.

3.3.4 Neurogenesis and lifespan of the early and late neurons

I followed the axon projection of the neurons labeled by the OMP-TetTag approach over time. I found a large amount of axons disappearing from the glomeruli. The speed of elimination was higher for the neurons labeled at early time points compared to the later stage. This raised the possibility that the early born neurons had a shorter life span. To test this hypothesis, I performed LacZ staining of the olfactory epithelium from the OMP-TetTag animal with doxycycline treatment at various time points. Surprisingly, the neurons labeled during the critical period were quickly removed from the system (Figure 3.3.4-1). When the neurons were labeled at P3, after 7 days, the LacZ staining decreased dramatically across the epithelium (Figure 3.3.4-1). After 21 days, it was very rare to see any remaining labeling. In contrast, the neurons labeled at P14 and P21 were very stable (Figure 3.3.4-1). After an initial rapid decrease between P21 to P28, the numbers of LacZ positive neurons remained stable for 20 days. After 20 days, the labeling started to gradually decrease again. Adult-generated neurons, which were labeled at P35 and P42 were very stable. A dense labeling could be seen after 85 days. Many of the labeled neurons could be seen even after 138 days. A detailed quantification using the posterior olfactory epithelium section is shown in (Figure 3.3.4-1).

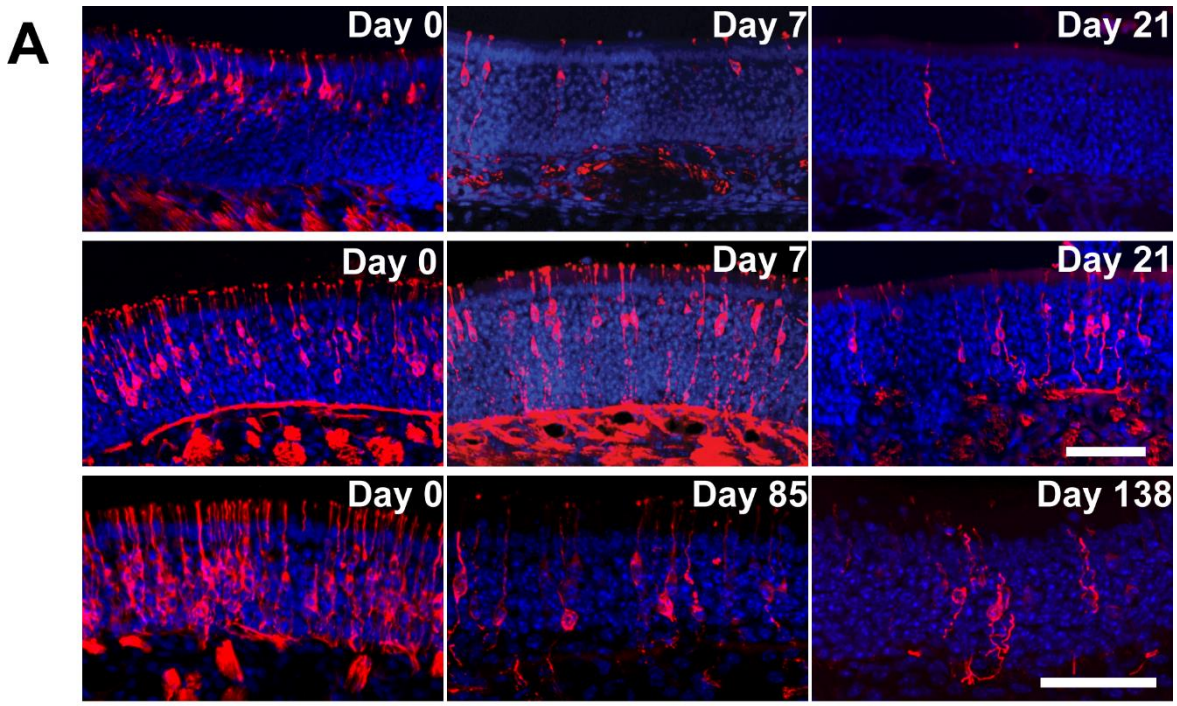
A
Day 0
Day 7
Day 21
Day 0
Day 7
Day 21
Day 0
Day 85
Day 138

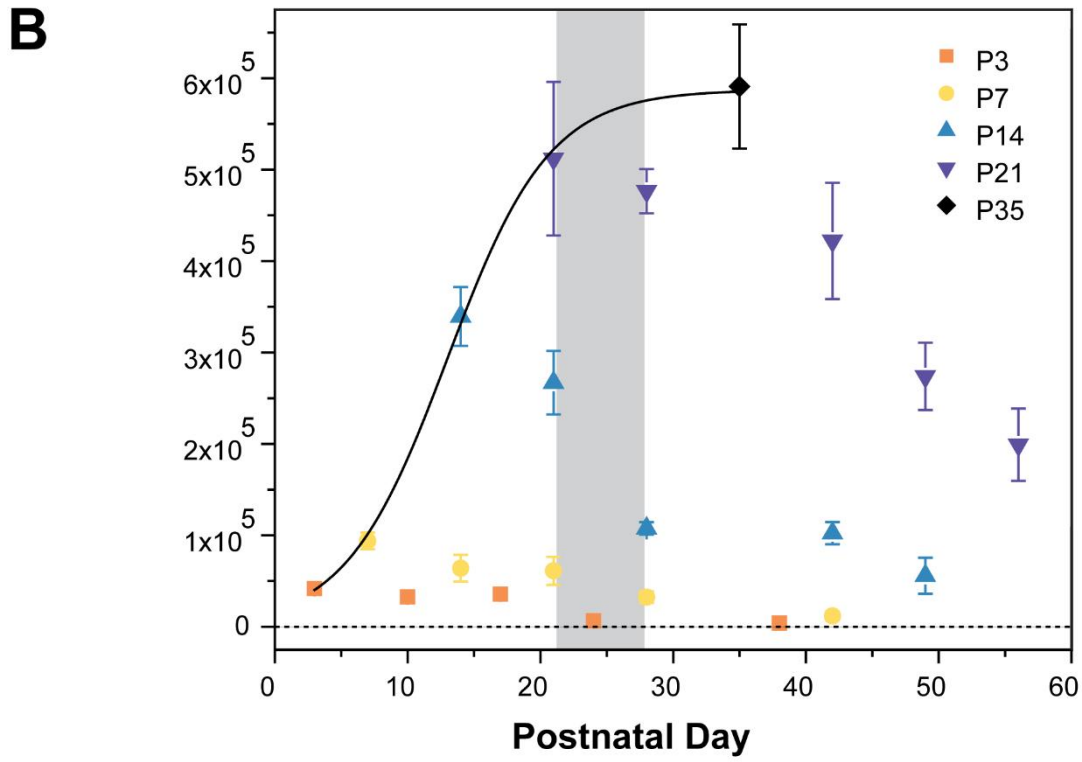
B
6x10^5
5x10^5
4x10^5
3x10^5
2x10^5
1x10^5
0
0
10
20
30
40
50
60
Postnatal Day
P3
P7
P14
P21
P35

Figure 3.3.4-1 Analysis of the lifespan of the OSNs generated at various stages.

(A) Representative images of the olfactory epithelia from the OMP-TetTag animals labeled at P3, P21 and P35 (adult), and observed after 0, 7, 21, 85, 138 days. Sections are stained against LacZ (red) and counterstained with DAPI (blue). Scale bar: 100 μm.

(B) Quantification of the number of neurons after DOX is given. OMP-TetTag animals are labeled at P3 (orange square), P7 (yellow dot), P14 (light blue triangle), P21 (purple triangle) and P35 (black diamond) for 0, 3, 7, 14, and 21 days. The shaded area indicates the weaning week. The black curve is the growth curve of OSNs without DOX treatment.

3.3.5 Changes of the axon innervation in the glomeruli during weaning.

In addition to exuberant growth, I also observed other changes in the axons labeled during postnatal period. Between P0 to P21, axons labeled in different glomeruli are eliminated with similar rate (Figure 3.3.4-1). Starting from P21, the elimination of axons from different glomeruli are different. The environment odorants change dramatically during the weaning period. I think the uneven decrease in LacZ signal during the weaning period is the result of selective punning of different OR types. To test this hypothesis, I quantified the glomeruli occupancy for 4 time points around the weaning period: P14 on DOX to P21 (before weaning), P21 (before weaning), P14 on DOX to P28 (after weaning), and P21 on DOX to P28 (after weaning). The innervation of individual glomeruli was ranked and normalized into the percentage of the pixels occupied by LacZ signals. The quantification showed a decrease in the glomeruli with less innervation comparing the labeling before and after weaning (Figure 3.3.5-1). Since one glomerulus has only one type of receptor, this result confirmed there is a selective pruning of OR types. The selectivity may be driven by neural activity since it is associated with the change of the odorants in the environment. Further investigation is required to test this hypothesis.

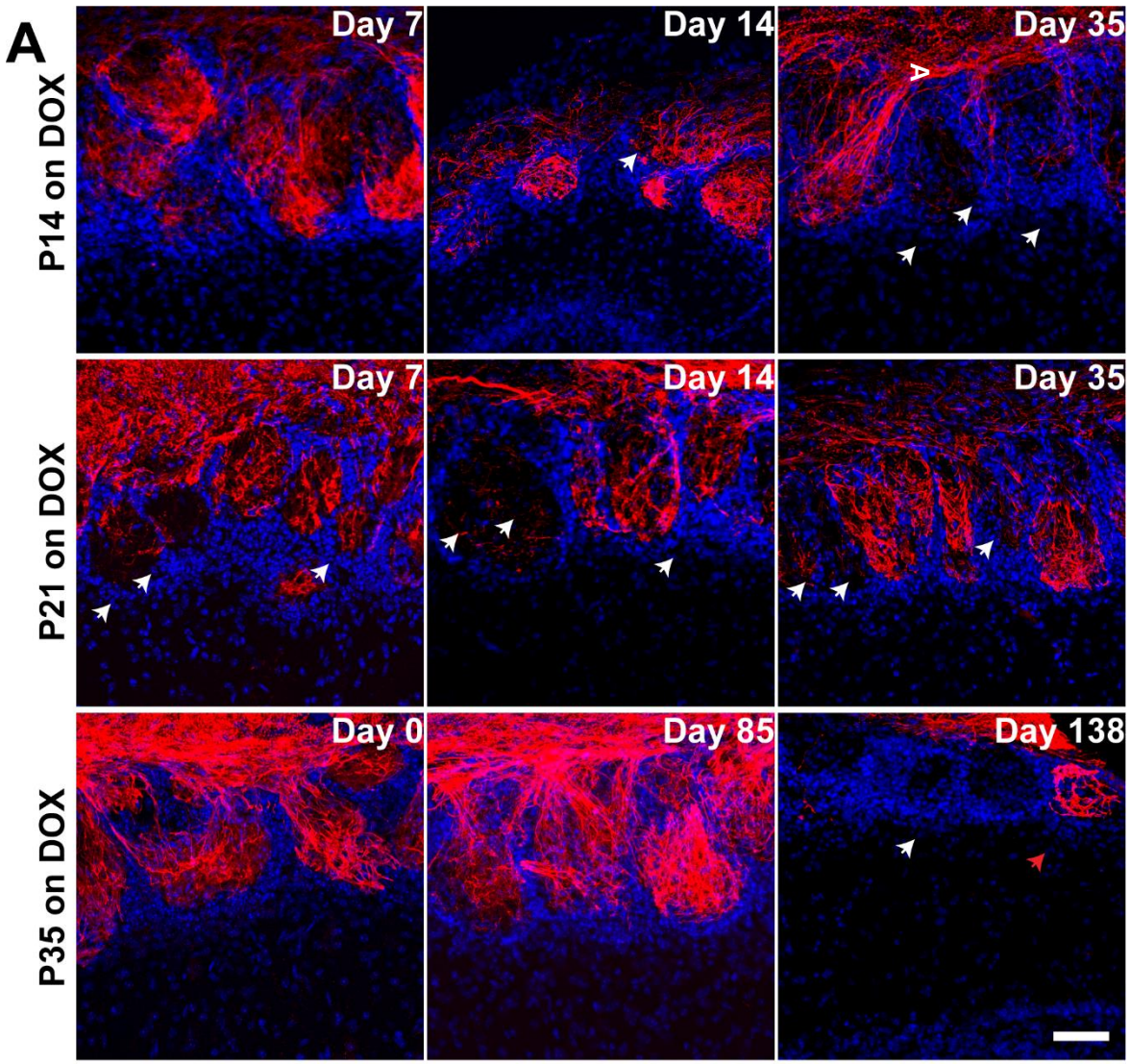
A
P14 on DOX
P21 on DOX
P35 on DOX
Day 7
Day 14
Day 35
Day 7
Day 14
Day 35
Day 0
Day 85
Day 138

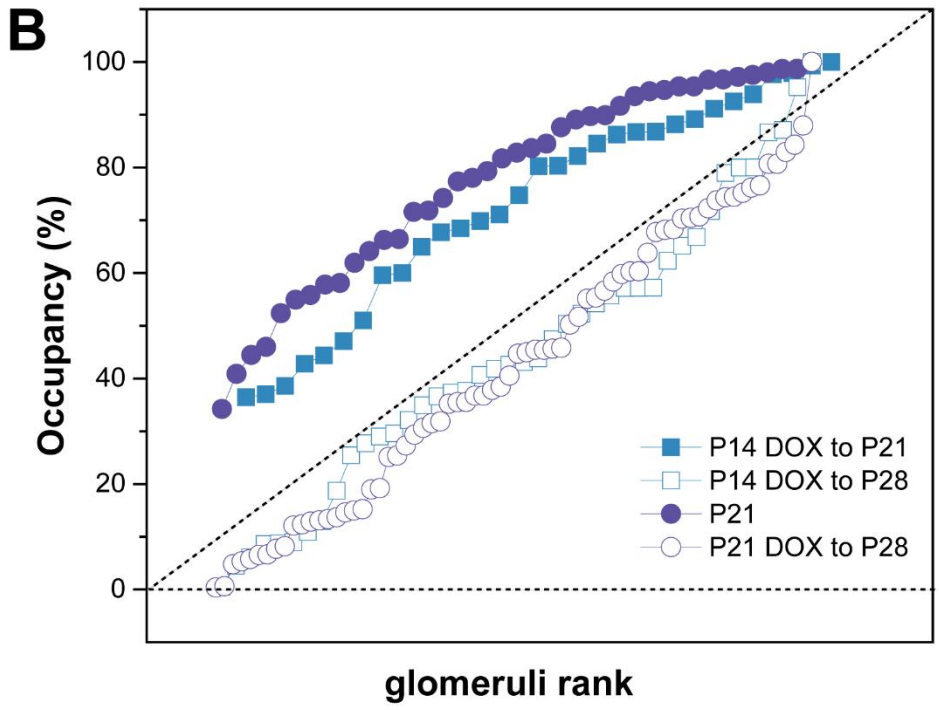
B
Occupancy (%)
100
80
60
40
20
0
glomeruli rank
P14 DOX to P21
P14 DOX to P28
P21
P21 DOX to P28

Figure 3.3.5-1 Axon pruning during the weaning week.

(A) Representative images showing the olfactory bulb of the OMP-TetTag animals sampled around the weaning week (P21 to P28) and adult (P35-P173). Animals given DOX at P14 don't shown obvious axon pruning before weaning (day 7), but start pruning during weaning (day 14). The animals labeled at the start of weaning (P21) also show significant axon pruning after 7 days. Axons labeled at adult stage (P35) do not show obvious pruning, until after a long period of time (day 138). The pruning is selective. Some of the glomeruli have empty space (white arrow), while some are fully innervated (red arrow). Scale bar: 100 μm.

(B) The quantification of the glomeruli occupancy from the P14 and P21 labeled animals observed before (P14 DOX to 21, blue square, P21 no DOX, purple dot) and after weaning (P14 DOX to P28, empty blue square, P21 DOX to P28, empty purple dot). The data is ranked by the percentage of maximal occupancy.

3.3.6 Extending the early neurons' lifespan through Bcl2 transgene promotes the axon exuberance growth.

The rapid elimination of OSNs born during the perinatal period and the observation that these neurons are highly dynamic in their axon projections suggest that eliminating these neurons may serve to remove a scaffold and limit unnecessary exuberant projections. It follows that by preserving these neurons we may extend the period of exuberant axon projections. I generated transgenic mice carrying tetO-Bcl2-IRES-Tdtomato allele, which expresses the long isoform of Bcl2 (Figure 3.3.6-1A) that encodes an anti-apoptotic protein and inhibits apoptosis when expressed transgenically (McDonnell et al., 1989; Sentman et al., 1991; Strasser et al., 1991). In compound heterozygotic OMP-IRES-tTA; Tet-Tag; tetO-Bcl2-IRES-Tdtomato (OMP-Bcl2-Tag for short) mice, the OMP-TetTag strategy allows the expression of Bcl2 only in the neurons generated before DOX is administrated (Figure 3.3.6-1B). In OMP-Bcl2-Tag mice fed with DOX at P2, we saw far more LacZ+ neurons remained at both P9 and P16 (Figure 3.3.6-1 C&D). Thus, the ectopic expression of Bcl2 extended the lifespan of the early born neurons.

Accompanied by the extended survival of early born neurons, we observed extended exuberant axons in the olfactory bulb. By P16, axons labeled at P2 were absent in control animals. Axons labeled at P9 were largely confined within the glomerular boundary. In contrast, P2-labeled axons in the OMP-Bcl2-Tag mice were observed in the bulb and extended into the EPL. P9-labeled axons exhibited higher level of exuberant growth in the Bcl2 than control (Figure 3.3.6-1 E&F). This experimental result demonstrate that the early-born neurons are sufficient to generate exuberant axons.

3.3.7 Extending exuberant axons leads to deficient convergence

The exuberant growth and retraction of early axons is tightly controlled. What is the consequence of extending the period of exuberant axon? We examined the projection patterns of M72 axons in the OMP-Bcl2-Tag mice and found ectopic glomeruli being innervated by the labeled axons. Axons were found projecting outside of the main glomerulus in a wide area of the dorsal OB (Figure 3.3.6-1 G). In sections, individual axons were observed entering different glomeruli in the vicinity of the main target (Figure 3.3.6-1 H). Quantification revealed a significantly increase in the number of glomeruli receiving input from the M72 axons in the Bcl2 mice. This result suggests that maintaining exuberant axons beyond the critical period is detrimental to the refinement process.

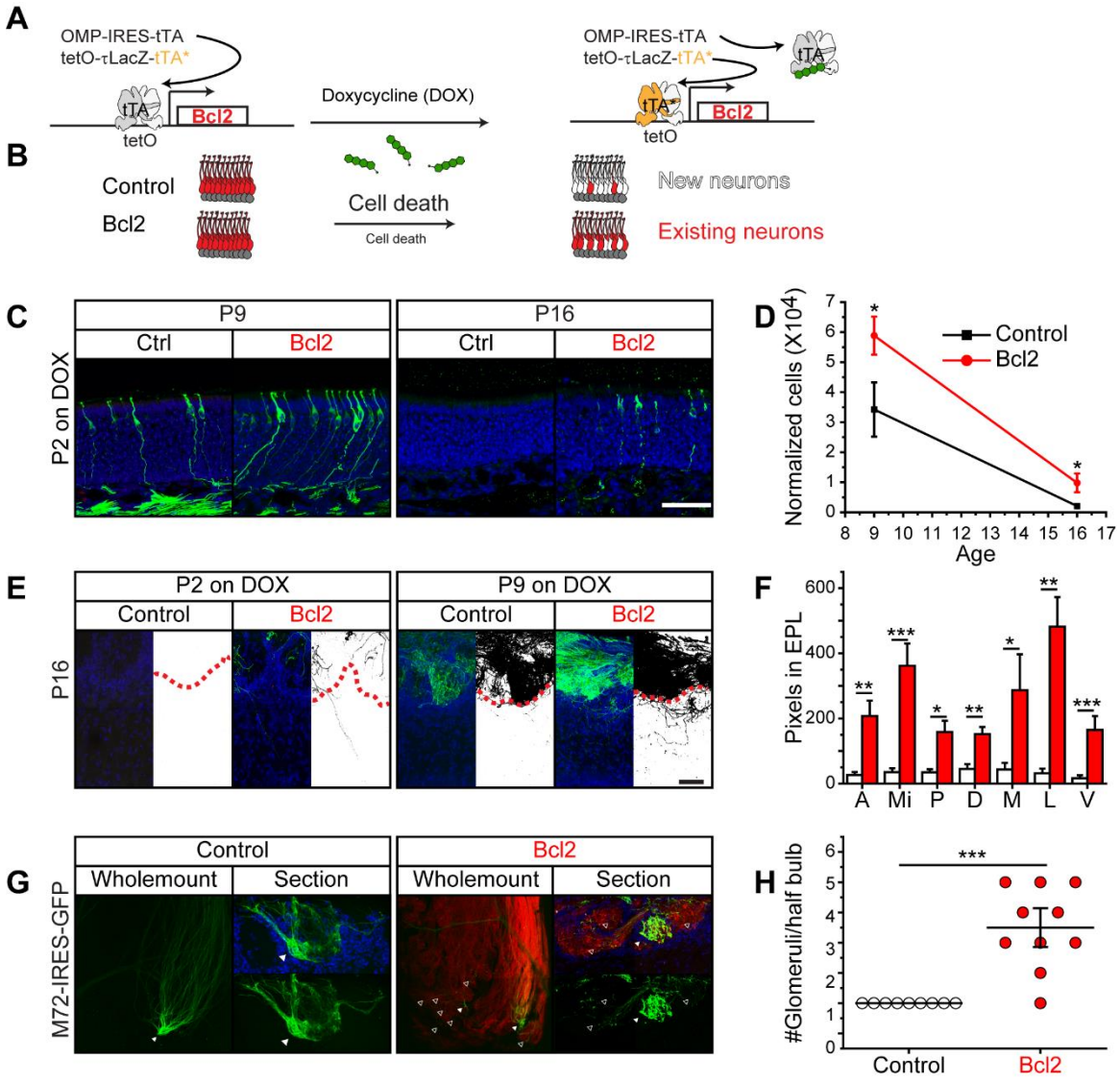
A
OMP-IRES-tTA
tetO-τLacZ-tTA*
tTA
Bcl2
tetO
Doxycycline (DOX)
OMP-IRES-tTA
tetO-τLacZ-tTA*
tTA
tTA*
Bcl2
tetO
B
Control
Bcl2
Cell death
Cell death
New neurons
Existing neurons
C
P9
P16
Ctrl
Bcl2
Ctrl
Bcl2
P2 on DOX
D
Normalized cells (X10^4)
Control
Bcl2
Age
E
P2 on DOX
P9 on DOX
Control
Bcl2
Control
Bcl2
P16
F
Pixels in EPL
A
Mi
P
D
M
L
V
G
Control
Bcl2
Wholemount
Section
Wholemount
Section
M72-IRES-GFP
H
#Glomeruli/half bulb
Control
Bcl2

Figure 3.3.6-1 Phenotype of the Bcl2 transgene.

(A) Illustration of the OMP-Bcl2-Tag transgene. In the OMP-Bcl2-Tag mice, the expression of tTA* leads to the continuous expression of Bcl2 in the labeled cells.

(B) The persistent expression of Bcl2 in the OMP-Bcl2-Tag animal reduces cell death and extends the lifespan of early born neurons (B).

(C) Representative images of OE at P9 and P16 from the control (OMP-TetTag) and OMP-Bcl2-TetTag animals treated with DOX at P2. Sections are stained against LacZ (green).

(D) Quantification of labeled cells from the control (black dot) and OMP-Bcl2-Tag (red square) animals.

(E) Representative images of OB at P16 from the control (OMP-TetTag) and OMP-Bcl2-TetTag animals treated with DOX at P2 (top) and P9 (bottom). Left panels show merged images of LacZ (green) and DAPI (blue) signals. Right panel shows the binary image of the green channel. Boundaries of the glomerulare layers are delineated with red dashed lines.

(F) Quantification of the axon exuberant growth at P16 from the control (white) and OMP-Bcl2-TetTag (red) animals treated with DOX at P9. Letters indicate the OB regions. A: anterior; Mi: middle; P: posterior; D: dorsal; M: medial; L: lateral; V: ventral.

(G) Representative images of M72 glomeruli in the control and OMP-Bcl2-TetTag animals.

(H) Quantification of the number of M72 glomeruli per half OB in the control and OMP-Bcl2-TetTag animals.

3.4 Discussion

3.4.1 The settler neurons

The neurons generated during the critical period have a significant difference in axon targeting plasticity compared to the neurons generated later. First of all, the exuberant growth from these neurons is precisely regulated, not a result of random targeting error from the initial axon sprout. Even though massive number of neurons are added to the epithelia around weaning, the exuberant growth is only seen during the critical period and only from the neurons generated around birth. Second, these neurons are different from those pioneering neurons, which are found during embryogenesis that trigger the development of the olfactory bulb (Treloar et al., 2010). Settler neurons are a group of neurons generated around birth. Considering the suppression induced by DOX takes 48 hours, the neurons born between P0 to P2 are the ones responsible for the exuberant growth. Third, these neurons are required for the correct axon targeting of the late generated neurons. Fourth, the lifespan of these neurons is much less than that of neurons generated at late stage. We refer them as the settler neurons.

3.4.2 The role of settler neurons in the formation of the olfactory map during critical period

OSNs are generated through the animal's life span. Exuberant axon growth is restricted to the critical period and limited to the settler neurons. Instead of all OSNs projecting to extra numeric targets and refining the target by massive pruning through competition, only this small group of neurons, at this specific period of time, are specifying potential targets. I postulate a "roaming and settle" model for the settler neurons. Before the critical period, the axons project to a proto-glomeruli that spans a coarse area around the targeting position. At the onset of the critical period, the settler neurons promote their axon growth to sample the area around them. As a result, they project into multiple glomeruli. This is the "roaming" phase. The refinement continues during the "settling" phase with the elimination of

ectopic projecting axons. Following the settling phase, the settler neurons are eliminated. Further investigation may require real-time imaging of the settler neurons during the critical period.

3.4.3 The dynamics of OSN axons during postnatal development

Our data indicates the re-organization of the olfactory sensory circuit is dynamic. The connection from the OSNs to the OB is under constant refinement. The dynamics of the connectivity after birth can be characterized into four stages.

During the critical period (P0-P7), the axon pruning is associated with the elimination of the settler neurons. By postnatal day 14, there is hardly any remaining settler neurons in the epithelium. At this stage, the pruning is also associated with the re-wiring of the axons. As many axons are seen crossing multiple glomeruli, it is not seen at the later stages.

The second stage is between the end of the critical period and the start of weaning (P7 to P21). After the first stage, the neurogenesis is greatly increased with a peak at P14. The elimination of neurons during this period is also significant, however, a large portion of the neurons remain in the system. The thickness of the epithelium and the mature neuron layer are greatly increased during this period. Before weaning, the elimination of axons appears in all glomeruli without selectivity.

Upon weaning, a significant number of axons are eliminated, and often left empty space in certain glomeruli, which is different from the previous two stages. This indicates the elimination of axon during this period is selective against certain receptor types. The selectivity against receptor type indicates an activity dependent mechanism. This stage lasts for about 1 week (P21 - P28).

Finally, at the adult stage, the axons are extremely stable. The glomeruli start to show empty spaces from 60 days after DOX treatment. The pruning during adult stage is similar to that of the pruning at the second stage, except the speed is much slower. Interestingly, there is no obvious change in the glomeruli density in the AOB, even after 150 days. The AOB axons may not be regenerated.

3.4.4 Development of synaptic connectivity during critical period

During the critical period when settler neurons generate exuberant axon outgrowth towards a broader area, their postsynaptic partner, the M/T cells, are also undergoing dendritic pruning. The M/T cells initially have multiple primary dendrites at birth. Pruning happens during the critical period. By the end of critical period, only one primary dendrite remains for each cell. The remaining dendrite only connects to a single glomerulus. There is a potential “synaptic matching” process between OSN and mitral cells during the critical period. The outgrowth of settler neuron axons may serve as a function to contact the mitral cell dendrites. One possible mechanism for establishing the synaptic connection is through competition. Within a defined proto-glomerulus area, the axons of different receptor types could transiently present as the settler neurons generate exuberant axon outgrowth. Only the correct axons of the same receptor types converge, making them the major population within that glomerulus. The mitral cell dendrites could also contact multiple types of receptors. It is likely that only synapses made with the converged axons are stable and remain after the critical period. To further test this hypothesis, it requires the labeling of synapses from a defined mitral cell and tracing of the dynamics of the synapse towards the glomeruli being contacted during the critical period.

4 Chapter IV. Transcriptome analysis of the olfactory sensory neurons during the critical period

4.1 Introduction

In the previous experiment, I identified the settler neurons, which are generated during the critical period and play an important role in mediating the olfactory map formation. This population of cells diminish after the critical period. Because of their unique axon guidance property, they may express a specific group of axon guidance molecules, as well as other transcription regulators that are different from the neurons generated after the critical period. I hypothesize that the switch between the settler neurons and the later generated neurons result in the transcriptome change of the olfactory epithelia during the critical period. Profiling the transcriptome of the olfactory epithelia will help understand the genetic machinery utilized by the settler neurons, and therefore provide genetic mechanism for the critical period.

4.2 Material and method

4.2.1 Animals

OMP-IRES-tTA mice and tetO-Kir2.1-IRES-tauLacZ mice (the Jackson laboratory, stock number 017754 and 009136 respectively) were described previously. All animals were maintained in Lab Animal Services Facility of Stowers Institute with a 14:10 light cycle, and provided with food and water *ad libitum*. Experimental protocols were approved by the Institutional Animal Care and Use Committee at Stowers Institute and in compliance with the NIH Guide for Care and Use of Animals.

4.2.2 RNA sample preparation

The olfactory epithelia were dissected from the nasal cavity. RNAs were extracted using Trizol (ThermoFisher). The poly-A selected library was constructed using Illumina True-seq kit. The sequencing was performed on illumina Hi-seq platform.

4.2.3 Sequence processing

The reads were aligned to the mouse genome (mm10) using STAR aligner. We then calculated TPM values and Z-scores for each gene based on counts of alignments to the unioned exon (uxon) space of the gene.

4.2.4 PCA analysis

TPM was used to perform the downstream analysis, including ANOVA, PCA, hierarchical clustering and GO term enrichment. All the analysis using TPM were conducted in R. The PCA was done using all the genes detected in the RNA-seq without filtering.

4.2.5 ANOVA analysis

Before the ANOVA, the genes were filtered. Only the genes with maximal TPM higher than 2 were used. P-value was corrected for multi-testing using “BH” method (Benjamini and Hochberg, 1995). Only the genes with adjusted P-value higher than 0.001 were used for the downstream analysis.

4.2.6 Hierarchical clustering analysis

The genes significantly changed through the ANOVA analysis were used for hierarchical clustering. The Spearman distance matrix between each gene's expression among the 5 data points were calculated. Ward's minimum variance method was used for clustering. The dendrogram was cut into 5 clusters.

4.2.7 GO term analysis

"Goseq" package was used for GO term enrichment analysis (Young et al., 2012). The enriched terms were then reconstructed into networks according to their connectivity in hierarchy.

4.2.8 In situ hybridization

The in situ hybridization was conducted as described in the previous chapters. The fluorescein labeled probe was used for the gene of interest; The DIG labeled probe was used for OMP to label the mOSNs. Fluorescein signal was detected through TSA amplification kit (ThermoFisher); The DIG signal was detected using HNPP/Fast red (Roche).

4.3 Results

4.3.1 Transcriptome profile of the olfactory epithelium during postnatal development

In order to understand the genetic program under the critical period, I performed bioinformatic analysis of the existing data in the lab. The poly-A selected transcriptome data I used were collected from the OE of the Kir2.1 and their littermate control animals at P0, P3, P7, P14 and P21. This data set is refered to OE-seq hereafter.

To resolve the cells expressing the genes detected in the OE transcriptome, I also performed a parallel analysis using sequencing after fluorescence active flow cytometry (FACS-seq) technology. The cells used in FACS-seq were from GFP positive cells from OMP-IRES-GFP and Neurog1-IRES-GFP animals, representing the mOSN and the progenitor cells. Since the sorted cells are limited, cells collected from about 10 animals were pooled and sequenced together for each time points. Totally three time points between P0 to P14 were used. Finally, the spatial localization of differentially expressed genes is confirmed using in situ hybridization.

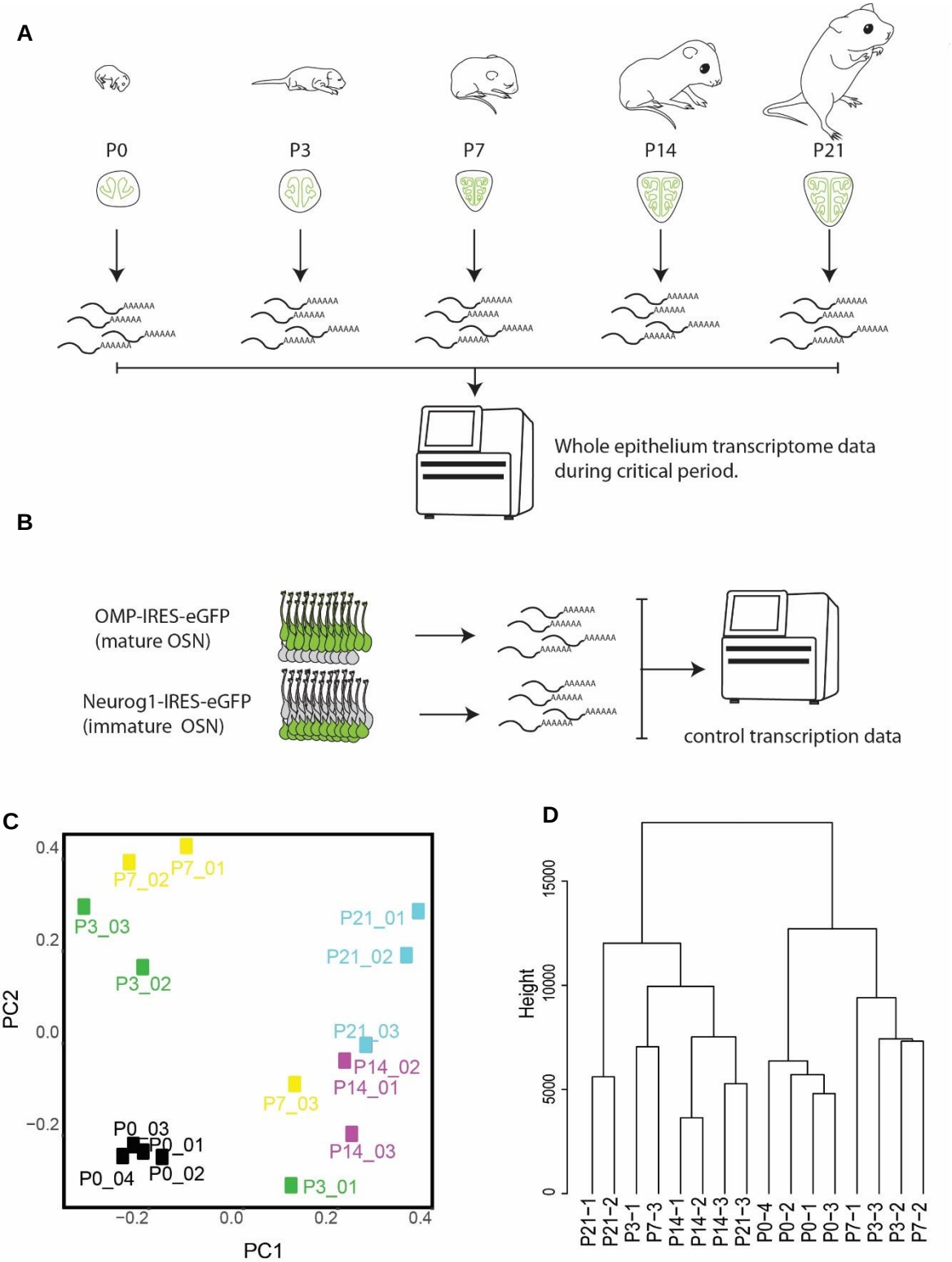
A
P0
P3
P7
P14
P21
Whole epithelium transcriptome data
during critical period.
B
OMP-IRES-eGFP
(mature OSN)
Neurog1-IRES-eGFP
(immature OSN)
control transcription data
C
PC1
PC2
P7_01
P7_02
P3_03
P3_02
P21_01
P21_02
P21_03
P14_02
P14_01
P7_03
P0_03
P0_01
P0_04
P0_02
P14_03
P3_01
D
Height
P21−1
P21−2
P3−1
P7−3
P14−1
P14−2
P14−3
P21−3
P0−4
P0−2
P0−1
P0−3
P7−1
P3−3
P3−2
P7−2

Figure 4.3.1-1 An overview of the transcriptome analysis.

(A) The schematic of OE-seq experiment. The olfactory epithelia (green) are collected from mice at P0, P3, P7, P14, P21. Poly-adenylated RNA is purified from the epithelia and sequenced.

(B) The schematic of FACS-seq experiment. Mice carrying OMP-IRES-GFP (mOSN) or Neurog1-IRES-GFP (progenitor cells) allele are used. GFP positive cells are collected from the two strains through FACS. The poly-adenylated RNAs are purified from the GFP positive cells and sequenced.

(C) The PCA analysis of the OE-seq. The samples are plotted against PC1 and PC2 on a two-dimension space. Early (P0) and Late (P14, P21) samples collapse together, while middle time points (P3, P7) fall in between.

(D) Clustering analysis of the OE-seq.

To analyze the sequencing results, I aligned the sequence using STAR aligner to the Ensembl release 67 (mm10) as reference annotation at the time of analysis. I used transcript per million reads (TPM) as a normalized measurement to compare the gene expression from samples across the five time points. I filtered out the genes with maximal TPM less than 2. This resulted in 20457 genes. These genes were defined as reliably detected by RNA-seq to be expressed in the OE from at least one sample ("expressed genes" for short). I then performed principle component analysis (PCA) on the expressed genes. The two top principle components PC1 and PC2 accounted for 78.05% cumulative variation. Along PC1, samples from P0, P14 and P21 clustered within the same time point. P3 and P7 samples were distributed separately. In the two-dimensional plot using PC1 and PC2, there appeared to be a line along the diagonal, where the sample fall onto in a chronicle order (Figure 4.3.1-1). This indicates age is one of the major factors in the gene expression profile. In addition, one of each samples from P3 and P7 were grouped with the P14 samples, indicating more variance in the samples collected during the critical period. The large variances of the P3 and P7 sample also suggest that they are transition states. The gene expression at these two timepoints is dynamic. This conclusion is also supported by the dendrogram of the hierarchical clustering between samples using UPGMA (Unweighted Pair Group Method with Arithmetic Mean) algorithm (Figure 4.3.1-1).

As an internal control, I looked at several marker genes with known expression profile. During the postnatal development, the proportion of mOSNs increases significantly, as shown in (Figure 4.3.1-2) by OMP in situ hybridization. The genes involved in olfactory receptor signaling, such as Gnal, Cnga2, Adcy3, were also increased with the growth of the mature sensory neurons. G protein subunit G gamma 8 (Gng8) has been shown to have an increased expression around P10 (Sathyanesan et al., 2013). This was also recapitulated by the RNA-seq (Figure 4.3.1-2). The stem cell markers, Neurog1, Ascl1, and Neurod1 all showed an increased expression at P3. The increase was correlated with the thickening of stem cell layer as seen in (Figure 4.3.1-2). All these genes served as positive controls were consistent with the published results.

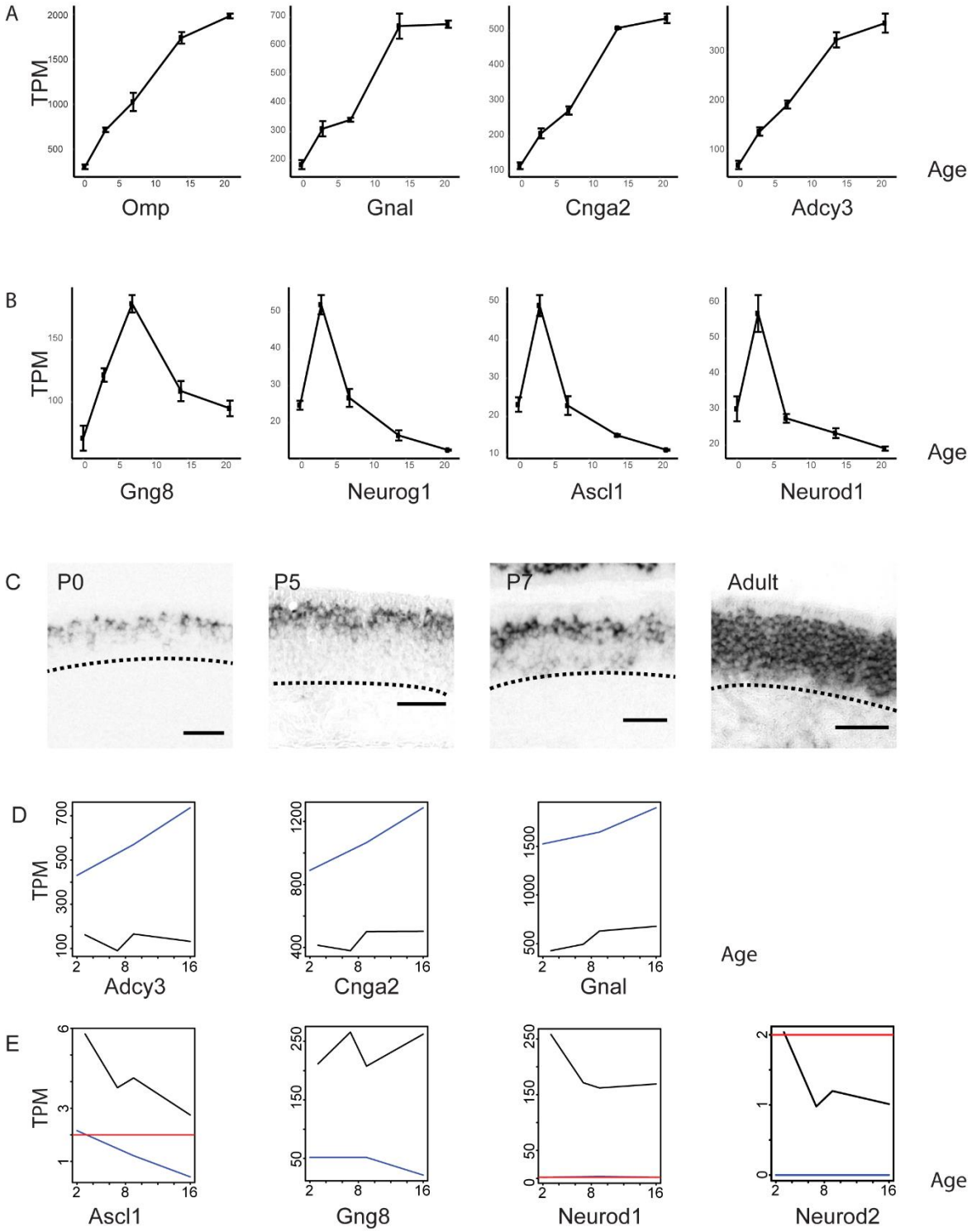
A
TPM
Omp
Gnal
Cnga2
Adcy3
Age
B
TPM
Gng8
Neurog1
Ascl1
Neurod1
Age
C
P0
P5
P7
Adult
D
TPM
Adcy3
Cnga2
Gnal
Age
E
TPM
Ascl1
Gng8
Neurod1
Neurod2
Age

Figure 4.3.1-2 Expression of the cell marker genes in the transcriptome.

(A) The expression of mOSN markers OMP, Gnal, Cnga2, and Adcy3.

(B) The expression of iOSN marker Gng8, and stem cell markers Neurog1, Ascl1, and Neurod1.

(C) Chromogenic *in situ* hybridization of OMP at various times (gray scale). The *in situ* signals indicate a continuous increase in the mOSN population in the OE. Dashed line indicates the bottom of the olfactory epithelium. Scale bar: 100 μm.

(D) mOSN marker genes' expression in the FACS-seq. blue line indicates the expression in OMP positive cells. Black line indicates the expression in Neurog1 positive cells. Red horizontal line indicates TPM=2.

(E) iOSN and progenitor cell marker genes' expression in the FACS-seq. blue line indicates the expression in OMP positive cells. Black line indicates the expression in Neurog1 positive cells. Red horizontal line indicates TPM=2.

I also examined the marker genes' expression in mOSN and progenitor cells from the FACS-seq. Mature neuron markers, such as ACIII, CNGA2, and Golf, were highly expressed in the OMP positive cell population (Figure 4.3.1-2). Markers of immediate progenitors, such as Neurod1, Neurod2, and NeuroG1, were highly expressed by the NeuroG1 positive cells. The immature neuron marker Gs and G gamma 8 and the neuronal fate marker Ascl1 were also expressed higher in the NeuroG1 positive cell population compared to the OMP positive cell population (Figure 4.3.1-2).

4.3.2 Genes differentially expressed during critical period

I then used ANOVA analysis to identify differentially expressed genes across the developmental stages. I used FDR to correct for multi-testing. There were 1992 genes with adjusted P-value lower than 0.001. There genes were defined as significantly differentially expressed genes in this study. To group the genes with similar expression patterns, I performed hierarchical clustering by first calculating the spearman distance of the mean, then linked the distance using Ward.D method. To define the clusters, I cut the dendrogram tree into 5 branches (Figure 4.3.2-1). Cluster 1, 2 and 3 genes showed an increase of expression over time. The difference among them was the onset of increase. Cluster 1 genes maintained a continuous increase. Cluster 2 and 3 genes did not increase until P7. Cluster 3 genes reached the plateau at P14 and remained constant between P14 and P21. Cluster 4 genes decreased over time. Cluster 5 genes showed a peak level of expression around P3, then kept decreasing. According to their expression profile, I grouped the genes into three types: pre-critical period genes (cluster 4), critical period genes (cluster 5), and post-critical period genes (cluster 1, 2 and 3) (Figure 4.3.2-1).

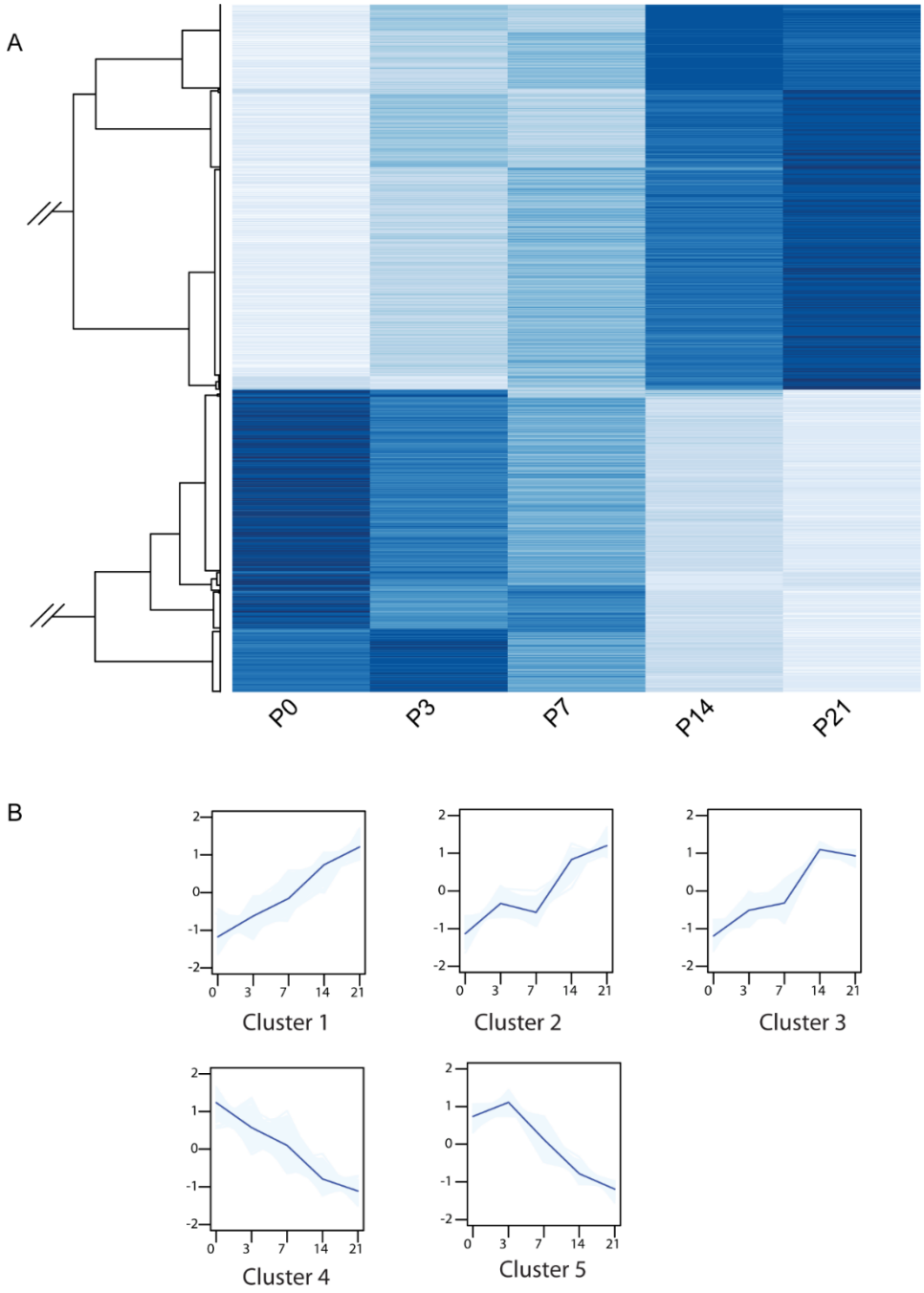

Figure 4.3.2-1 Expression profile of the differentially expressed genes in the OE-seq.

(A) Hierarchical clustering of the differentially expressed genes in the OE-seq. The differentially expressed genes from the transcriptome are plotted against the animals' age using z-scored log2.

(B) The 5 clusters identified by hierarchical clustering. Light blue indicates the z-score of individual gene's expression level. Dark blue indicates the mean.

To further understand the functions of the genes in the five clusters. I performed gene ontology (GO) term analysis. Standard GO analysis method gives biased results on RNA-seq data due to the over-detection of differential expression for long and highly expressed transcripts (Young et al., 2010). To count for the gene length and expression level bias, I adapted GOseq analysis (Young et al., 2012). The enriched GO terms were plotted in the topologic network plot in (Figure 4.3.2-2). The size of the circle indicated the significance (-log2 of adjusted P-value). The color indicated the number of terms with direct connectivity that were also enriched. For the limitation of the space, terms with overlapping phrases were not shown.

For the post-critical period genes, Olfactory receptors and its signaling were over-represented. It was not a surprise because the genes clustered in these 3 clusters were mainly expressed by the olfactory sensory neurons, and increasing with the increase number of cells.

For the pre-critical period genes, the most enriched terms in biological pathways were related to the localization of the protein, regulation of the signaling, metabolic process, and the regulation of development. The highest enriched terms in cellular location were related to cell membrane. The genes associated with these terms were involved in cell signaling. This result indicated that cell signaling molecules were involved for the onset of critical period.

For the critical period genes, many of them were known progenitor cell markers, such as Ascl1, Neurog1, and Neurod1. The genes expressed by the immature neurons were also detected in this cluster. When compared to pre-critical period genes, some of the GO terms were similar. There were 2 new groups of terms detected only in the critical period genes. One group had the terms related to the cell adhesion. The other was related to the response of hormone. The cell adhesion terms were from many axon guidance genes. The enrichment of these terms indicated a unique set of axon guidance molecules used during the critical period. Within the response of hormone group, insulin signaling stood out with very high significance. Insulin-like growth factors (IGF) are known to be involved in the axon guidance of the OSNs. Several IGF binding proteins were seen in critical period genes. In addition, Wnt signaling terms were also seen among the critical period genes.

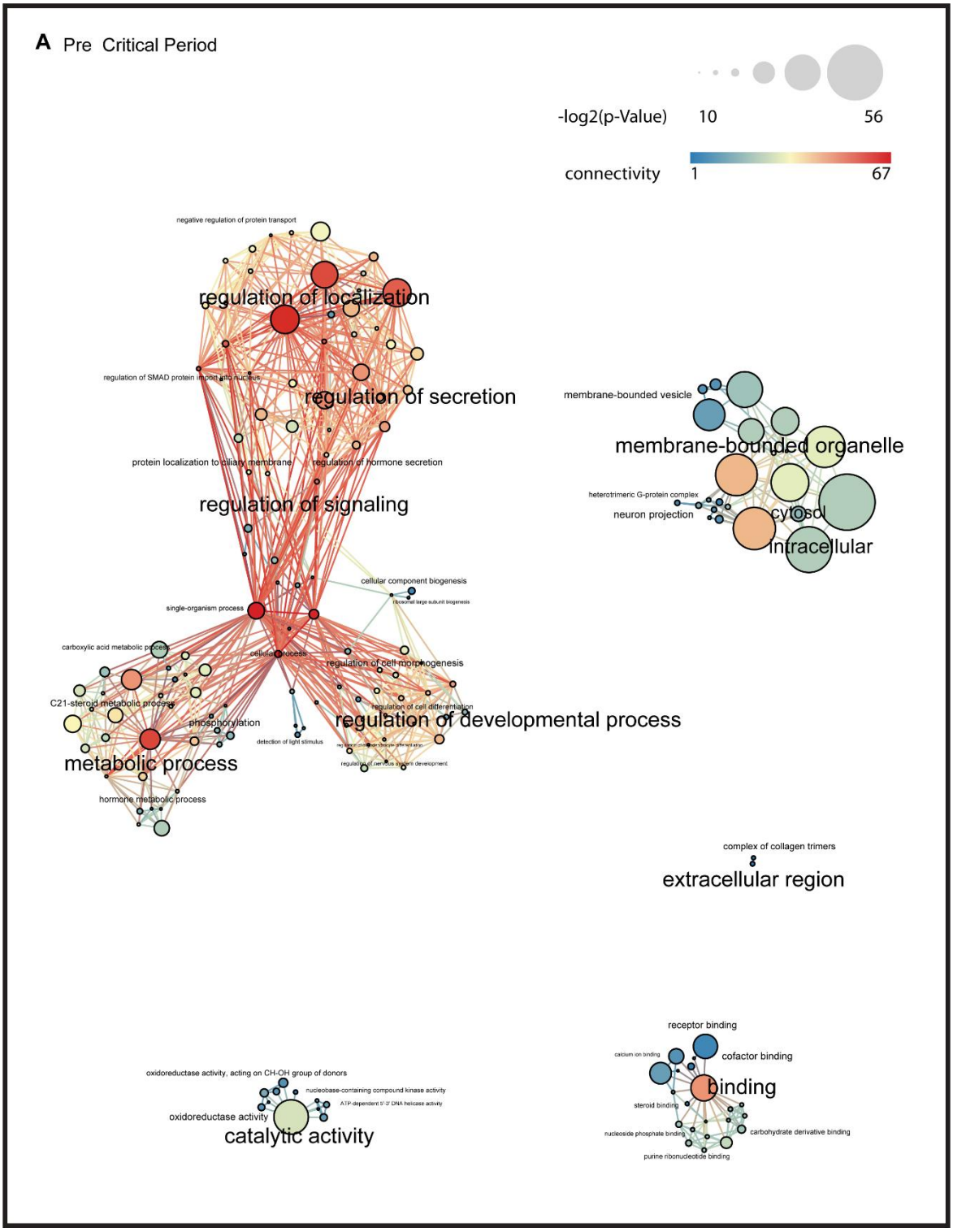
A Pre Critical Period
-log2(p-Value) 10 56
connectivity 1 67
negative regulation of protein transport
regulation of localization
regulation of SMAD protein import into nucleus
regulation of secretion
protein localization to ciliary membrane
regulation of hormone secretion
regulation of signaling
cellular component biogenesis
ribosomal large subunit biogenesis
single-organism process
carboxylic acid metabolic process
cellular process
regulation of cell morphogenesis
C21-steroid metabolic process
regulation of cell differentiation
phosphorylation
detection of light stimulus
regulation of developmental process
metabolic process
hormone metabolic process
membrane-bounded vesicle
membrane-bounded organelle
heterotrimeric G-protein complex
neuron projection
cytosol
intracellular
complex of collagen trimers
extracellular region
receptor binding
calcium ion binding
cofactor binding
binding
steroid binding
nucleoside phosphate binding
carbohydrate derivative binding
purine ribonucleotide binding
oxidoreductase activity, acting on CH-OH group of donors
nucleobase-containing compound kinase activity
ATP-dependent 5'-3' DNA helicase activity
oxidoreductase activity
catalytic activity

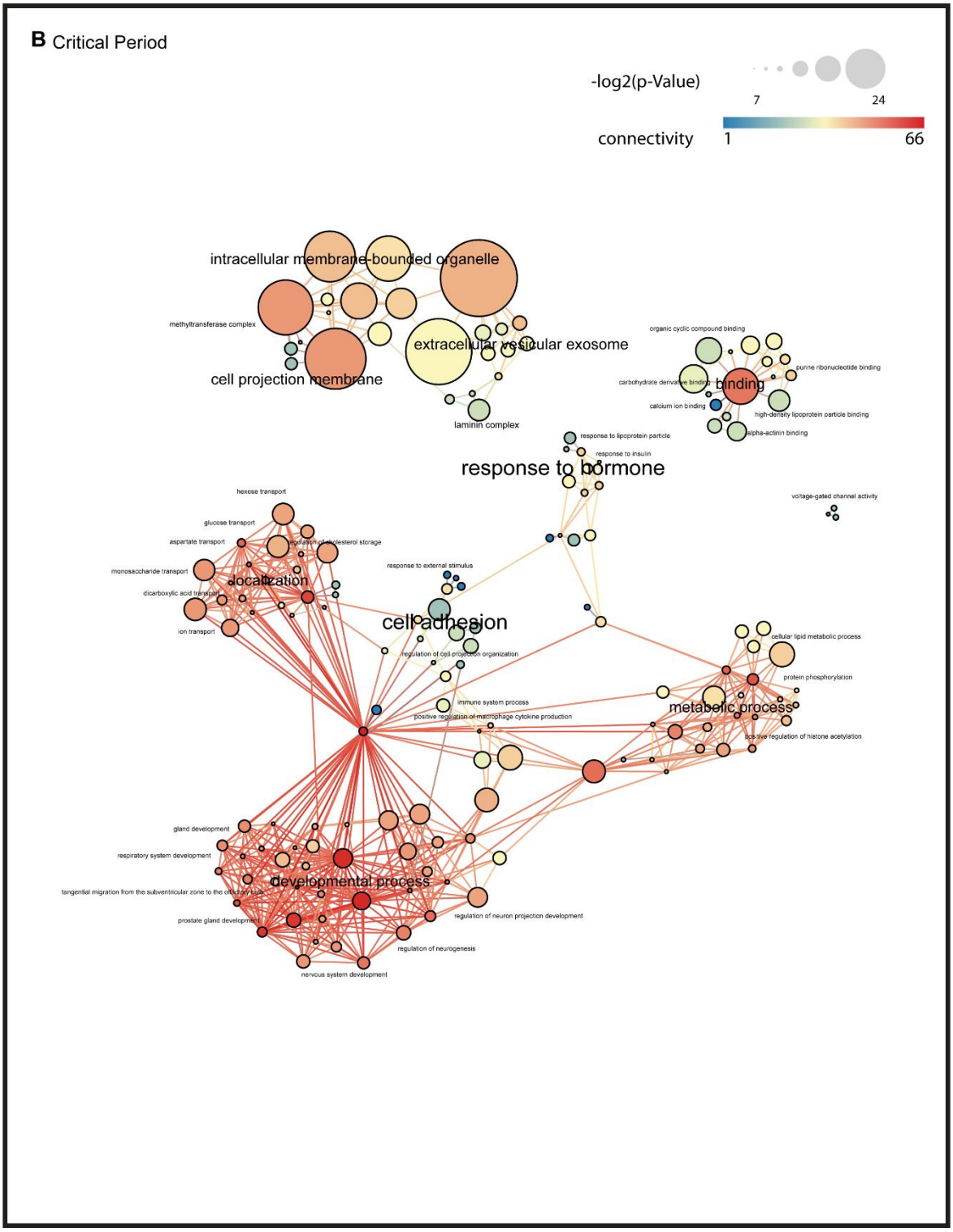
B Critical Period
-log2(p-Value)
7
24
connectivity
1
66
intracellular membrane-bounded organelle
methyltransferase complex
extracellular vesicular exosome
cell projection membrane
laminin complex
organic cyclic compound binding
purine ribonucleotide binding
carbohydrate derivative binding
binding
calcium ion binding
high-density lipoprotein particle binding
alpha-actinin binding
response to lipoprotein particle
response to insulin
response to hormone
voltage-gated channel activity
hexose transport
glucose transport
aspartate transport
regulation of cholesterol storage
monosaccharide transport
localization
dicarboxylic acid transport
ion transport
response to external stimulus
cell adhesion
regulation of cell projection organization
cellular lipid metabolic process
protein phosphorylation
immune system process
positive regulation of macrophage cytokine production
metabolic process
positive regulation of histone acetylation
gland development
respiratory system development
developmental process
tangential migration from the subventricular zone to the olfactory bulb
prostate gland development
regulation of neuron projection development
regulation of neurogenesis
nervous system development

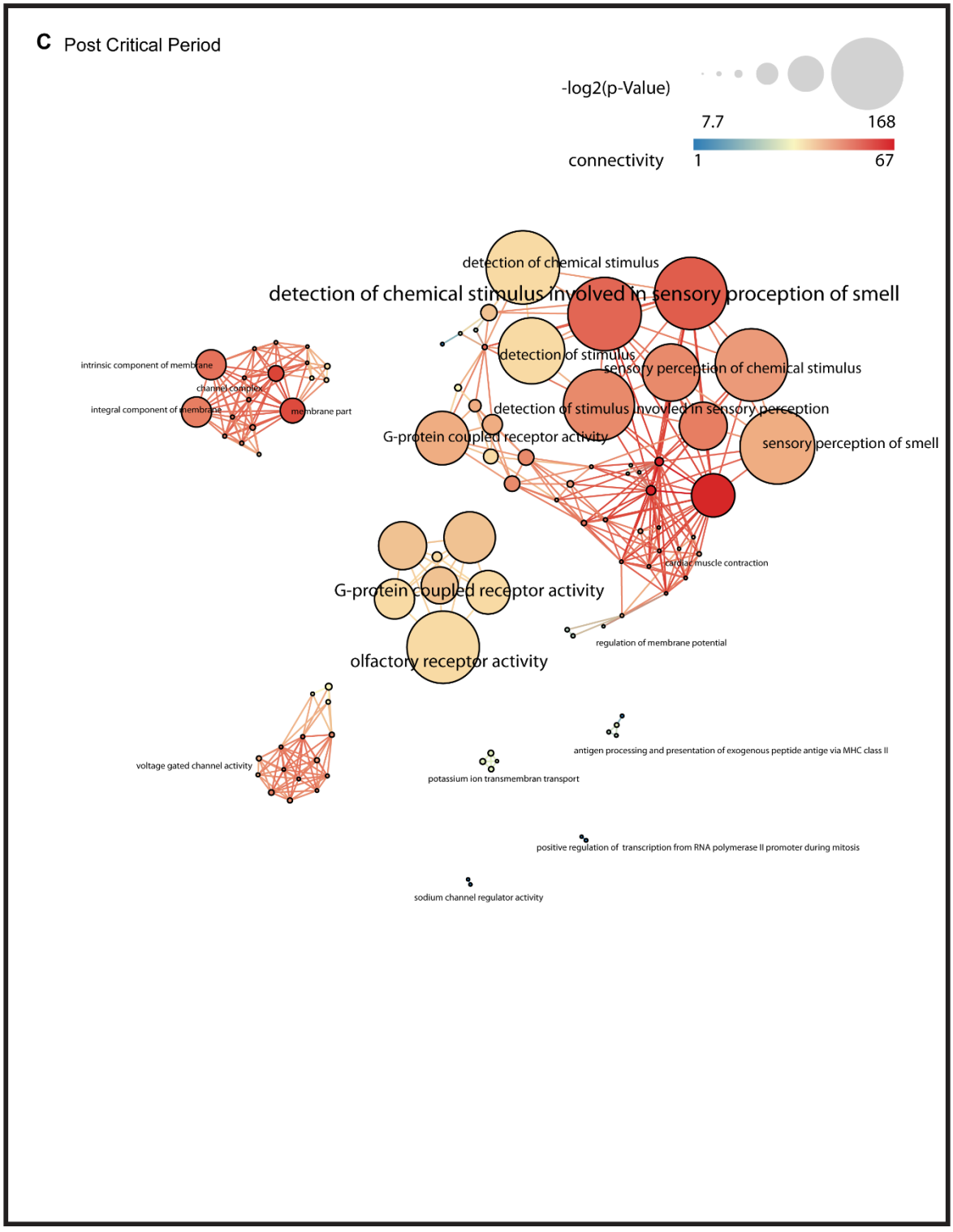
C Post Critical Period
-log2(p-Value)
7.7
168
connectivity
1
67
detection of chemical stimulus
detection of chemical stimulus involved in sensory proception of smell
detection of stimulus
sensory perception of chemical stimulus
detection of stimulus involved in sensory perception
G-protein coupled receptor activity
sensory perception of smell
intrinsic component of membrane
channel complex
integral component of membrane
membrane part
cardiac muscle contraction
G-protein coupled receptor activity
regulation of membrane potential
olfactory receptor activity
antigen processing and presentation of exogenous peptide antige via MHC class II
voltage gated channel activity
potassium ion transmembran transport
positive regulation of transcription from RNA polymerase II promoter during mitosis
sodium channel regulator activity

Figure 4.3.2-2 Gene ontology term analysis.

(A) Enriched GO terms of the pre-critical period genes.

(B) Enriched GO terms of the critical period genes.

(C) Enriched GO terms of the post-critical period genes.

Color code indicates the number of terms connected to a defined term. The size of the term indicates the significance of the enrichment using -log2 of the adjusted P-value.

From the GO term analysis, I found different groups of cell adhesion molecules, as well as signaling pathways, were enriched for different stages. Wnt signaling pathway (6 genes out of 168 genes) and IGF signaling pathway (4 genes out of 232 genes) associated terms were enriched for the critical period. Since different cell signaling pathways were enriched before and during critical period, there is a signaling switch at the critical period. The changes in the cell signaling receptors may be the potential regulators of the critical period.

4.3.3 Identification of regulatory motifs in the genes differentially expressed during the critical period

Surprisingly, based on the FACS-seq data, majority of the genes enriched during the critical period were highly expressed in the INPs instead of OSNs. Their specific expression profiles were strongly correlated with the axon guidance switch at P7. This indicated that the progenitor cells might be involved in the axons guidance switch. To understand how the expression change was regulated for this group of genes, I sought to identify the transcription regulators. I performed motif enrichment analysis using MEME (Bailey and Elkan, 1994). As a positive control, I first did the MEME analysis on the post critical period genes. I was able to see the binding signature of the known transcription factors of the Olf-1/EBF family. This result showed that the MEME analysis was able to discovery meaningful motifs from our data. I then applied the motif search to the critical period genes. I found there was a "CCAAT" 5mer motif highly enriched in the 500 bp upstream region of the transcription starting sites of about 30% of the critical period genes (61 sites out of ~200 genes, figure 4.3.3-1). This motif was the binding motif of several know transcription regulators, including CCAAT enhancer binding proteins (C/EBPs) and nuclear factor Ys. These genes were expressed constantly in the OSNs between P0 to P21. Their expression level in the INPs were higher compared to that in the mOSNs. The expression within mOSNs also did not change significantly over time (Figure 4.3.3-2). These evidences indicated that additional component might be interacting with the CCAAT motif. In the MEME analysis, other motifs, such as multiple "A/T"s, multiple "C/G"s, "CCCCTCCCC", and "CA" repeats, were also

showing significant enrichment. These motifs could be identified from pre- and post-critical period genes, as well as from random sets of genes from the expressed genes (data not shown). Therefore, these motifs were not specific to the critical period genes.

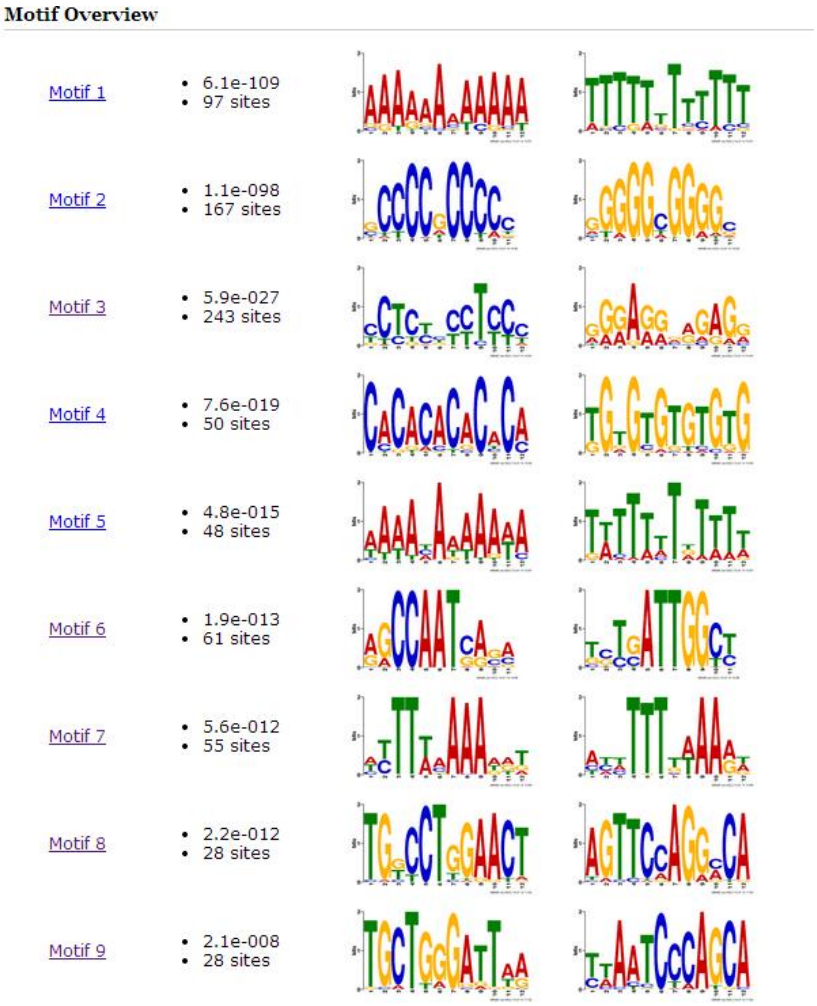

Figure 4.3.3-1 Motif analysis of the critical period genes

The MEME motif analysis result for the critical period genes. The p-Value and number of sites are listed at the second column. The consensus sequence and the reverse complement sequence are shown in the third column. The heights of the characters indicate the frequency.

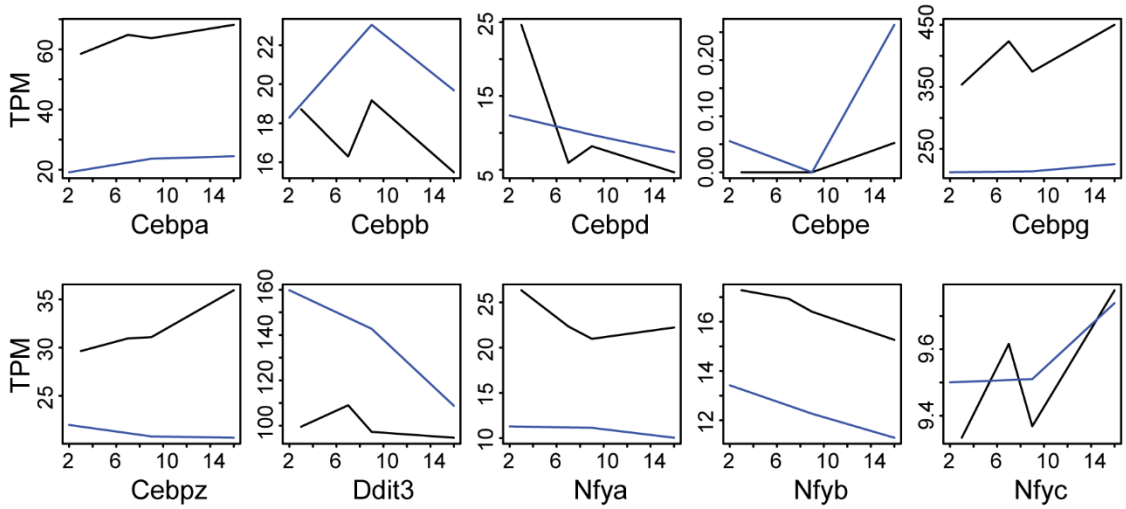

Figure 4.3.3-2 Expression profiles of the genes interacting with "CCAAT" motif.

The expression profiles of the genes interacting with "CCAAT" from the FACS-seq data are shown as TPM. Blue lines indicate the expression in the OMP positive population. Black lines indicate the expression in the Neurog1 positive population.

4.3.4 Identification of GPCRs specifically expressed during critical period

According to the activity dependent model, OR signaling through the cAMP is critical for axon guidance. The ORs are G protein coupled receptors (GPCRs). In the OSNs, they are coupled to Gs and Golf. Other GPCRs are also able to couple to these two G proteins to change the cAMP level. Signaling from other GPCRs expressed in the cell could influence the signaling of ORs through Golf and Gs. This possibility makes non-OR GPCRs genes of interest in the analysis. I examined 344 GPCRs from the GPCR database (http://www.guidetopharmacology.org/). About 125 GPCRs were detected in the OE transcriptome with a minimal TPM of 2 from at least one sample (Figure 4.3.4-1A). Among them, 25 GPCRs were differentially expressed (adjusted P-value lower than 0.001 in ANOVA, Figure4.3.4-1B). Among the 25 GPCRs, 4 GPCRs showed increased expression profile during the critical period: Cckbr, Celsr1, Cxcr4, and Fzd1 (Figure4.3.4-1C, 4.3.4-2A). Cckbr and Cxcr4 were shown to be involved in early neuron migration and axon outgrowth (Lee and Soltesz, 2011; Nishimura et al., 2015). Cxcr4 was expressed in the stem cells rather than the OSN (Toba et al., 2008). Fzd1 was a receptor involved in Wnt signaling pathway. Celsr1 (also known as flamingo 2 homolog) was a co-receptor of Wnt (Gordon and Nusse, 2006). In the FACS-seq data, only Fzd1, Fzd2, Celsr1, and Smo, a less significant GPCR (P-value less than 0.05 from ANOVA), were expressed in the neurons. The expression of Celsr1 and Fzd2 were higher in the progenitor cells compared to neurons (Figure4.3.4-1B). Based on this analysis, Fzd1 was the only GPCRs specifically expressed in the mOSNs during the critical period. Other Frizzled receptors were also detected in our data (Figure 4.3.4-2C). The C/EBPs that binds to the "CCAAT" motif were also associated with Wnt signaling. Even though the proteins binding to the "CCAAT" motif were not enriched during the critical period, the specific expression of Wnt signaling molecules could provide an additional control to the "CCAAT" motif during the critical period. In addition, Wnt signaling was also enriched in the GO term analysis. The evidence strongly associates Wnt signaling with the critical period.

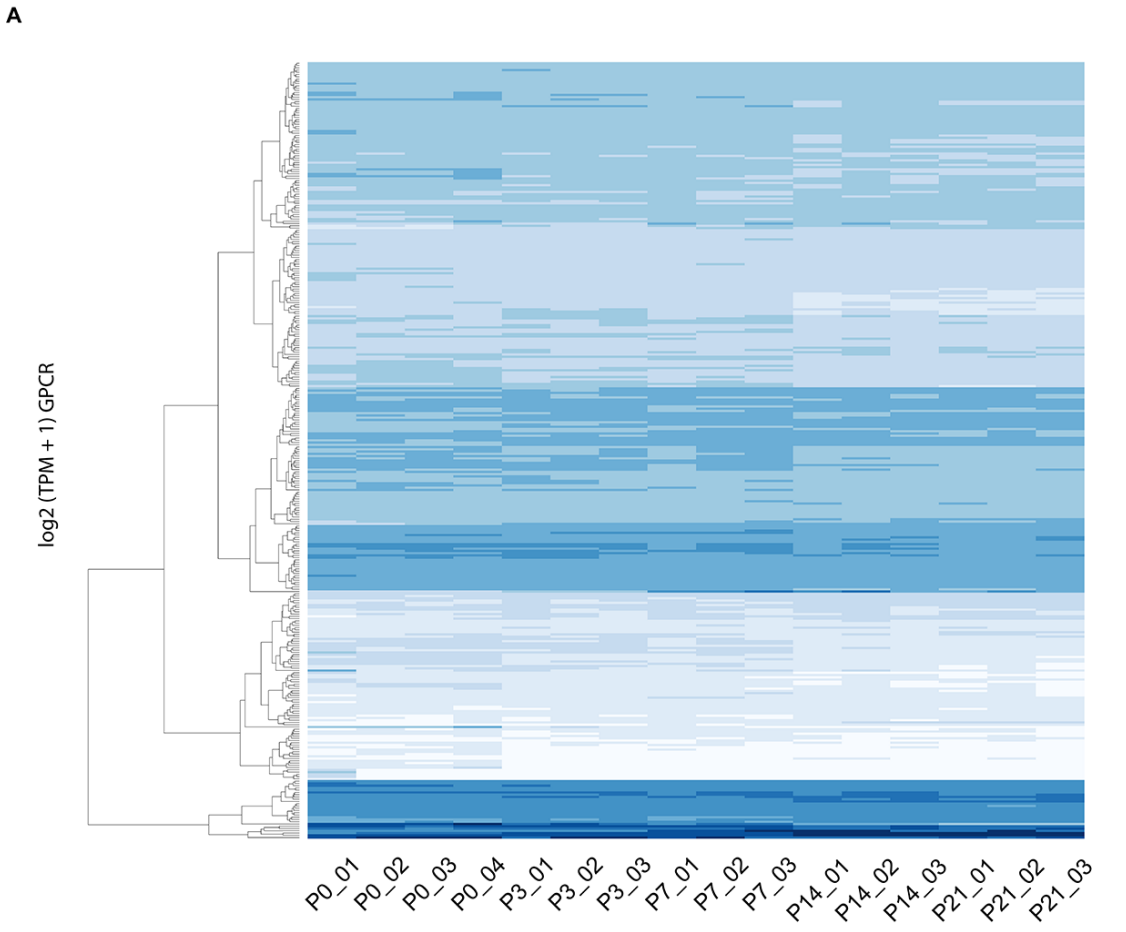
A
log2 (TPM + 1) GPCR
P0_01
P0_02
P0_03
P0_04
P3_01
P3_02
P3_03
P7_01
P7_02
P7_03
P14_01
P14_02
P14_03
P21_01
P21_02
P21_03

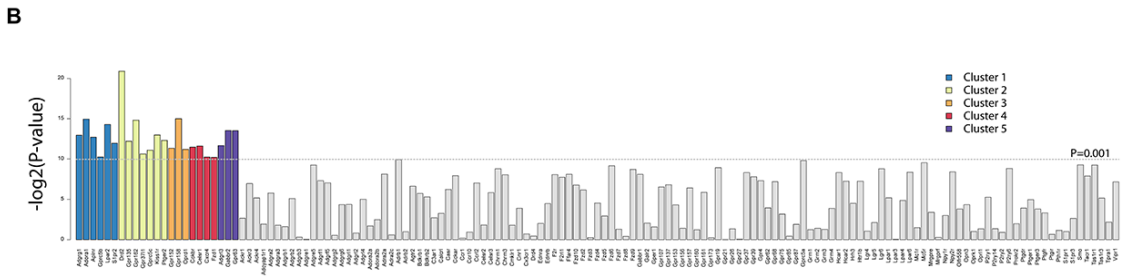
B
-log2(P-value)
Cluster 1
Cluster 2
Cluster 3
Cluster 4
Cluster 5
P=0.001

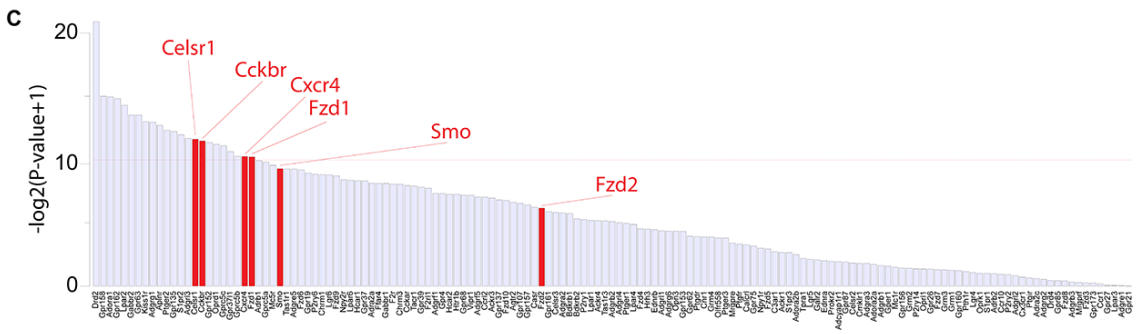
C
-log2(P-value+1)
Celsr1
Cckbr
Cxcr4
Fzd1
Smo
Fzd2

Figure 4.3.4-1 Identification of potential GPCRs expressed during the critical period.

(A) The expression profiles of 344 GPCRs examed. The heatmap shows the expression levels of these GPCRs in individual samples. 125 of them show expression in the OE.

(B) Bar plot showing the significance of the expressed GPCRs (-log2 P-value in the ANOVA analysis). 6 cluster 1 GPCRs (blue), 7 cluster 2 GPCRs, 3 cluster 3 GPCRs, 4 cluster 4 GPCRs, and 3 cluster 5 GPCRs are differentially expressed.

(C) The GPCRs in (B) ranked by p-Values. Red bars indicate the GPCRs enriched at P3.

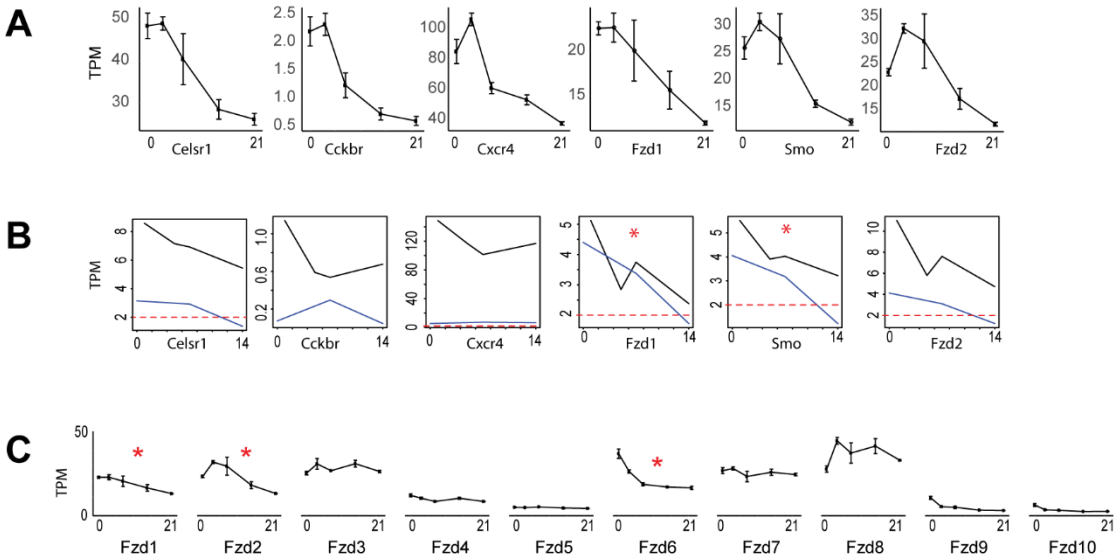

Figure 4.3.4-2 Expression of the GPCRs enriched during critical period.

(A) Expression profile of the GPCRs significantly enriched at P3 from OE-seq.

(B) Expression profile of the GPCRs shown in (A) from the FACS-seq data. Blue lines indicate the expression in OMP positive population. Black lines indicate the expression in Neurog1 positive population. Red dashed lines indicate TPM equals to 2.

(C) Expression of all the Frizzled receptors from OE-seq.

4.3.5 Olfactory receptors are dynamically expressed during the critical period

One olfactory sensory neuron only expresses one olfactory receptor type from a single allele. This allelic exclusive expression pattern is also called “one neuron one receptor” rule. Even though this idea is challenged by the recent discovery that iOSNs could express multiple receptors (Hanchate et al., 2015; Tan et al., 2015), the single receptor type expression in the mature neurons is still shown to be stringent. As discussed in Chapter I, previous studies showed that olfactory receptors are cell identity code during the axon guidance. Changing the receptor identity changes the position of the glomerulus. We wonder whether the expression of ORs changes during the critical period.

To study the dynamics of olfactory receptor expression, I examined the olfactory receptors detected in the RNA-seq data (Figure 4.3.5-1). As the proportion of mOSNs in the OE increases during the postnatal development, one would expect the ORs’ expression to increase. Surprisingly, a large group of ORs did not show an increase. Some of them even decreased over time and could be barely detected at P21. This observation was confirmed by FACS-seq (Figure 4.3.5-1). Similar to the whole-OE result, a lot of ORs did not show an increasing expression pattern. Some of the ORs were rather highly expressed in Neurog1 positive cells, but not in the OMP positive cells.

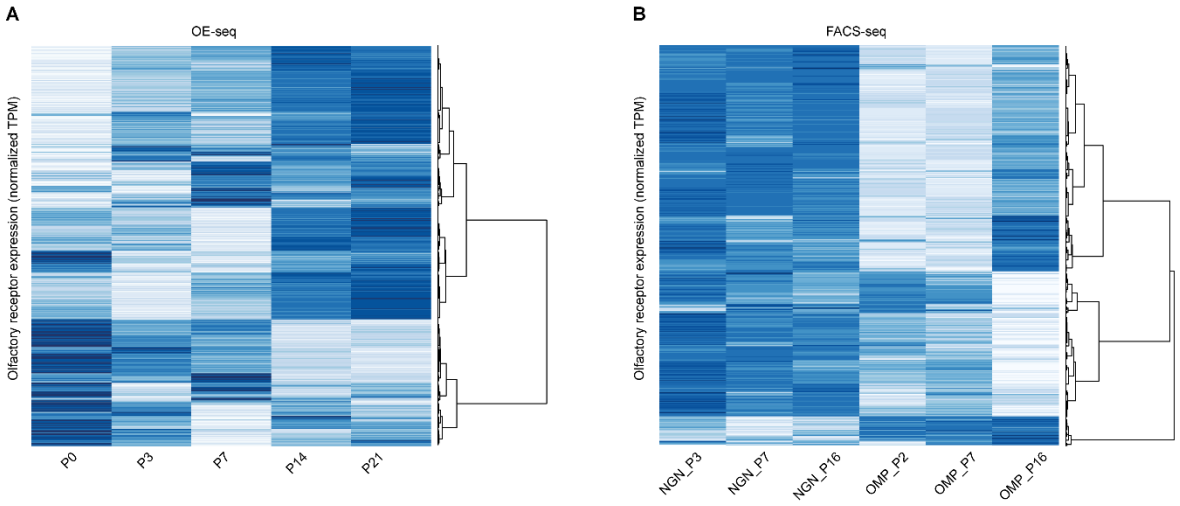

Figure 4.3.5-1 Expression profile of the olfactory receptors during postnatal development.

(A) Expression profile of the olfactory receptors in the OE-seq.

(B) Expression profile of the olfactory receptors in the FACS-seq.

To further confirm this result, I performed in situ hybridization using specific 3-UTR probes against the detected receptors at 3 stages, P0, P7, P14. The expression pattern was recapitulated in the in situ hybridization (Figure 4.3.5-2).

All of the ORs tested in the in situ hybridization showed expression outside of the mOSN layer marked by OMP probe (red). Examples of other abnormal receptors included: Olfr225, Olfr1164, and Olfr1136 were detected in the mOSN layer only at P0 and P7, not at P14. Olfr885, initially highly expressed in the mOSN layer, showed increased expression outside mOSN layer at later stages (Figure 4.3.5-2).

When looking at the distribution of these receptors in the entire OE, the ORs that were only expressed during early stages were all located at the medial dorsal zone in the nasal cavity (Figure 4.3.5-3). Olfr195 and Olfr1413, whose expression pattern increased over time as other normal receptors, did not show this preference (Figure 4.3.5-3). They were detected at the lateral end of the nasal cavity. The medial dorsal zone was the most accessible zone to air flow. The distribution of early receptors in the medial dorsal zone indicated an activity dependent mechanism. Since these receptors were only expressed at early stages, they might be needed for biological functions that only exist during this period, such as locating the milk.

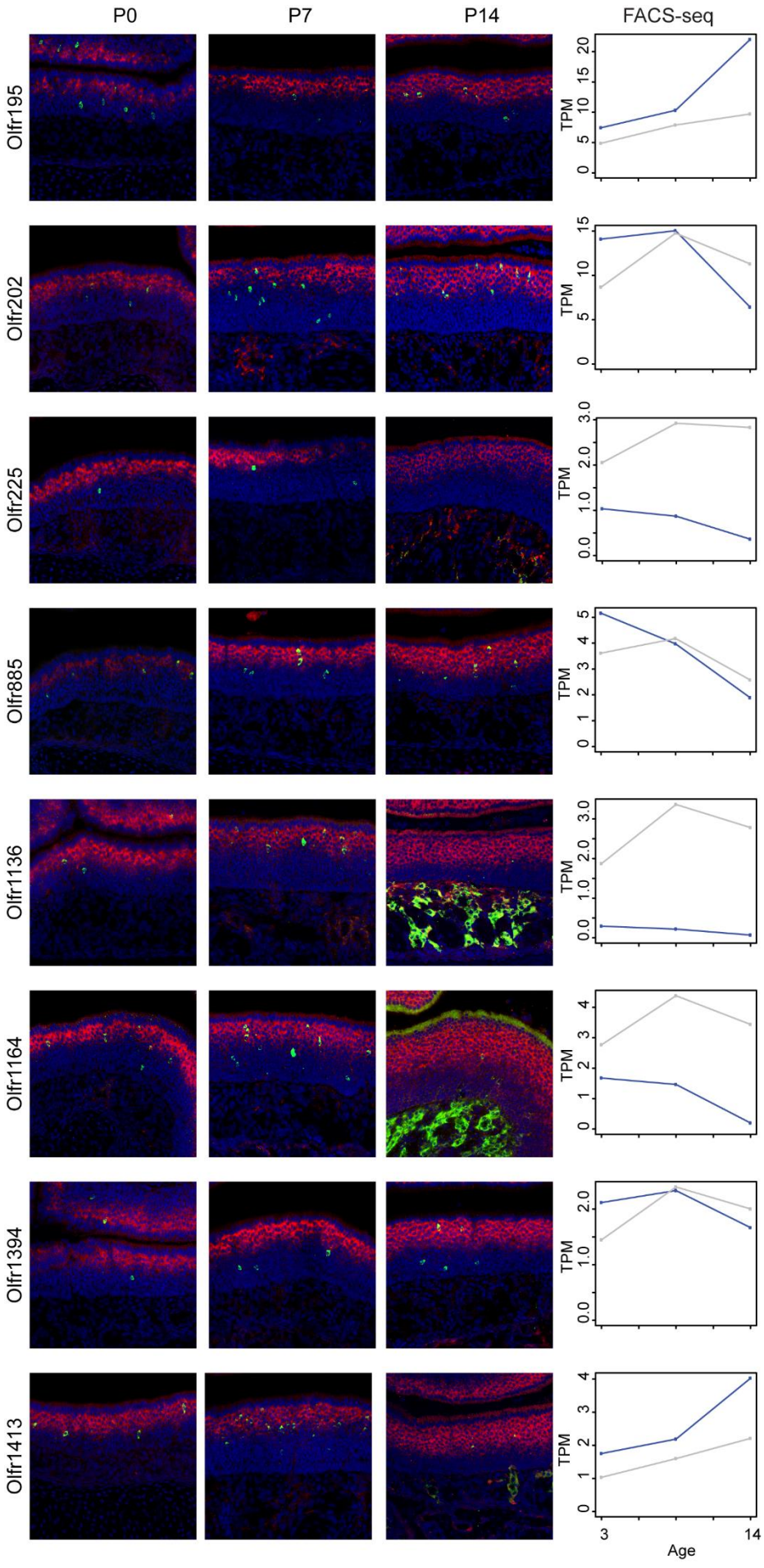
P0
P7
P14
FACS-seq
Olfr195
Olfr202
Olfr225
Olfr885
Olfr1136
Olfr1164
Olfr1394
Olfr1413
TPM
0 5 10 15 20
0 5 10 15
0.0 1.0 2.0 3.0
0 1 2 3 4 5
0.0 1.0 2.0 3.0
0 1 2 3 4
0.0 1.0 2.0
0 1 2 3 4
3
14
Age

Figure 4.3.5-2 The spatial and temporal dynamics of the olfactory receptors.

Left panels show the double *in situ* hybridization for OMP (red) and olfactory receptors (green) at three time points (P0, P7, P14). The corresponding expression levels in the OMP positive (dark blue) and Neurog1 positive cells (gray) from the FACS-seq are shown on the right.

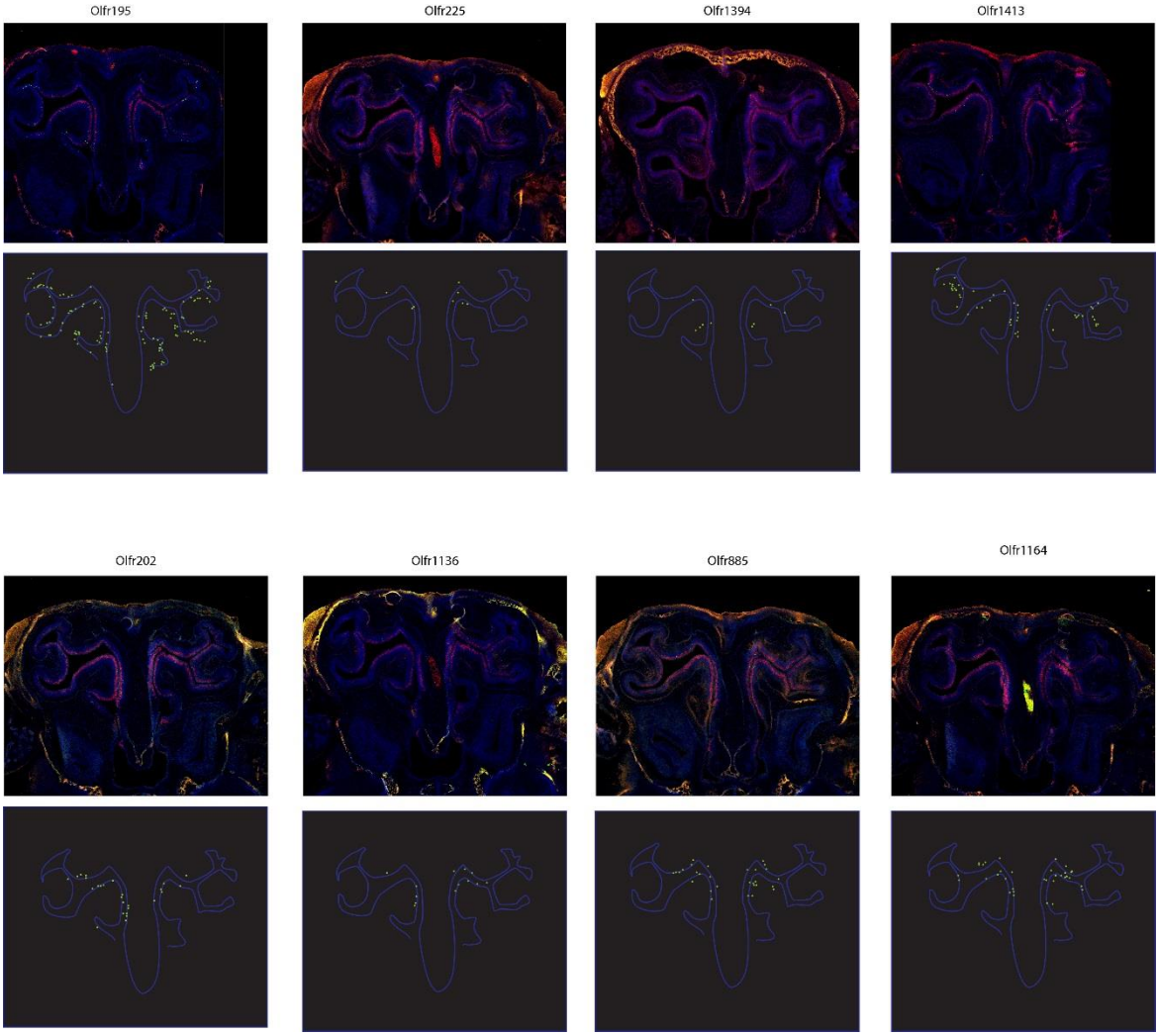

Figure 4.3.5-3 The olfactory receptors expressed early are located in the center of the air duct.

The upper images are double *in situ* hybridization of OMP (red) and olfactory receptors (green) at P0. The lower images are camera lucida drawings from the *in situ*, showing the outline of olfactory epithelium (blue) and the OR in situ signals (green dots).

4.3.6 Transcriptome change under activity deprivation

The Kir2.1, LBR and M71 experiment indicated neural activity doesn't change the timing of the critical period. To test this hypothesis, I conducted RNA-seq analysis for the Kir2.1 animal during critical period.

The heatmaps of differentially expressed genes between Kir2.1 and littermate control mice showed similar pattern (Figure 4.3.6-1). I performed hierarchical clustering using the same parameter as in the wildtype analysis. The 5 clusters showed same expression pattern (Figure 4.3.6-1). These results support the hypothesis that the activity deprivation doesn't change the time of the transcriptome switch during the critical period.

The Kir2.1 animal has a disrupted axon projection pattern as the result of activity deprivation. To identify the activity dependent molecules, that could be involved in axon projection, I compared the gene expression to that of the wildtype animal through ANOVA analysis. I identified 92 activity dependent genes with an adjust p-value less than 0.05. These genes were presumably influenced by the neural activity deprivation. Interestingly, all the olfactory receptors in the list were dramatically down-regulated. Since the number of mOSNs did not change in the Kir2.1 animal, this result confirmed the activity dependent regulation of olfactory receptors. Most of the genes in the list, except ORs, were up-regulated (Figure 4.3.6-2). From the GO term analysis, immune related GO terms were enriched for the up-regulated genes. These genes were mostly involved in interferon-gamma signaling pathway. A recent study indicated that interferon pathways are likely to be involved in the brain circuit development (Filiano et al., 2016).

I performed the in situ hybridization to verify the expression pattern of the up-regulated genes in the Kir2.1 mice. The in situ hybridization results showed these genes were expressed by the OSNs, not by the immune cells. The expression in the OSNs were higher compared to the control animal, which was consistent with the RNA-seq (Figure 4.3.6-3).

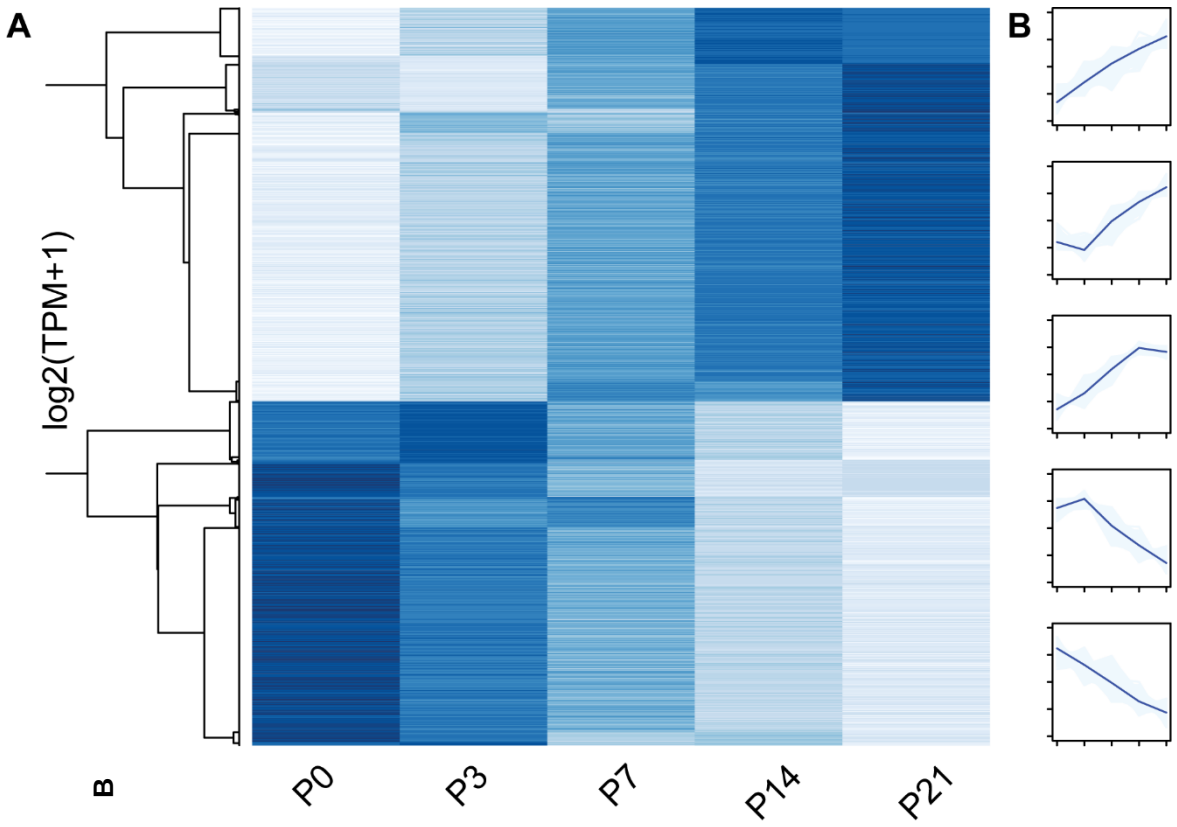

Figure 4.3.6-1 Transcriptome changes under neural activity deprivation.

(A) The expression profile of differentially expressed genes in the Kir2.1 mutant during postnatal development.

(B) The 5 clusters identified from the hierarchical clustering analysis show a similar pattern compared to the wild type animals.

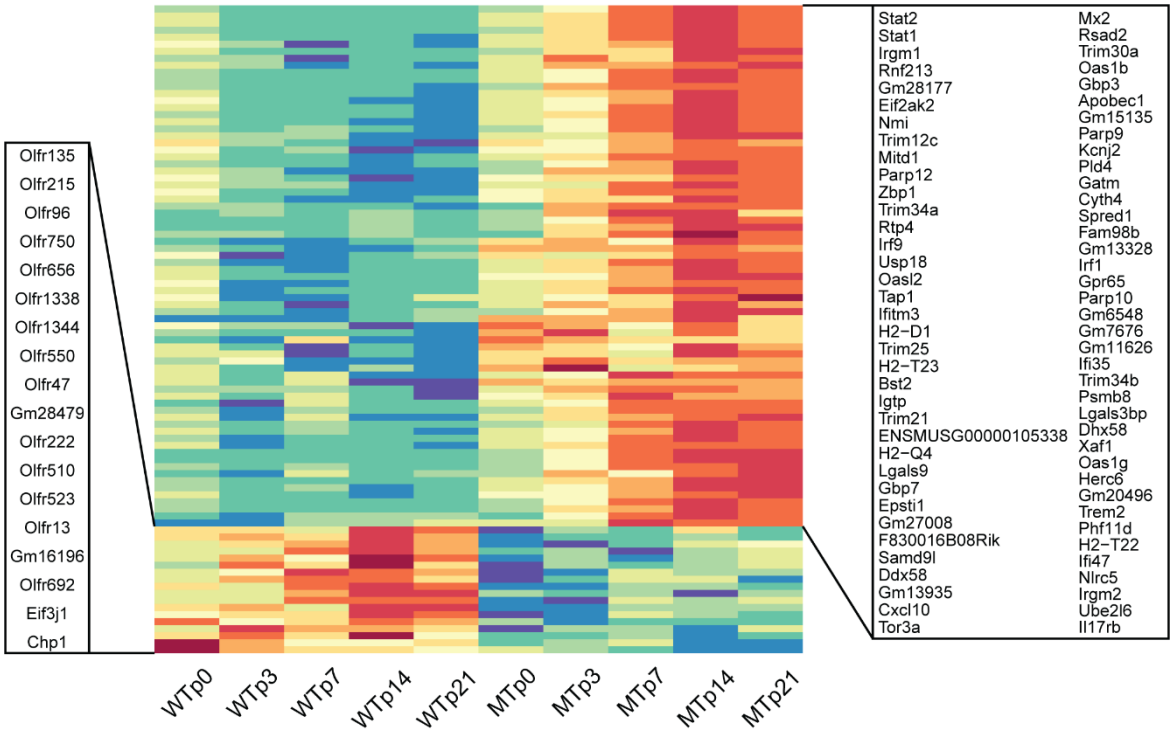

Figure 4.3.6-2 The activity dependent genes revealed by the Kir2.1 transgenic mice.

The heatmap shows the differentially expressed genes in wildtype (WT) and Kir2.1 (MT) animals during the postnatal development. The genes upregulated in the wildtype animals are mainly olfactory receptors (list on the left). The genes upregulated in the Kir2.1 animals are mainly from the interferon signaling pathways, including the two major receptors Stat1 and Stat2 (list on the right). The interferon pathway genes upregulated in the Kir2.1 animals also show an increase in expression during postnatal development.

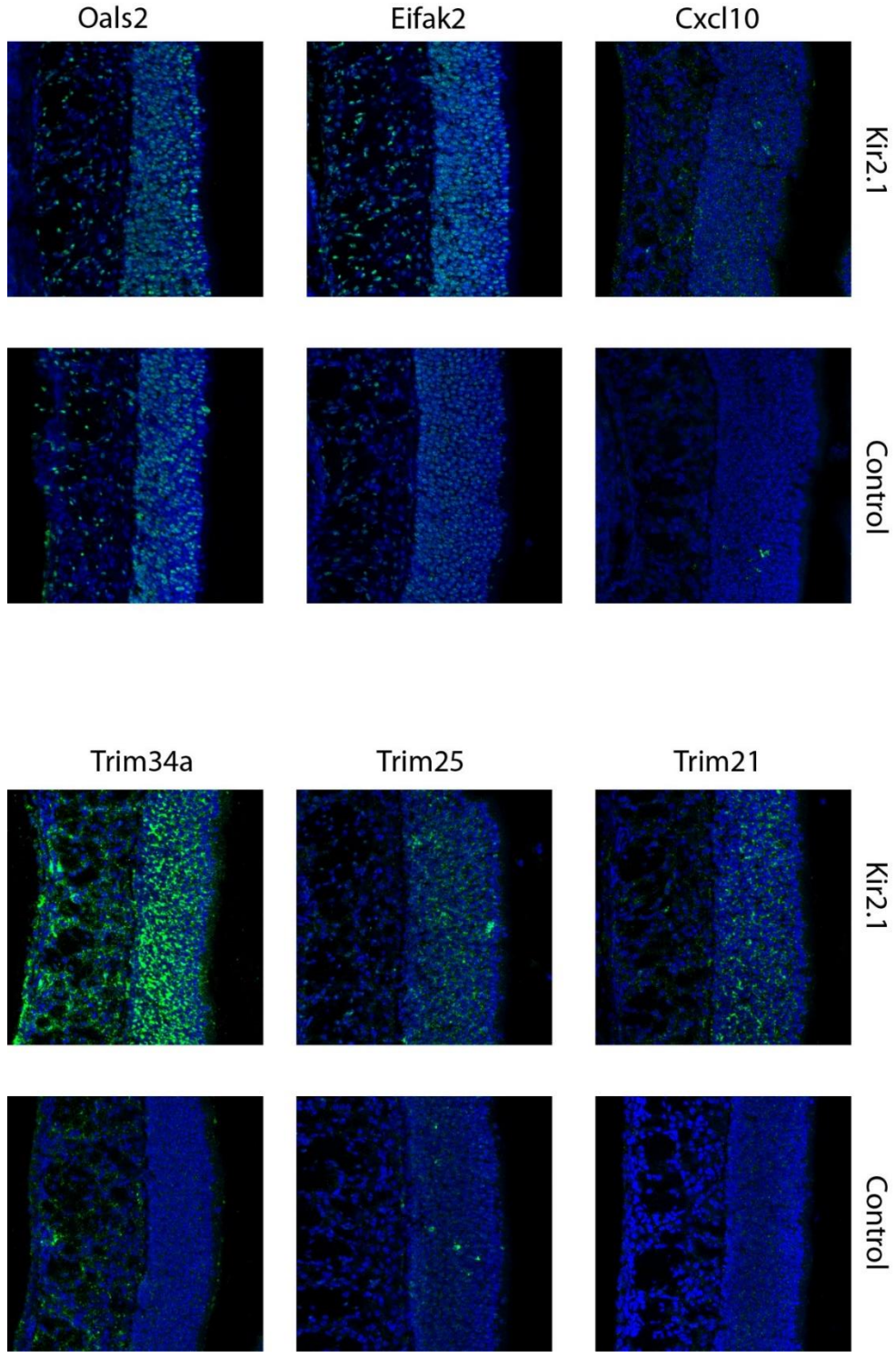

Figure 4.3.6-3 Interferon pathway genes are upregulated in the Kir2.1 animals.

The *in situ* hybridization signals (green) of six up-regulated genes in the Kir2.1 animals. The signals are detected in both neurons and other cells in the OE.

4.3.7 New cell markers label the constant changing cell populations

I next tried to identify the genes specifically expressed by different cell types by comparing the expression levels between the Neurog1 and OMP positive cell population in the FACS-seq data. When a gene's TPM from the three time points are higher in one cell type, I consider this gene as specific to the cell type. From all genes being detected in the FACS-seq data, I found 5211 genes specific to mature neurons, and 8501 genes specific to INPs.

I then plotted the expression profile of these cell type specific genes using the whole OE transcriptome data. For the genes specific to OMP-positive cells, most of them were following the cluster 3 expression pattern. While the genes specific to Neurog1-positive cells followed the expression pattern of cluster 1 and 2. This was expected as the mOSN population was increasing in the OE. However, there were genes that did not follow this trend. There were 29 mOSN specific genes showing a decreased expression pattern, and 38 INP specific genes showing an increased expression pattern. There were three highly enriched GO terms related to "epithelial cell proliferation" in the 29 mOSN specific genes. There were highly enriched GO terms related to "oxidoreductase activity" in the 38 INP specific genes. Several neuron-specific genes were also included in the 38 genes list, such as Homer2 (glutamate receptor), 3 olfactory receptors, calbindin, and Tac4 (neurotransmitter).

I also performed the in situ hybridization experiment for the differentially expressed genes in the FACS-seq. I found additional genes that were very specific to certain cell types (Figure 4.3.7-1). For example, Chd1l was only expressed by the glands. E03002O03rik was only detected on P0 at the *col de sac* region, where the GC-D neurons are normally located (Greer et al., 2016). Coch and Ldhd were specific to the microvilli cells. Kcne1l and Magix were expressed by most of the cells in the epithelium but rarely expressed by the sustentacular cells. Their distribution within a cell was very specific to the nucleolus.

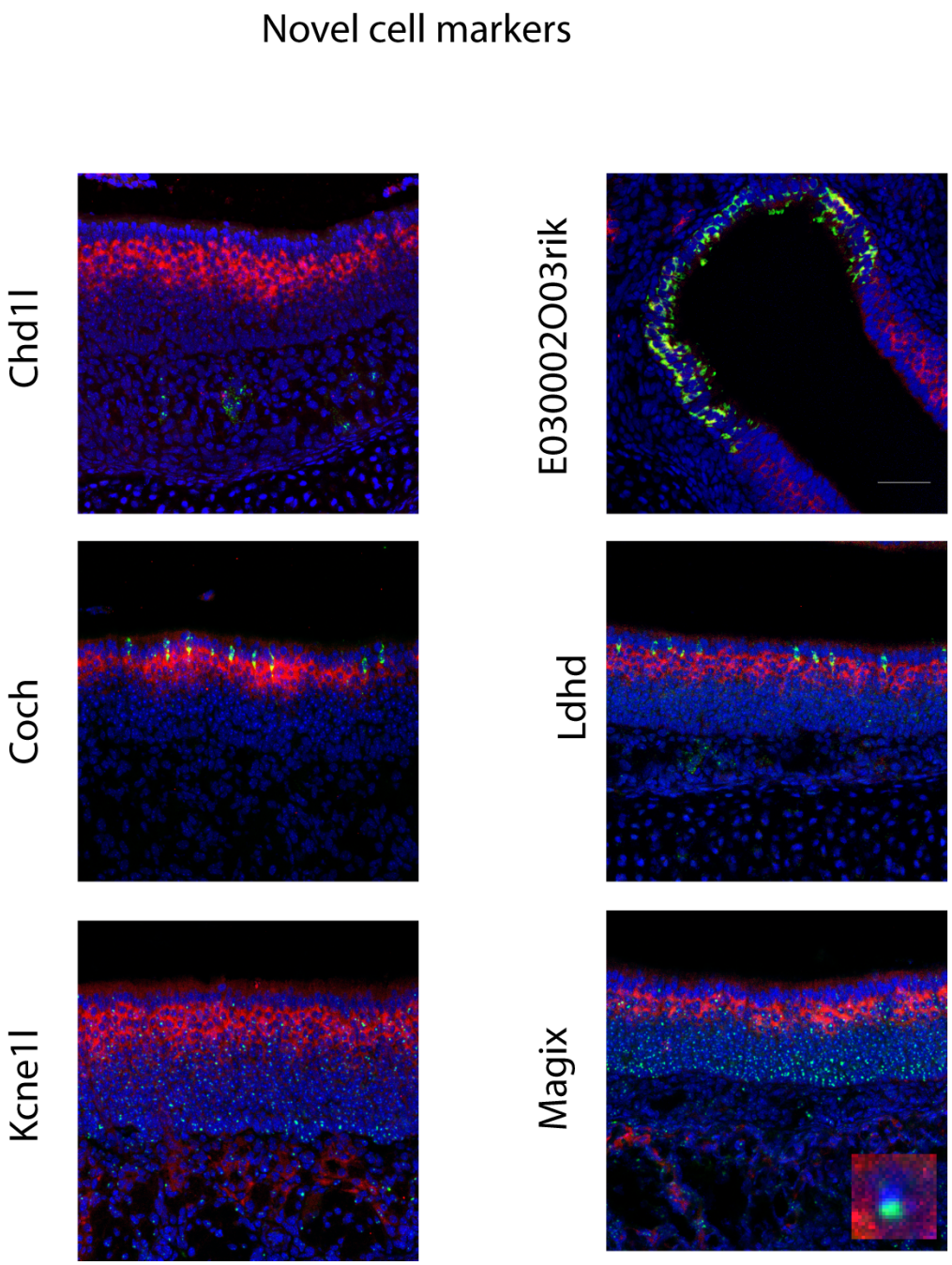

Figure 4.3.7-1 Representative images of six cell markers.

Chd1l is mainly expressed in the basal layer of the Bowman's gland. E030002O03rik is mainly expressed in the GC-D neurons only during the critical period. Coch is mainly expressed in microvilli cells. Ldhd is mainly expressed in microvilli cells. Kcne1l is expressed in both neurons and other cell types in the OE. The signals are enriched in the nucleolus. Magix signals are enriched in the nucleolus of the basal cells.

4.3.8 Gland specific markers

OSNs are covered by mucus. Mucus is secreted by the glands and the supporting cells. These cells are critical for the function of the nose. However, naris gland is much less studied compared to the neurons and stem cells in the nasal cavity. At least three types of gland have been observed in the olfactory epithelium including Bowman gland, nasal septal glands, and lateral nasal glands. There is no known molecular marker for them. It is not known whether their molecular identities are different or not. In the in situ hybridization experiment, I initially attempted to identify the genes specifically expressed by different cell types, and genes that were differentially expressed during the postnatal period. From the genes I tested, some of them were expressed by the glands. Three of the confirmed genes, Bpifb3, Lcn3, and Vmo1 were shown in Figure 4.3.8-1. It was very surprising to see, that different glands expressed different genes. Even within the Bowman gland population, the cells' molecular identities were different from each other. The cells expressing Bpifb3 were located in the lateral region of the cavity and did not express Lcn3. The cells expressing Lcn3 were only located in the medial region. These results revealed the heterogeneity among the gland cells. The gland cell may have different functions depending on their locations in the nasal cavity. Further investigation requires generation of GFP reporter mice and the physiology study of the specific cell type.

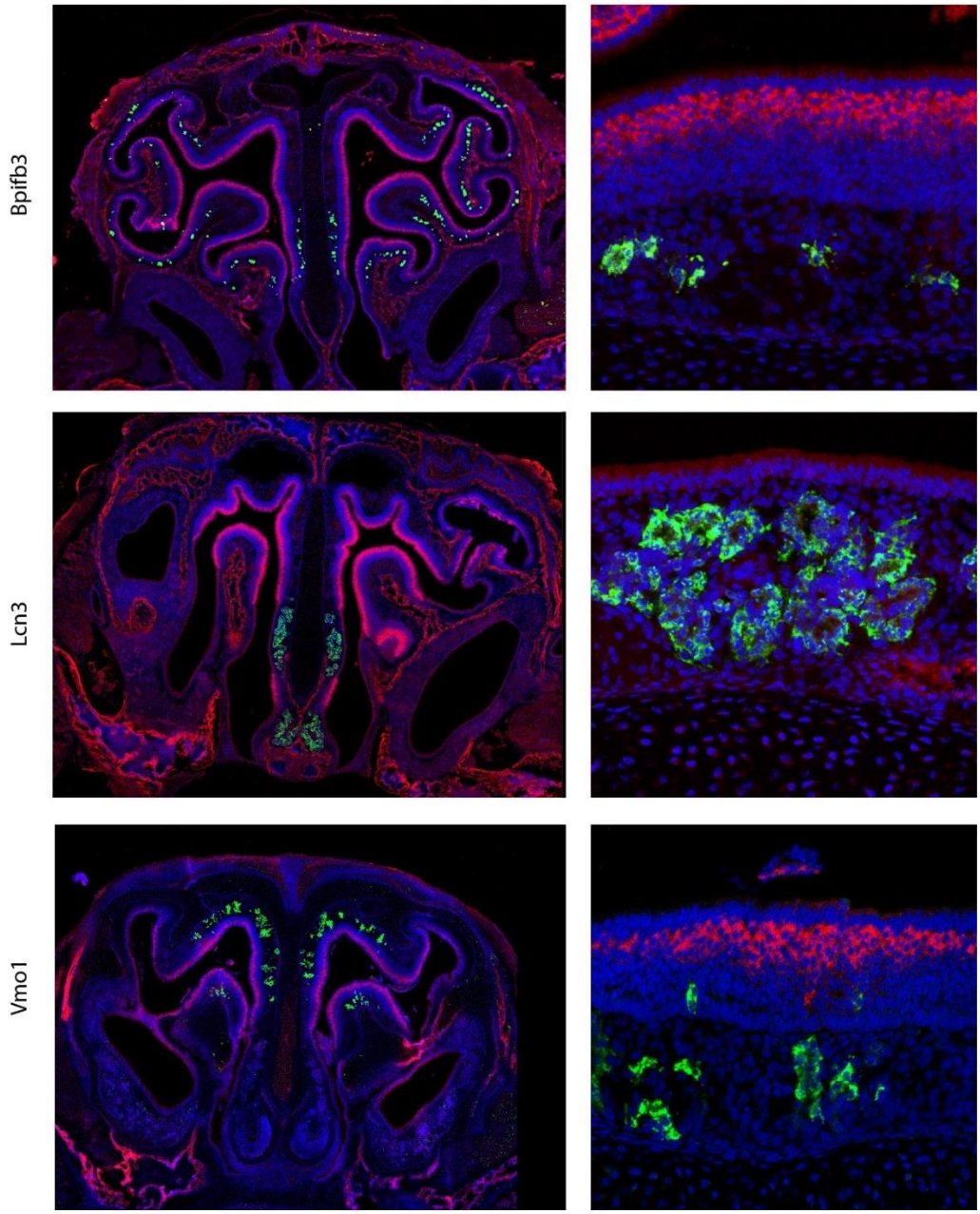

Figure 4.3.8-1 The gland specific genes.

The representative images showing double *in situ* hybridizations of OMP (red) and three genes expressed in the glands (green). The whole OE sections of P7 mice are shown on the left. The zoom-in images are shown on the right.

Bpifb3 is expressed by the ventral Bowman's gland.

Lcn3 is mainly expressed by the lateral gland.

Vmo1 is mainly expressed by the Bowman's gland in the central region of the air duct.

4.3.9 Novel cGMP cyclase

Recently, it has been recognized that sub-olfactory systems exist in the olfactory epithelium These include GC-D neurons, Gruenenburg ganglion and the type B cells in OE. These different subtype neurons express a different type of guanylate cyclase as their molecular markers. Here I identified 3 more guanylate cyclases Gucy2c, Gucy1b3, and Gucy1a3 (Figure 4.3.9-1). Gucy1a3 and Gucy1b3's expression is only detected at P0 and P3 and diminish over time. Gucy2c expression remains constant during the development. They could potentially label new types of cGMP neurons in the epithelium.

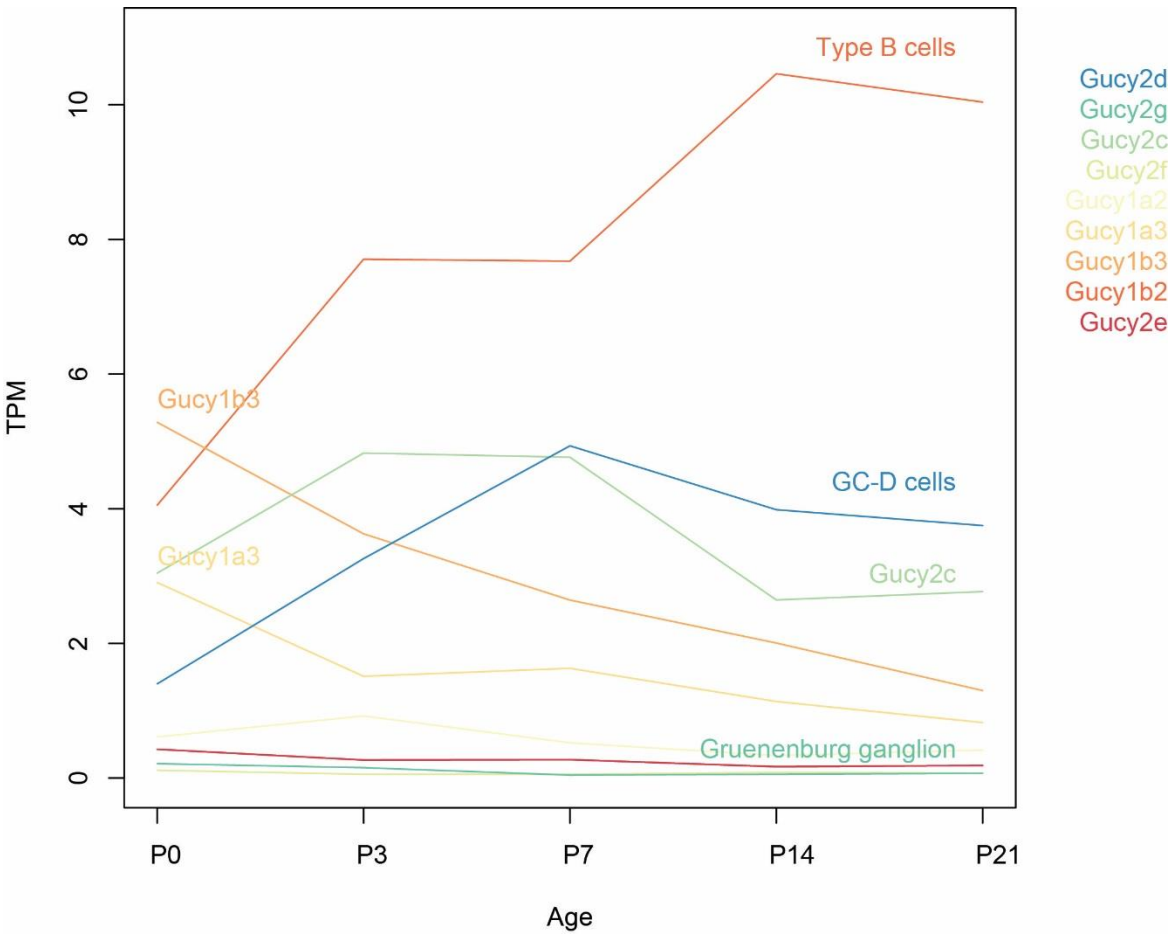

Figure 4.3.9-1 Expression profiles of nine guanylate cyclases detected in the OE-seq.

Gucy1b2 is shown to be specifically expressed in the Type B OSNs. Gucy2d is shown to be expressed by GC-D cells. Gucy2g is shown to be expressed by the cells in the Gruenenburg ganglion. Additionally, Gucy1b3, Gucy2c, Gucy1a3 are also detected in the OE-seq.

4.4 Discussion

4.4.1 Transcriptome change reveals a genetic program under the critical period

From the transcriptome analysis, we can see that the transcriptome of the olfactory epithelium is very dynamic during postnatal development. Many genes are differentially expressed during postnatal development (under the current algorithm, ~2000 genes showed significant changes). There is a transition around P7, where the genes expressed at early and late stages switch the expression profile. This change corresponds to the critical period. Different sets of axon guidance molecules are expressed between the early and late neurons. Genes expressed at the same stage share transcriptional control elements, such as the "CCAAT" domain. When neural activity is deprived, the developmental change of the transcriptome remains largely unaltered. Within the small group of genes that are altered by activity deprivation, GO terms associated with immune response are highly enriched.

4.4.2 Transcriptome analyses reveals the change of cell identity in OSNs during the critical period

In the previous chapter, I defined the settler neurons, which exhibit exuberant axon outgrowth during the critical period. Here, I identify a cluster of genes that are expressed by the settler neurons. These genes include axon guidance molecules and cell signaling molecules. The Igf signaling and Wnt signaling GO terms are enriched for these genes. Wnt signaling and Igf signaling have multiple functions, including axon guidance, cell proliferation and others. For the settler neurons, they are more likely to be involved in axon guidance rather than cell proliferation. Cell proliferation is highest at P14, which is after the closure of the critical period (Chapter 3). These terms are not enriched at P14. Axon growth defects have been observed in both Wnt signaling in vitro (Rodriguez‐Gil and Greer, 2008),

and Igf signaling in vivo (Scolnick et al., 2008b). However, it is not known whether these signaling pathways are associated with the OR-based axon sorting. Further experiment is required to test this hypothesis. Known activity dependent axon guidance molecules, such as Kirrels and EphrinAs, are only enriched after the critical period. They are likely to be used by the late neurons. In another word, neurons generated before and after the critical period express different sets of axon guidance molecules and adopt different axon guidance mechanisms. The transcriptome analysis shows that there is a switch from the settler neurons to the later generated OSNs at the closure of the critical period.

5 Chapter V. Wnt signaling and the critical period

5.1 Introduction

In the activity dependent model of OSN axon guidance (Serizawa et al., 2006), difference in neural activity drives differential expression of the axon guidance molecules to sort the OSN axons. In this model, neural activities between two different receptor types must be different enough to drive a transcriptional change in the downstream axon guidance molecules. However, in the case of M71 and M72 receptors, the two receptors are very similar, with only several amino acid differences (Feinstein and Mombaerts, 2004). They share the same types of ligands. Therefore, their activity levels are presumably very similar. However, the neurons expressing the two receptors can always distinguish each other. In the extreme case, the mutant with a single amino acid difference can distinguish itself from another form (Feinstein and Mombaerts, 2004). The mutations do not necessarily result in the change in the OR activity, but result in the separation of axons (Feinstein and Mombaerts, 2004). I think additional molecules are involved in the tuning of OR signaling to facilitate the axon sorting. These molecules should be able to amplify the difference from the G protein signaling generated downstream of ORs. ORs are GPCRs. GPCRs form receptor complex by binding to other membrane receptors (Parmentier, 2015). The association between GPCRs could be a potential mechanism to alter the downstream signaling. In the previous chapter, I identified Fzd1, a GPCR specifically expressed during critical period in the mOSNs. Fzd1 is a receptor of the Wnt signaling pathway. Previously, Wnt signaling is reported to be involved in axon guidance process (Zou, 2004). In the Drosophila olfactory system, Wnt signaling directs the specification of the olfactory dendritic map (Wu et al., 2014; Yao et al., 2007). Its role in axon guidance in the mammalian olfactory system has also been proposed (Rodriguez‐Gil and Greer, 2008). In this chapter, I will provide a detailed analysis of the Fzd1 receptor's function during the critical period.

5.1.1 Wnt signaling

Fzd1 is a receptor of the Wnt signaling pathway. The first mammalian Wnt, Wnt-1 was discovered by Roeland Russe and Harold Varmus as Int-1, an oncogene (Nusse et al., 1984). It later turned out to be an ortholog of the already characterized gene Wingless (Wg), in Drosophila. Developmental studies conducted by Christiane Nüsslein-Volhard and Eric Wieschaus have established Wg as a morphogen, involved in body polarity formation (for details of the history, see review by Nusse (Nusse, 2005)). Later, other Wnt signaling molecules were discovered. (Nusse et al., 1991)

Wnt signaling starts with the binding of the Wnt ligand to the Frizzled receptor. Frizzled receptors are G protein coupled receptors (GPCRs). The ligand-receptor binding activates a signaling cascade within the cell. In the classic definition, Wnt signaling is further divided into canonical and non-canonical pathways. In the canonical pathway, the signaling starts with the binding of Wnt to the receptor complex containing Frizzled receptors and other co-receptors. The activation of the receptor complex results in a signaling cascade that results in the accumulation of beta-catenin, an adhesion molecule. Beta-catenin then translocates into the nucleus and activates the downstream gene transcription by binding to transcription activators, TCFs. (Clevers, 2006). The binding also recruits many other transcription co-activators to form a transcription activation complex. The transcription complex activates the transcription of downstream genes. Depending on the genes being activated, Wnt signaling can be involved in different functions, such as cell differentiation, the establishment of cell polarity, axon guidance, and programmed cell death (Nusse, 2005). The noncanonical Wnt pathway is generally also referred to beta-catenin independent pathway. It includes two types, the PCP-pathway and Wnt/Ca2+ pathway (Gordon and Nusse, 2006). Both don’t rely on beta-catenin for gene expression. In some cases, the downstream transcription is not activated.

5.1.2 Wnt signaling and the axon guidance

Wnt signaling can act as an axon guidance cue in mammalian neural system during development. There are many examples. Wnt signaling gradient direct spinal cord commissure neuron axon guidance (Lyuksyutova et al., 2003). It is also involved in the topographic patterning in the chicken tectum (Schmitt et al., 2006). In mammalian sensory neurons, secreted frizzled inhibitors are involved in the axon guidance of retinal ganglion cells (Liu et al., 2008; Rodriguez et al., 2005). In the mouse olfactory sensory neurons, the expression of Wnt and receptors are detected during development (Rodriguez‐Gil and Greer, 2008). Non-canonical Wnt signaling ligand, Wnt5a, has been shown to promote neurites growth *ex vivo* (Rodriguez‐Gil and Greer, 2008).

Wnt signaling has other functions in neuron development, such as synaptogenesis (Packard et al., 2003), and dendritic development. In Drosophila, Wnt signaling directs the dendritic patterning of the secondary projection neurons in the olfactory system (Wu et al., 2014). Wnt signaling is also shown to stimulate dendritic morphogenesis (Rosso et al., 2005).

5.1.3 Interaction between Wnt receptors

Frizzled (Fzd) receptors are the receptors of Wnt, a family of GPCRs. It is not known whether they couple to Golf or Gs, which are the two major G proteins expressed in the olfactory sensory neurons. Fzd receptors have many co-receptors. The receptors and co-receptors form receptor complexes. In addition to the association with co-receptors, Fzds can couple to different types of other Fzd proteins to form heterodimers. Heterodimerization alters the signaling property of Frizzled (Carron et al., 2003). The formation of heterodimers between different types of Frizzled could be a potential mechanism for fine tuning the signaling.

Based on the evidence of receptor complex, there are two possible ways for the Fzds to interact with ORs. First, the Frizzled receptors are structurally similar to the olfactory receptors in that both have 7

transmembrane domains, and PDZ domains (Schulte and Bryja, 2007). The Frizzled receptors could couple to the OR signaling through direct binding to form receptor complex. On the other hand, the signaling can be altered through indirectly affecting the downstream messengers, such as cAMP and PKC.

5.2 Material and method

5.2.1 Animals

Fzd1-lacZ, Fzd2-lacZ, M71-IRES-tauGFP, M72-IRES-tauGFP, and OMP-IRES-tTA mice (the Jackson laboratory 012820, 012821, 006676, 006678, and 017754, respectively) were described previously. All animals were maintained in Lab Animal Services Facility of Stowers Institute with a 14:10 light cycle, and provided with food and water *ad libitum*. Doxycycline (DOX) treatment was performed by either weaning the pups onto DOX diet or by fostering the pups to CD1 moms fed with DOX diet at least 48 hours earlier. Experimental protocols were approved by the Institutional Animal Care and Use Committee at Stowers Institute and in compliance with the NIH Guide for Care and Use of Animals.

5.2.2 Transgenesis

Fzd1 and Fzd2 coding sequences were cloned from plasmids pRK5-mFzd1 (addgene#42253) and pRK5-mFzd2 (addgene#42254) into MluI and PacI sites of the plasmid tetO-v1rj3-IRES-Tdtomato (Haga-Yamanaka et al., 2014). Next, the plasmids were linearized with AscI and FseI. The fragments containing the tetO-Fzd1-IRES-Tdtomato and tetO-Fzd1-IRES-Tdtomato were gel extracted using Zymo Research gel extraction kit (Zymo). The extracted DNA was then purified by Phenol-Chloroform-IAA (25:24:1), 50% Isopropanol, 100% Ethanol, and 80% Ethanol. The resulting DNA was diluted into 10ng/µl concentration in embryo injection buffer. FVB strain embryos were collected

and injected with a standard protocol (He et al., 2008). The founders were screened through PCR using a probed detecting Tdtomato by Transnytex. The positive founders were mated to OMP-IRES-tTA; OR-IRES-eGFP compound heterozygote mice for further experiment.

5.2.3 Immunohistochemistry

Immunohistochemistry was conducted as described in the previous chapter. The additional antibodies used in this chapter include: Goat anti-Fzd1 (B&D systems). Rabbit anti-Fzd2 (Abcam).

5.2.4 Cloning and vector construction

All the vectors in this chapter were cloned using Q5 polymerase (NEB) and assembled through HIFI assembly kit (NEB). ORs and RTP1 were cloned from C57/bl6j strain mouse olfactory epithelia cDNA.

5.2.5 Imaging of histological samples

Histology staining was imaged using Zeiss 700 confocal microscope.

5.2.6 RNA-seq analysis

Tdtomato positive cells were sorted from tet-Fzd1 animal using Biorad S3 sorter. The GFP positive cells were sorted from tet-GCaMP2 animals. The RNAs were extracted and sequenced the same way as describe in the previous chapter.

5.2.7 Whole mount imaging of the glomeruli

The olfactory bulb samples were mounted onto a class bottom petri dish (Celvic) using a home-made mounting media (Y-mount). The images were taken using Zeiss 780 with QUASER detector. The spectrum images were separated using Zeiss Zen software.

5.2.8 FRET

Acceptor bleaching experiment was done on Zeiss 700 confocal microscope. Vectors expressing Fzd1::RFP and OR::GFP were transfected into Neuro2A cells using Lipofactamine 3000 (ThermoFisher). The red fluorescence was ablated using 100% laser power with 30 iterations. 4 images before the bleaching and 5 images after bleaching were used to analyze the FRET.

5.2.9 Surface expression test

Vectors containing Fzd1::RFP, Fzd2::RFP, OR-2A-RTP1-2A-nucBFP were transfected into HEK293 cells using lipofactamine 3000. Images were taken through Zeiss 700 confocal microscope.

5.3 Results

5.3.1 Frizzleds expression during the critical period

From the transcriptome analysis in the previous chapter, Fzd1, Fzd2 and Celsr1 were detected to be expressed in the OE during the critical period following slightly different timelines. Fzd1 was specific to the mOSN. while Fzd2 and Celsr1 were also expressed by the progenitor cells. Fzd1 was expressed highly at P0 and P3, then started to decrease at P3. Fzd2 was also detected to be expressing at P0, reaching a peak at P3, then started to decrease at P7. There was a 2-day difference in when the receptor was expressed at the highest level. They both decreased to a significantly low level at P10 and remained the low expression level to P21.

I conducted immunohistochemistry staining using a previously described Fzd1 antibody (Rodriguez‐Gil and Greer, 2008), and a new Fzd2 antibody. The Fzd2 antibody didn't produce any staining. The Fzd1 antibody produced strong staining at P3. The signal was lower at P14, which was consistent with the published results. The signal was enriched at the cell membrane, as well as on the axons. This pattern was slightly different from the published result, probably due to different staining conditions.

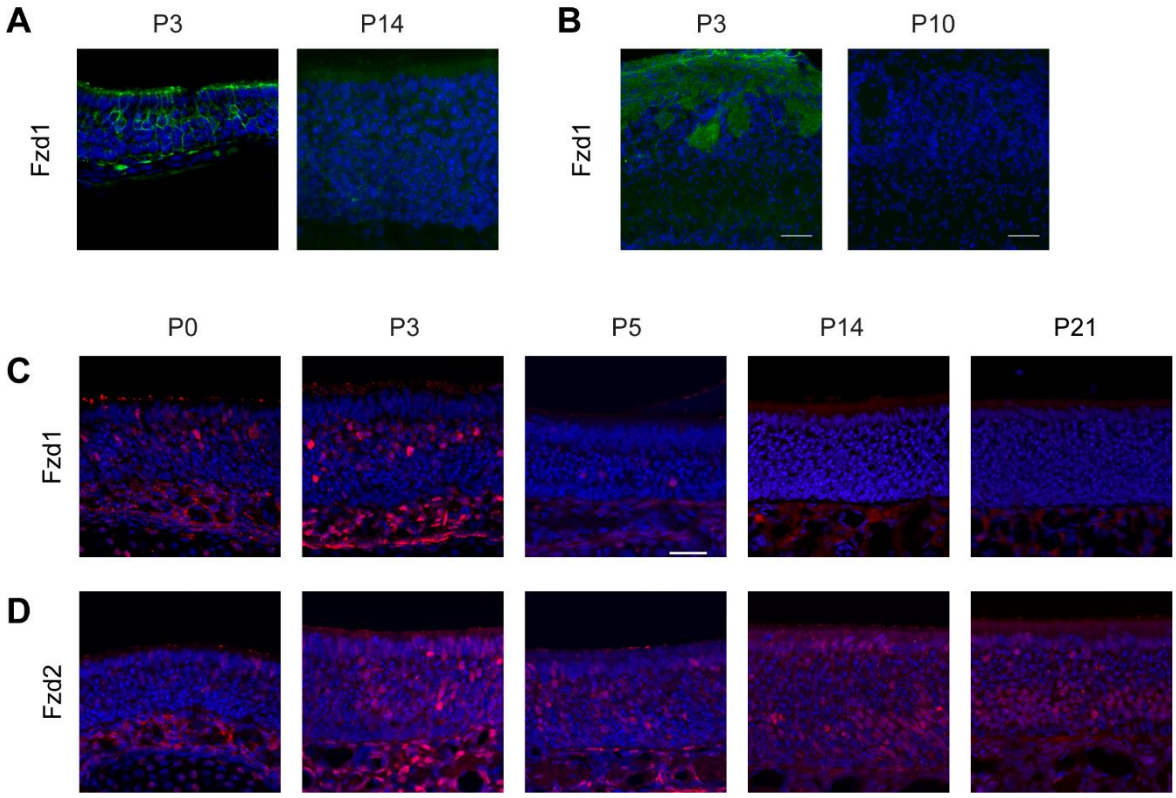

Figure 5.3.1-1 The expression patterns of Fzd1 and Fzd2 during the critical period.

(A) Immunostaining of Fzd1 in the OE (green) at P3 and P14.

(B) Immunostaining of Fzd1 in the OB (green) at P3 and P10.

(C) Time course stainings of LacZ (red) in Fzd1-lacZ animal in the OE.

(D) Time course stainings of LacZ (red) in the Fzd2-lacZ animal in the OE.

Sections are counter-stained with DAPI (blue). Scale bar: 50 μm.

To further confirm the expression timeline of Fzd1 and to validate the Fzd2's expression from RNA-seq, I used the Fzd1-LacZ and Fzd2-LacZ transgenic animals. These two mice were created by the Jeremy Nathans lab in the study of Fzds' function during development (Yu et al., 2010). Both mice were created by inserting a LacZ gene inside the open reading frame of the original Frizzled receptors. LacZ staining or antibody staining against LacZ protein could be used to identify the cells expressing the Fzds. The relative expression levels of Fzds at different ages could be inferred from the levels of LacZ.

In the Fzd1-LacZ animal, the LacZ antibody staining showed a similar trend as the Fzd1 antibody staining in wildtype animals (Figure 5.3.1-1C and D). I performed double staining to simultaneously detect OMP and LacZ. The LacZ staining was mosaic among the OMP positive cells, indicating the expression of Fzd1 is mosaic among mOSNs (Figure 5.3.1-2).

In the Fzd2-LacZ animal, the LacZ staining was seen not only in mOSNs, but also in other cell types (Figure 5.3.1-2). The expression of LacZ in the mOSNs followed the same trend as detected by RNA-seq (Figure 5.3.1-2). Similar to Fzd1, the expression level of LacZ in Fzd2-LacZ animals was also mosaic. Interestingly, the iOSNs seemed to express Fzd2 with a higher level (Figure 5.3.1-2). The nonspecific Fzd2 expression pattern was not from background autofluorescence, because the signal was only seen in the nucleus. Between P0 to P21, the LacZ signal in the Fzd2-lacZ animals was decreasing from the mOSN, but remained stable in other cell types (Figure 5.3.1-1D).

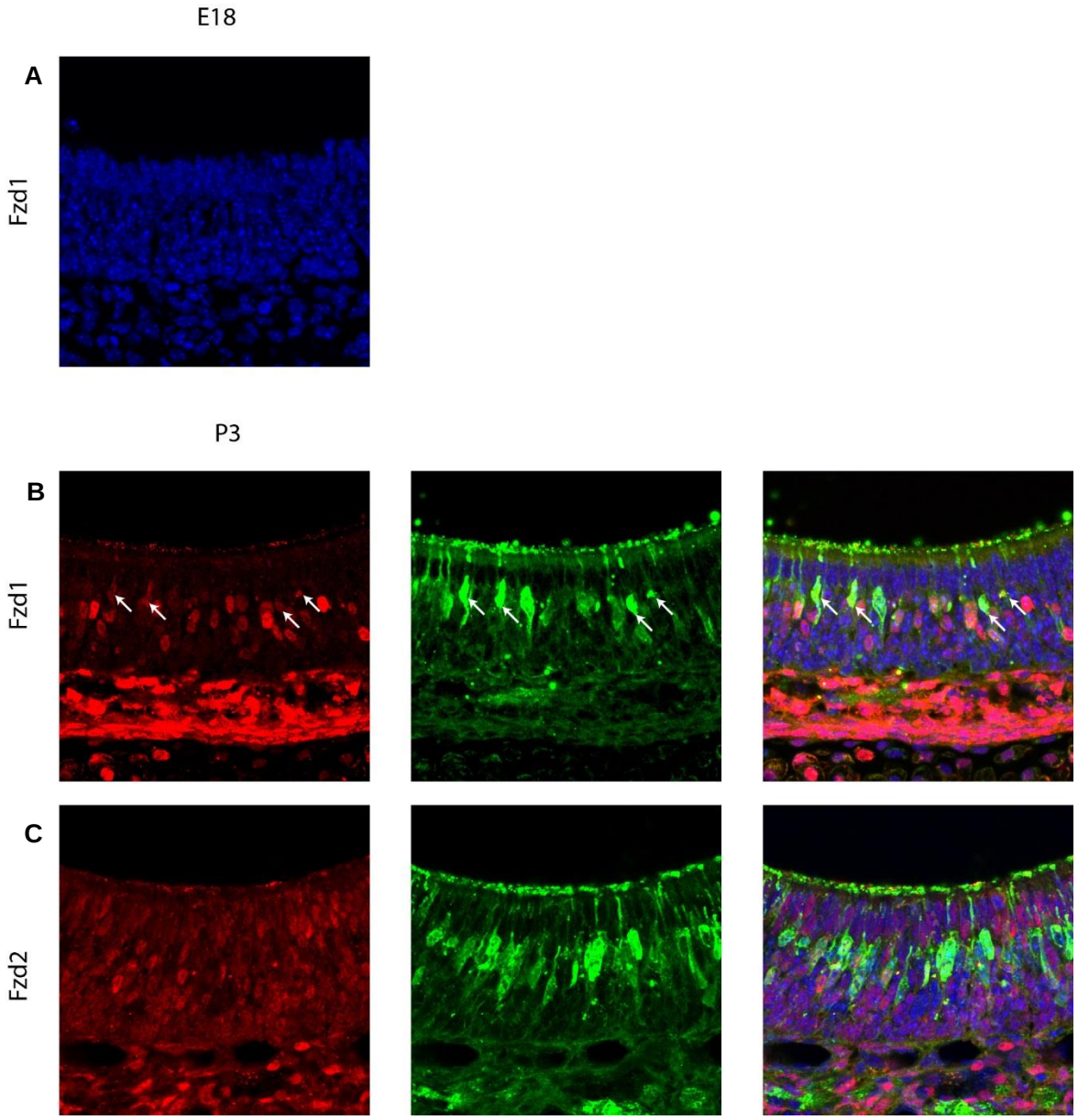

Figure 5.3.1-2 The expression of Fzd1 and Fzd2 during the critical period, continued.

(A) Representative image of the OE at E18 from the Fzd1-lacZ animal. The LacZ signal is not detected in the Fzd1-lacZ animal at E18.

(B) Representative image of the OE from the Fzd1-lacZ animal stained with LacZ (red) and OMP (green) at P3.

(C) Representative image of the OE from the Fzd2-lacZ animal stained with LacZ (red) and OMP (green) at P3. Fzd2 is expressed by all cell types within the olfactory epithelium.

From the RNA-seq, immunohistochemistry, and genetic marker staining experiment, both the Frizzled receptors were enriched during the critical period. Fzd2's expression was not specific to OSNs, but did decrease specifically from mOSNs. Because of the strong correlation between the timing of Frizzled receptors' expression and the critical period, I hypothesize that the Frizzled receptors are involved in regulating the olfactory map formation during the critical period. To test this hypothesis, I adopted a genetic approach to manipulate the expression of Fzd1 and Fzd2 during the critical period.

5.3.2 Genetic manipulation of Frizzled 1 and Frizzled 2

To understand the correlation between Fzds and the critical period, dis-correlate the two is a preferred approach. To achieve this goal, I generated tetO-Fzd1-IRES-Tdtomato and tetO-Fzd2-IRES-Tdtomato mice (tet-Fzd1, and tet-Fzd2 animal for short) (Figure 5.3.2-1). When mated with OMP-IRES-tTA mice, the compound heterozygote mice carrying both alleles express Fzd1 or Fzd2 in the mOSNs. The expression can be shut down by DOX, making it possible to change the timing of the Fzds' expression.

In the tet-Fzd1 animal, Fzd1 expression was maintained through the lifespan in the absence of DOX as detected by immunohistochemistry. The staining signal was also increased compared to the control animal (Figure 5.3.2-1). Different glomeruli had different expression levels as estimated by the intensity of Tdtomato fluorescence in the OB (Figure 5.3.2-1). The glomeruli projection was altered from birth to the adult stage (Figure 5.3.2-1). I examed the axon projection of 3 OR types, M71, M72 and MOR28. They showed different phenotypes. M71 glomeruli showed a diffusive projection pattern, with fibers spreading around the original position. M72, which is quite similar to M71 in amino acid sequence, did not show any glomerulus at the dorsal olfactory bulb (Figure 5.3.2-1). MOR28 glomeruli located at the ventral olfactory bulb was also affected. The glomeruli still form. But two or three extra glomeruli were seen around the original MOR28 glomeruli.

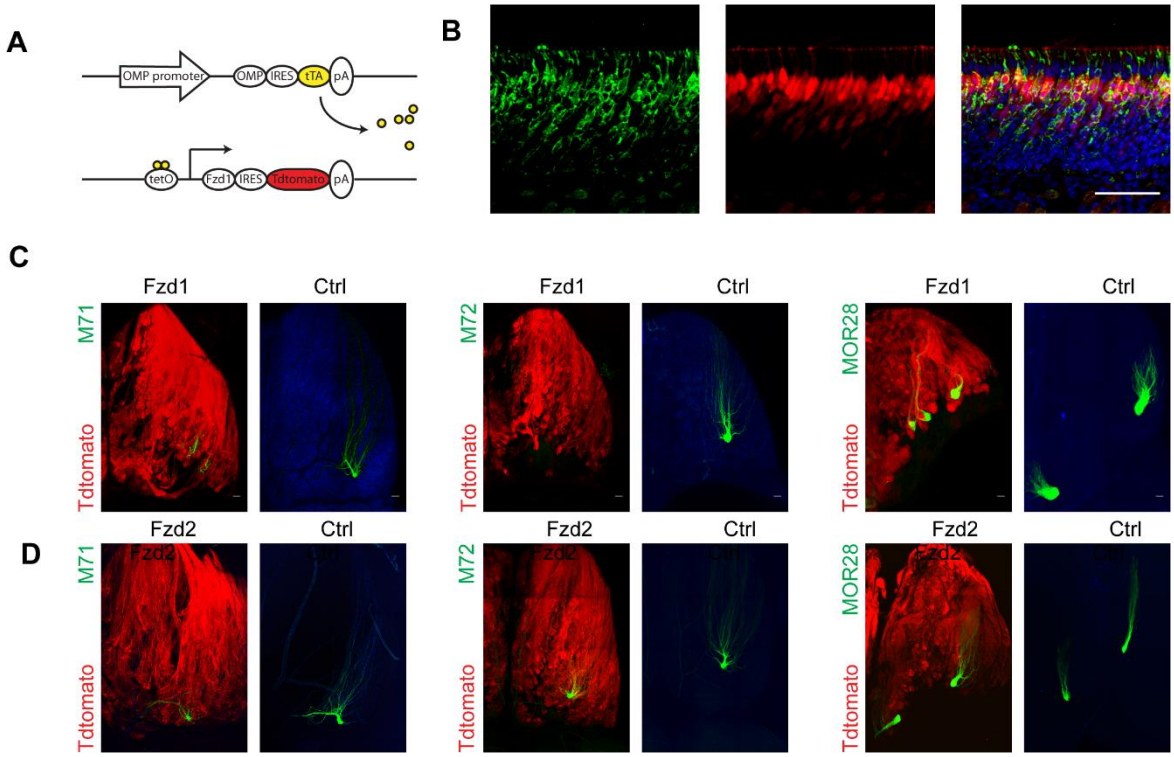

Figure 5.3.2-1 Overexpression of Fzd1 and Fzd2 through tetracycline trans-activation system.

(A) Schematic illustration of the tet-Fzd1 transgenic animal.

(B) Expression of Fzd1 detected by immunostaining (green) in the OSNs in the tet-Fzd1 animal.

(C) Axon projection patterns of M71, M72 and MOR28 neurons in the tet-Fzd1 and control animals.

(D) Axon projection patterns of M71, M72 and MOR28 neurons in the tet-Fzd2 and control animals.

The tet-Fzd2 transgene did not change the singular glomerulus projection pattern for any of the three olfactory receptor types (Figure 5.3.2-1D). This result indicates that the ectopic expression after the critical period nor increased expression of Fzd2 during the critical period does not affect the axon guidance of OSN.

5.3.3 Ectopic expression of Frizzled 1 promotes exuberant axon projection

The settler neurons are critical for the olfactory map formation during the critical period. Fzd1 is expressed in the settler neurons. I hypothesize that the Fzd1 could promote axon outgrowth of settler neurons, which results in the exuberant projection during the critical period. I performed staining of OSN axons in the tet-Fzd1 animals. As expected, the neurons generated after the critical period are showing more exuberant projection compared to the OMP-TetTag animals (Figure 5.3.3-1A). From a systematic quantification, the pruning of the exuberant projection was delayed by about one week (Figure 5.3.3-1C). At P14, when the exuberant growth was pruned in the OMP-TetTag animals, tet-Fzd1 animals showed highest level of exuberant axons (Figure5.3.3-1A, B). This gain-of-function phenotype indicates the Fzd1 indeed contributes to the settler neurons' exuberant axon growth.

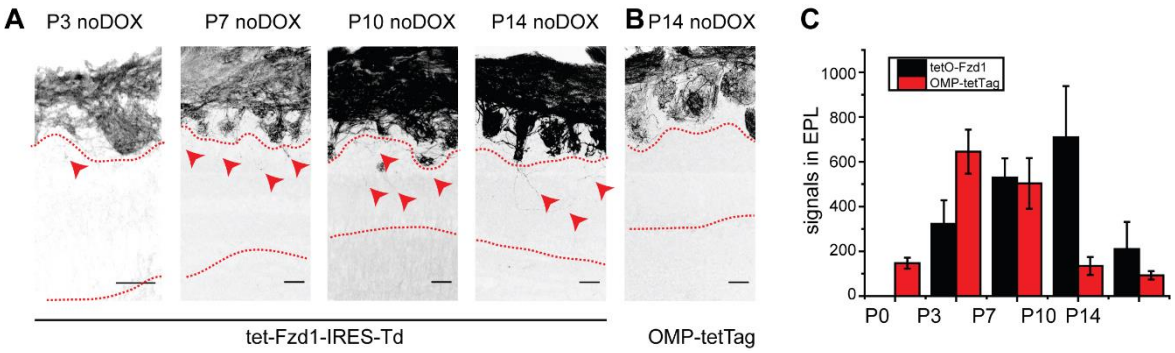

Figure 5.3.3-1 Ectopic expression of Fzd1 promotes the axon exuberant growth.

(A) Representative images showing the OSN axons stained against tdTomato (red) in the tet-Fzd1animals at P3, P7, P10 and P14.

(B) Representative images showing the OSN axons stained against LacZ (red) in the OMP-TetTag animals at P14.

(C) Quantification of the axon exuberant growth in the OMP-TetTag and the tet-Fzd1 animals.

5.3.4 Turning off ectopic expression of frizzled 1 causes precocious closure of the critical period

Using the genetic tools, I investigated the role of Fzd1 and Fzd2 during the critical period through ectopic expression. The Fzd1 expression was tightly coupled to the closure of the critical period. A straight forward hypothesis is that Fzd1 controls the closure of the critical period. This is also supported by the phenotype of the ectopic expression, which can be explained as follows: Wnt signaling normally results in the activation of downstream genes. If the Fzd1's presence is to shut down the critical period, the genes expressed by the late neurons will be induced by the Fzd1. These late genes will prevent the neurons from repairing the mis-projection even during the critical period and result in a discrupted projection pattern. Since the tet-Fzd1 has a disrupted glomeruli pattern, I want to take advantage of this phenotype to study if the OSNs will still be able to repair the disrupted projection when the Fzd1 is turned on and off earlier, before the normal closure time of the critical period.

First, I tested when the Fzd1 expression was shut down after the animal was given DOX. I fostered tet-Fzd1 animal to DOX fed CD1 mom and did a time series of immunostaining against Fzd1. The immunostaining showed that it took 48 hours to shut down the Fzd1 expression (Figure 5.3.4-1).

Second, I tested whether endogenous Fzd1's expression time course was altered in the tet-Fzd1 animals. I mated the Fzd1-lacZ with tet-Fzd1 animals, and gave the offspring DOX at P3. By P3, not only the Fzd1 from the tet-Fzd1 stopped expression, the endogenous allele that expressed LacZ was also shut down (Figure 5.3.4-2).

These results showed that using DOX with the tet-Fzd1, I could manipulate the time course of the Fzd1's expression. I continued to foster the tet-Fzd1 pups at different time points between P0 to P21 to DOX fed CD-1 moms, and counted the glomeruli at the adult stage, the same way to measure the timing of the critical period in the pervious experiment. I observed three OR types: M71-GFP, M72-GFP, MOR28-GFP. Surprisingly, the restoration of the disrupted projection never happened for the

MOR28 and M72 glomeruli, no matter when the Fzd1 expression was shut down (Figure 5.3.4-2). For the M71 glomeruli, only when the doxycycline was given at P0, the glomeruli projection was restored to singular projection pattern (Figure 5.3.4-1).

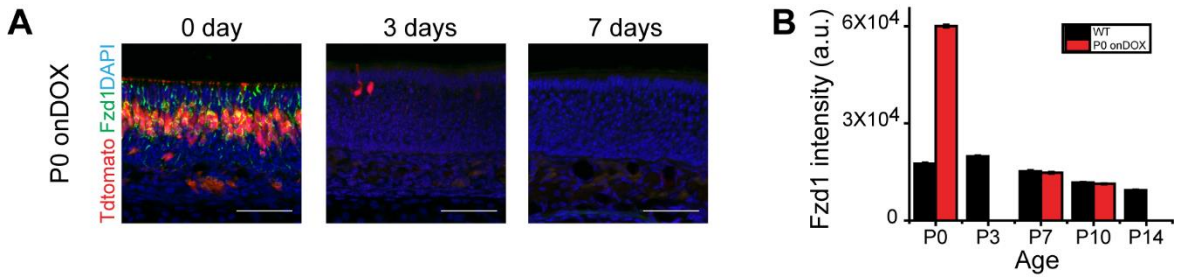

Figure 5.3.4-1 Manipulating Fzd1 expression using tet-Fzd1 transgene.

(A) Representative images showing the Fzd1 (green) and tdTomato expression (red) in the tet-Fzd1 OSNs before given DOX at P0, after given DOX for 3 days (P3), and after given DOX for 7 days (P7).

(B) Quantification of Fzd1 expression in the glomeruli before (P0) and after (P3-14) given DOX in the tet-Fzd1(red) and control animals (black).

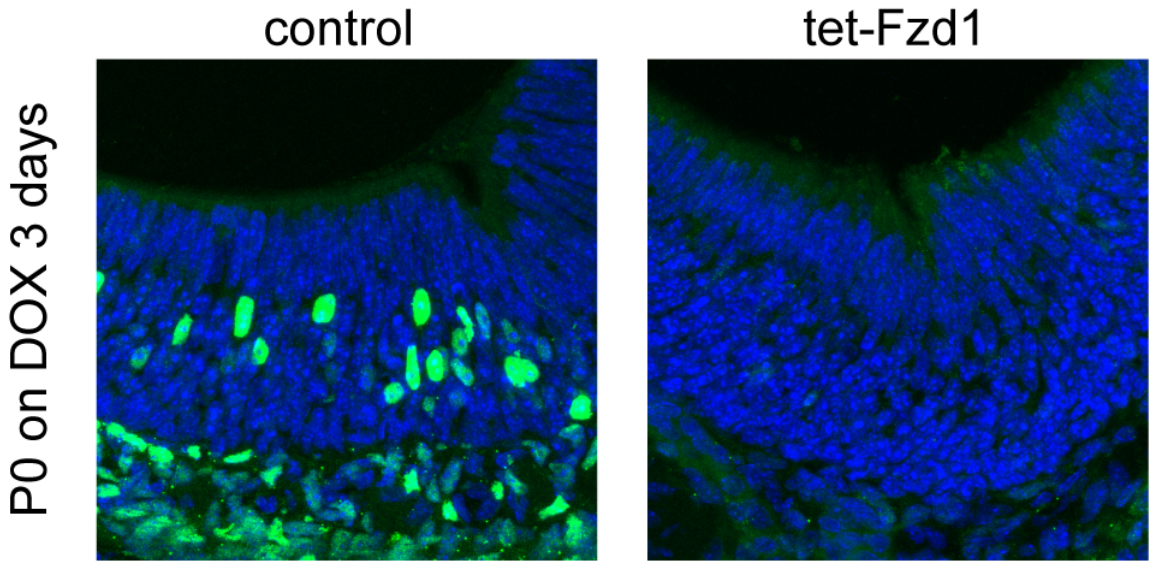

Figure 5.3.4-2 Down-regulation of Fzd1 suppresses the endogenous Fzd1 expression.

Immunostainings of LacZ (green) in the OE from the control (left) and tet-Fzd1 (right) animals given DOX at P0 for 3 days. Sections are counterstained with DAPI.

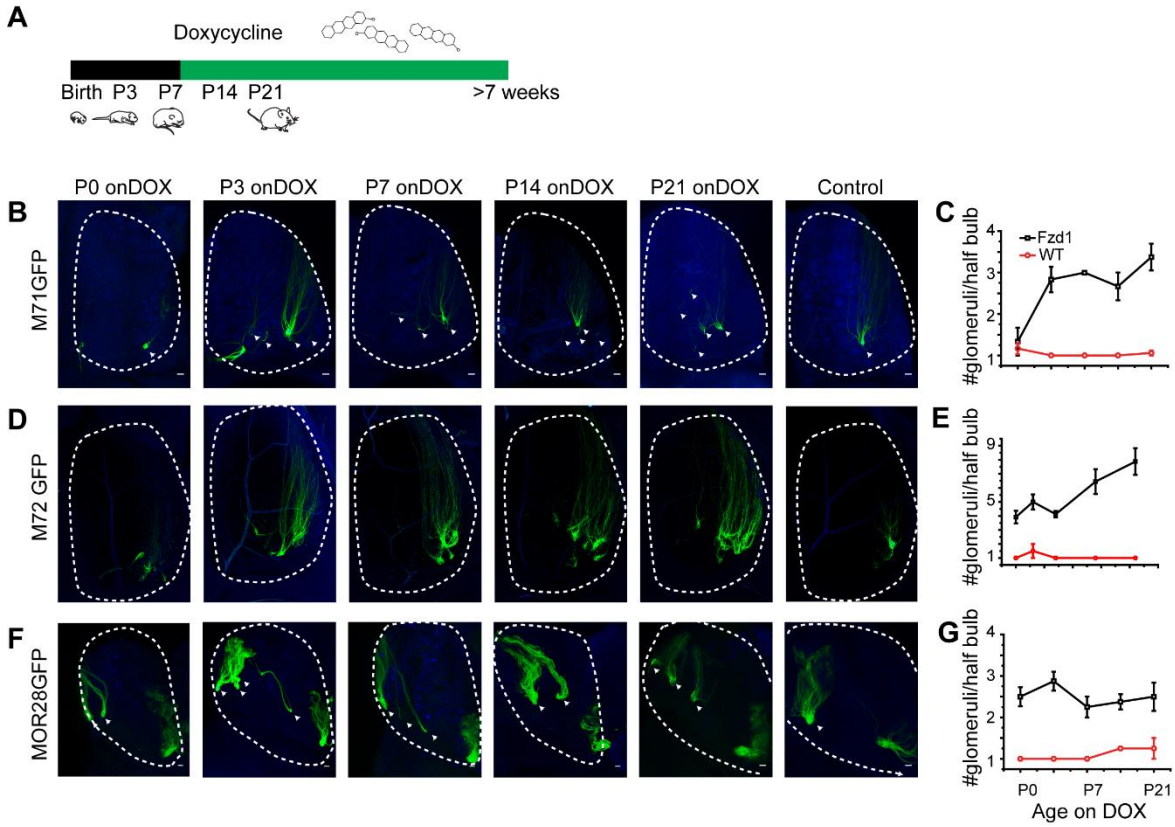
A
Doxycycline
Birth P3 P7 P14 P21 >7 weeks
P0 onDOX
P3 onDOX
P7 onDOX
P14 onDOX
P21 onDOX
Control
B
M71GFP
C
#glomeruli/half bulb
Fzd1
WT
D
M72 GFP
E
F
MOR28GFP
G
P0 P7 P21
Age on DOX

Figure 5.3.4-32 Down-regulation of Fzd1 before the closure of the critical period results in precautious closure.

(A) Schematic illustration of the time-course on-DOX experiment on the tet-Fzd1 animals.

(B) Representative images for the adult M71-GFP animals given DOX at various time points.

(C) Quantification of the results showing the number of glomeruli per half bulb at adult stage for M71 glomeruli.

(D) Representative images for the adult M72-GFP animals given DOX at various time points.

(E) Quantification of the results showing the number of glomeruli per half bulb at adult stage for M72 glomeruli.

(F) Representative images of the adult MOR28-GFP animals given DOX at various time points.

(G) Quantification of the results showing the number of glomeruli per half bulb at adult stage for MOR28 glomeruli.

5.3.5 Knockout of Frizzled 1 postpones the closure of the critical period

I also tested whether Fzd1 and Fzd2 knockout directly affect axon guidance of the OSNs. Due to the breeding difficulty of the Fzd1-lacZ and Fzd2-LacZ animals, I was not able to acquire all the genotypes. The data acquired from the viable animals were shown in Figure 5.3.5-1. Both the heterozygote and homozygote Fzd1-LacZ or Fzd2-LacZ occasionally generate ectopic glomeruli for the three receptor types that I have examined (Figure 5.3.5-1). Fzd2-LacZ homozygote mice have a higher frequency to generate extra glomeruli at the adult stage than Fzd1-lacZ animals (Figure 5.3.5-1A, B). However, the phenotype is not statistically significant. The results indicate the two genes may not be directly affecting the targeting of OSNs. Alternatively, the two genes can complement each other's function. I think the later is unlikely considering the non-overlapping spatial expression pattern of the two receptors.

If the down-regulation of Fzd1 is responsible for the closure of the critical period, will permanently removing this down-regulation prevent the critical period from closing? I repeated the Kir2.1 time course experiment under the Fzd1 knockout background. Strikingly, the glomeruli restoration happened in the Fzd1-LacZ knockout animals even after the critical period (Figure 5.3.5-2). It was more striking that the heterozygote and homozygote shared similar time course (Figure 5.3.5-2). Singular projection pattern could be seen in animals treated with doxycycline even at P14 (Figure 5.3.5-2). This result suggests that removing Fzd1 indeed opens the critical period. Removing one allele is sufficient to achieve the openning.

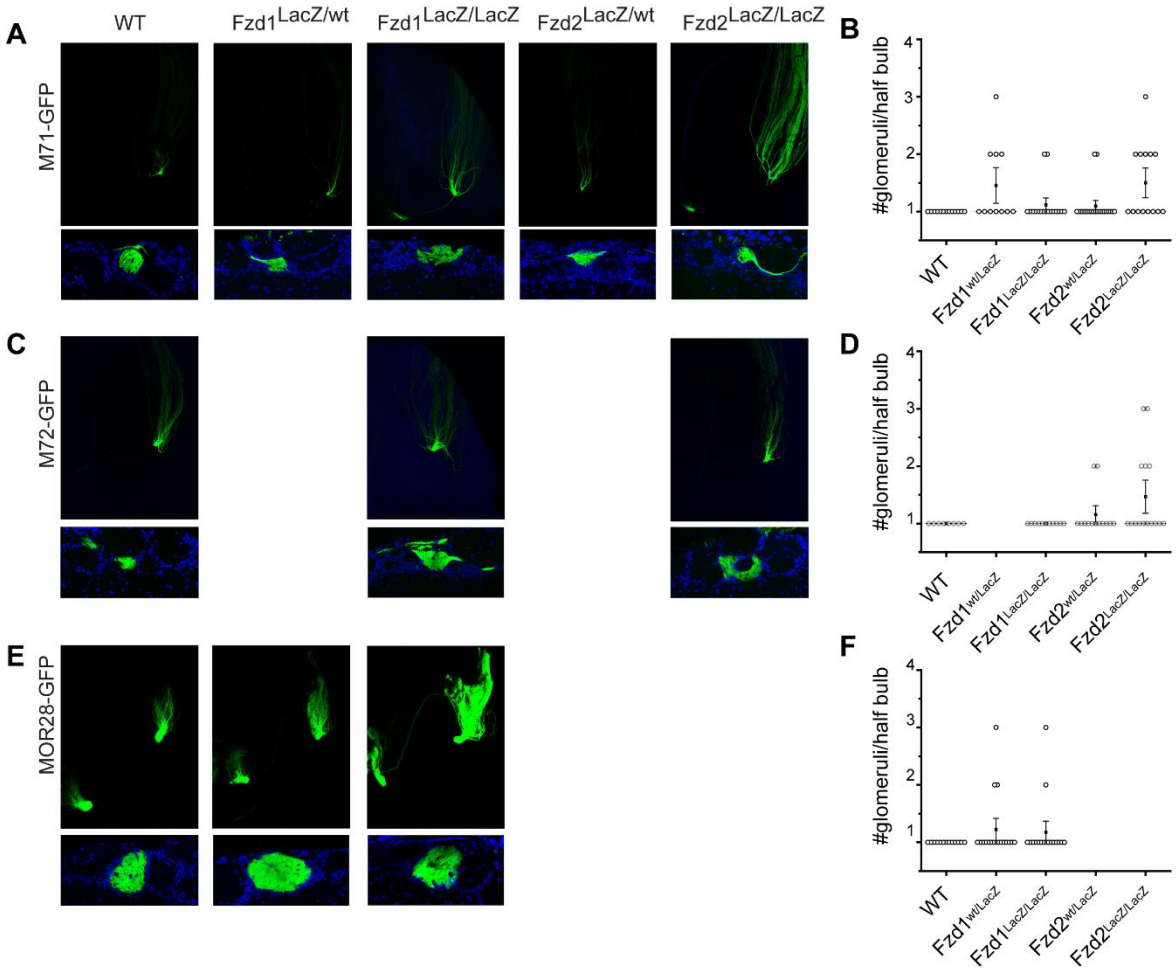
A
WT
Fzd1LacZ/wt
Fzd1LacZ/LacZ
Fzd2LacZ/wt
Fzd2LacZ/LacZ
M71-GFP
B
#glomeruli/half bulb
WT
Fzd1wt/LacZ
Fzd1LacZ/LacZ
Fzd2wt/LacZ
Fzd2LacZ/LacZ
C
M72-GFP
D
#glomeruli/half bulb
E
MOR28-GFP
F
#glomeruli/half bulb

Figure 5.3.5-1 Axon projection in the absence of Fzd1 and Fzd2.

(A) Representative wholemount images (up) and sections (bottom) showing the M71-GFP glomeruli in the wildtype, Fzd1-lacZ, and Fzd2-LacZ animals.

(B) Quantification of the numbers of glomeruli per half OB in (A). Each circle represents one half OB.

(C) Representative wholemount images (up) and sections (bottom) showing the M72-GFP glomeruli in the wildtype, Fzd1-lacZ, and Fzd2-LacZ animals.

(D) Quantification of the numbers of glomeruli per half OB in (C). Each circle represents one half OB.

(E) Representative wholemount images (up) and sections (bottom) showing the MOR28-GFP glomeruli in the wildtype, and Fzd1-lacZ animals.

(F) Quantification of the numbers of glomeruli per half OB in (E). Each circle represents one half OB.

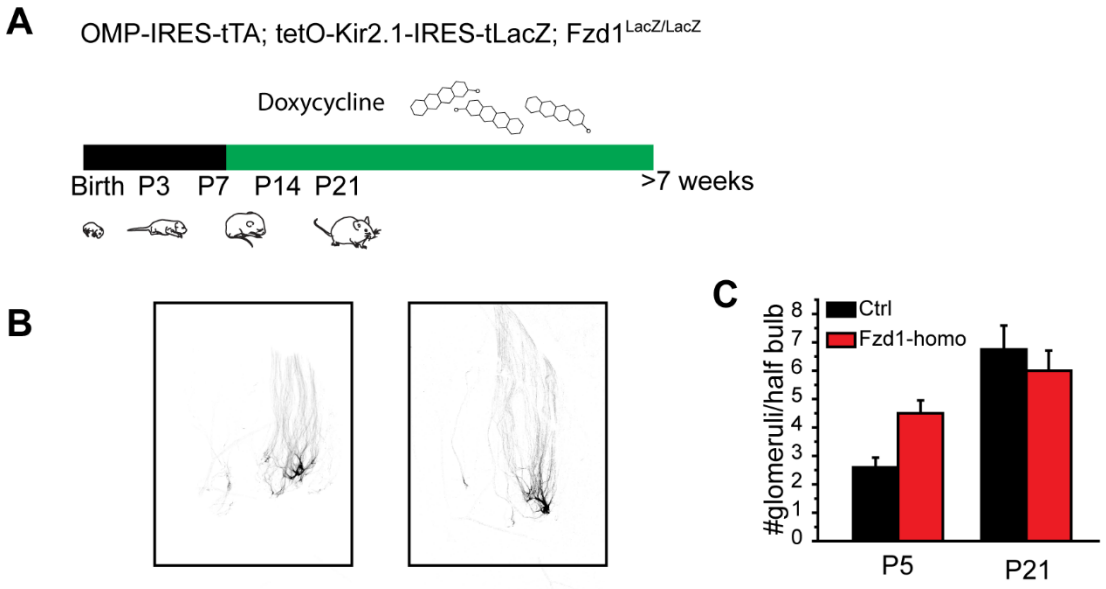

Figure 5.3.5 2 Design of the experiment testing whether knocking out Fzd1 affects the critical period.

(A) The schematic the experiment.

(B) Representative images for the M72-GFP glomeruli in the OMP-IRES-tTA; tet-Kir2.1-IRES-tauLacZ; Fzd1-lacZ (right) and control (left) animals

(C) Quantification of the number of M72 glomeruli per half bulb at P5 and P21 in the control (ctrl, black) and OMP-IRES-tTA;tet-Kir2.1-IRES-tauLacZ; Fzd1-lacZ homozygote (Fzd1-homo, red) animals.

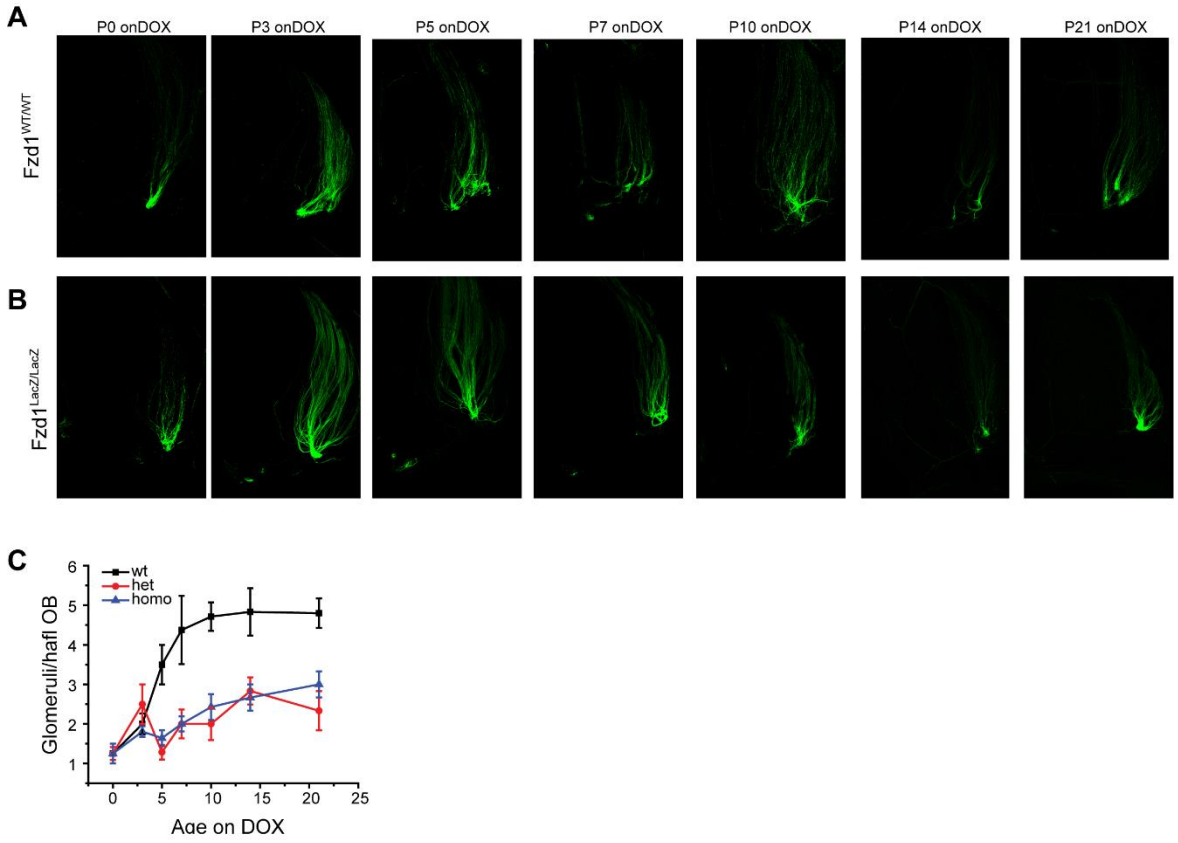

Figure 5.3.5-3 The result of the experiment described in Figure 5.3.5-2 using M72-IRES-GFP animals.

(A) Representative wholemount images showing the M72-GFP glomeruli at adult stage from the control animals given DOX at various time points.

(B) Representative wholemount images showing the M72-GFP glomeruli at adult stage from the Fzd1-LacZ homozygote animals given DOX at various time points.

(C) Quantification of the results.

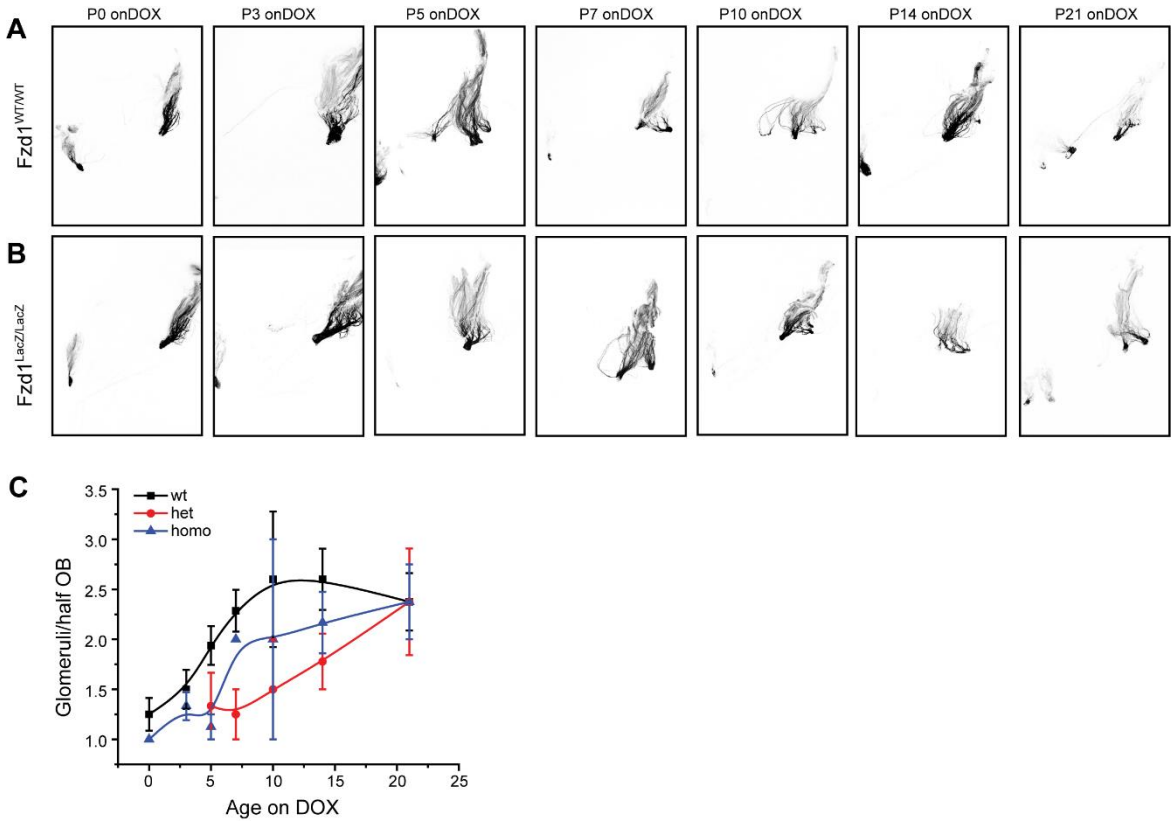

Figure 5.3.5-4 The result of the experiment described in Figure 5.3.5-2 using MOR28-IRES-GFP animals.

(A) Representative wholemount images showing the MOR28-GFP glomeruli at adult stage from the control animals given DOX at various time points.

(B) Representative wholemount images showing the MOR28-GFP glomeruli at adult stage from the Fzd1-LacZ homozygote animals given DOX at various time points.

(C) Quantification of the results.

5.3.6 Frizzled receptors interact with olfactory receptors

Next, I tested whether Fzd1 directly interacts with olfactory receptors. I first conducted FRET experiment by constructing adenoviruses (AV) vectors that expressed GFP fusion proteins with olfactory receptor I7(AV181), MOR28(AV189), M71(AV182), M72(AV186), or P2(AV187), as well as RFP fusion proteins with Fzd1 (AV183), Fzd2(AV184) or Fzd3(AV185). I expressed these constructs in the HEK293 cells, which did not express the mouse olfactory receptors, and performed acceptor bleaching experiment to quantify the amount of FRET. Across the ORs and Frizzled receptors that I tested, all of them showed robust FRET when compared to GFP or RFP alone as controls (Figure 5.3.6-1). The amount of FRET was different for different OR types (Figure 5.3.6-1). One limitation of this experiment was the artificial environment *in vitro*. For example, HEK293 cells lacked the receptor transport protein (RTP) necessary for the OR to locate on the membrane (Saito et al., 2004). This limited the amount of ORs that could interact with Frizzled receptors on the membrane. To test whether Fzds and ORs translocate together, I co-expressed the previously reported RTP1 with ORs and Fzds fused with RFP in the HEK293 cells. Surprisingly, not only the ORs, the Frizzled receptors were also translocated onto the membrane when co-expressed with RTP1 (Figure 5.3.6-2). This suggests that the Frizzled receptors interact with the RTP-OR complex.

For the GPCRs that can form receptor complex, a conserved three amino acid motif can be widely seen between the binding pairs (Borroto-Escuela et al., 2016). These three amino acid motifs could serve as affinity guides to determine which receptors interact with each other. This hypothesis is called the “Triplet guide” hypothesis. In the olfactory receptors, many conserved three amino acids motif exist (Figure 5.3.6-2B). Some of them are in the transmembrane region. I found “MYF” in the extracellular region, “FLL” and “YFF” in the transmembrane region that were conserved between ORs and Fzd1 (Figure 5.3.6-2A). Under the Triplet guide hypothesis, these three conserved motifs could be the interaction sites between ORs and Fzd1. To test this, I constructed four mutant versions of Fzd1 at L405, L369, Y305, as well as triple mutant containing all three sites, by replacing the amino acids with alanine (Figure 5.3.6-2C). When expressed in the same fashion, triplet mutant was not able to localize

onto the membrane in the presents of RTP1 (Figure 5.3.6-2C). This result indicates these three sites are important for the interaction between ORs and Fzd1.

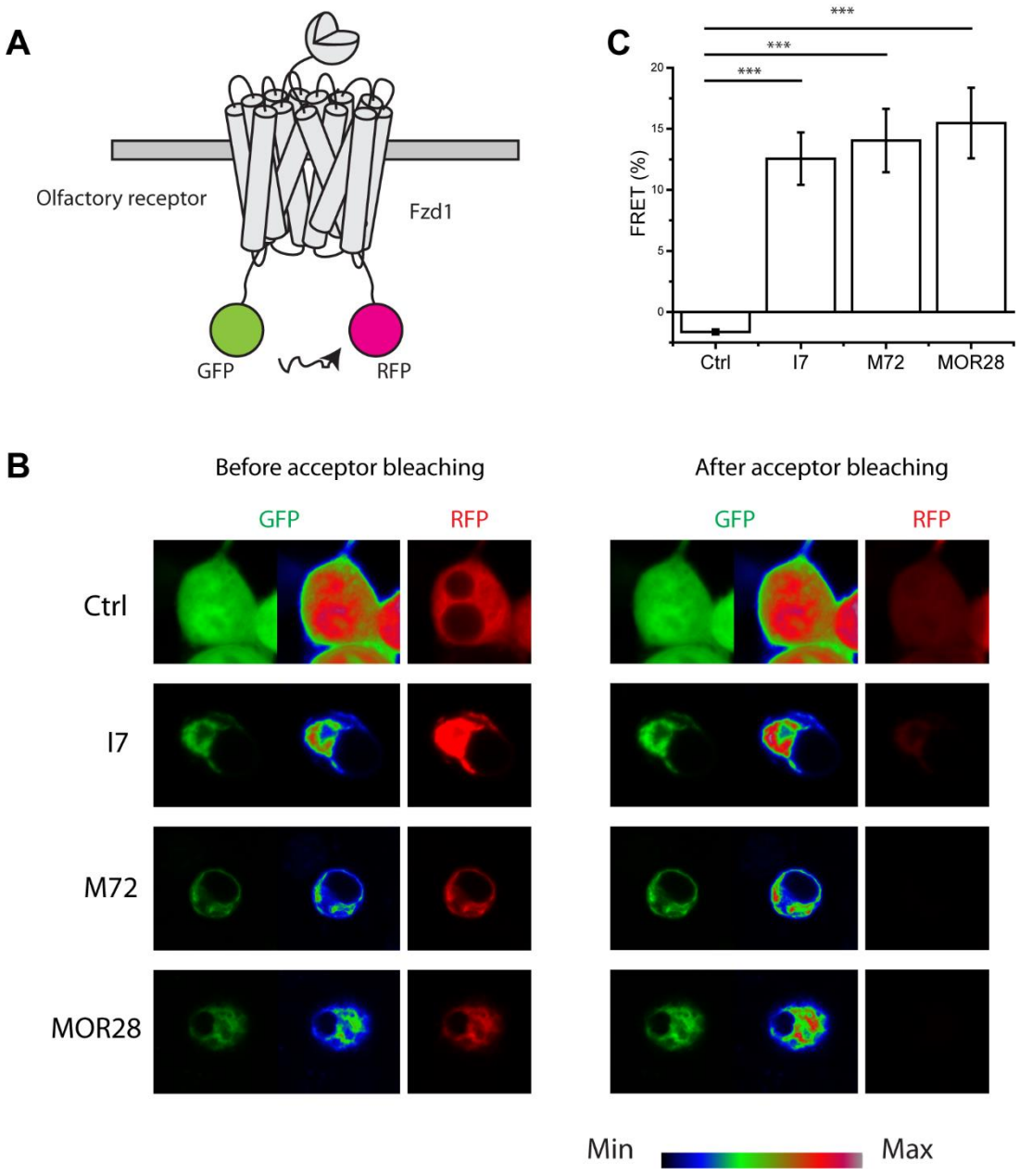
A
Olfactory receptor
Fzd1
GFP
RFP
C
***
***
***
FRET (%)
20
15
10
5
0
Ctrl
I7
M72
MOR28
B
Before acceptor bleaching
After acceptor bleaching
GFP
RFP
GFP
RFP
Ctrl
I7
M72
MOR28
Min
Max

Figure 5.3.6-1 FRET analysis of the OR-Frizzled interaction.

(A) Schematic illustration of the FRET design.

(B) Representative images showing the eGFP signal (green) and the mRFP (red) signals in Neuro2A cells before and after bleaching of the mRFP.

(C) Quantification of the FRET between different ORs and the Fzd1. The stars indicate the P-value in student t-test. *:<0.05. **:<0.01. ***:<0.001.

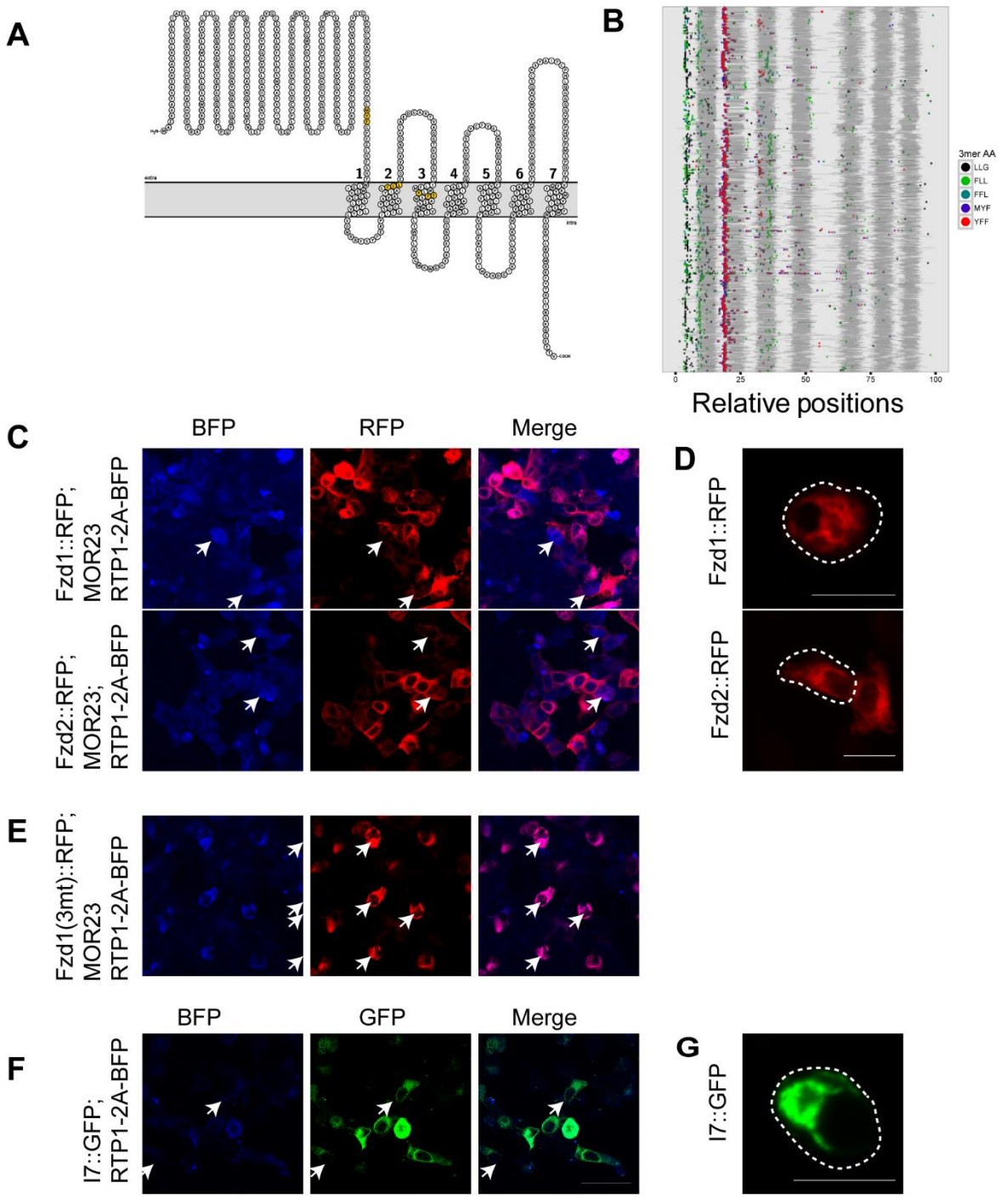
A
1
2
3
4
5
6
7
B
3mer AA
LLG
FLL
FFL
MYF
YFF
0
25
50
75
100
Relative positions
C
BFP
RFP
Merge
Fzd1::RFP;
MOR23
RTP1-2A-BFP
Fzd2::RFP;
MOR23;
RTP1-2A-BFP
D
Fzd1::RFP
Fzd2::RFP
E
Fzd1(3mt)::RFP;
MOR23
RTP1-2A-BFP
F
BFP
GFP
Merge
I7::GFP;
RTP1-2A-BFP
G
I7::GFP

Figure 5.3.6-2 Association analysis with receptor transporter protein.

(A) Three conserved triplet motifs between ORs and Fzd1.

(B) The highly conserved triplet motifs and their relative distributions on the ORs.

(C) Membrane expression tests for Fzd1 and Fzd2 in association with MOR23 and RTP1. Cells showing membrane expression of RFP are labeled with white arrows.

(D) Localization of Fzd1 and Fzd2 without the association with ORs and RTP1.

(E) Membrane expression tests for mutant Fzd1 (Y305A, L369A, F405A) in association with MOR23 and RTP1. Cells with expressing the mutant Fzd1 are indicated with white arrows.

(F) Control expression tests using I7 receptor fused with eGFP in association with RTP1. Cells showing membrane expression of eGFP are labeled with white arrows.

(G) Localization of I7 without association with RTP1.

5.4 Discussion

5.4.1 Fzd1 induces axon outgrowth

The enhanced axon exuberant growth and the disrupted axon projection pattern indicate that Fzd1 promotes axon outgrowth during the critical period. The overgrowth could allow the axons to sample the nearby axons and correct the mistakes in the projection. The extended exuberant growth after the closure of the critical period caused extranumeric glomeruli at the adult stage. It indicates that the persistence of exuberant growth is not good for the correct targeting. The mechanism needs to be shut down after the formation of intact glomeruli to prevent further remodeling. This task is likely to be conducted by the down regulation of Fzd1. The axon exuberant growth was eventually pruned in the tet-Fzd1 animals. It indicates additional molecules could reduce the exuberant growth after the critical period with a less prominent effect.

5.4.2 Down regulation of the Fzd1 triggers the closure of the critical period

The on-DOX experiment in the tet-Fzd1 animal indicates the Fzd1's down regulation determines the closure of the critical period. This is achieved by switching a group of axon guidance genes as suggested by the RNA-seq. The switch of axon guidance genes switches the neurons' ability to independently target the glomeruli. The neurons start to depend on the existing axons to find the target after the switch. It is important to note that it is the change in expression level, not the expression itself that triggers the closure. This can explain the Fzd1 knockout phenotype as well. The Fzd1 is never down regulated in the knockout. Therefore, the critical period is never closed. As a result, neurons at a later stage could target the correct glomeruli without the existing correct route. These evidences also indicate the Fzd1's role is very specific. It is involved in controlling the timing of the critical period,

not the targeting capacity. This is also supported by the evidence that there is no obvious disruption of the map in the knockout animals.

The Fzd1 knockout phenotype is counter intuitive. The gene's expression is only present during the critical period. However, removing it extended the critical period. A similar molecule observed in the critical period study in the visual system is the PirB. PirB is a receptor for the MHC peptide, which is identified to be expressed specifically during the critical period (Syken et al., 2006). however, removal of PirB, instead of ablating the critical period, increased the circuit plasticity and maintains the critical period into the adulthood. There could be a general principle for how the critical period is regulated. The circuit plasticity is a default for the neurons. The signaling through cell surface molecules is utilized to stop the plasticity. The change in expression, not the existence of the molecule itself, is the signal to close the critical period. As such, the removal of the receptor acts in the opposite direction of what people would expect.

5.4.3 Coupling between Frizzled and ORs as a potential mechanism for fine tuning of the OR signaling

The activity dependent model for olfactory map formation has been proposed for nearly a decade. It is still under debate as contradictory results emerge. First, odor-evoked activity alone is not sufficient for correct glomeruli targeting. This can be seen from the negative results of Cnga2 knockout, Golf knockout, as well as the separation of mutant receptors in the M71-M72 mutant swapping experiment (Feinstein and Mombaerts, 2004). Odorant-evoked activity is eliminated in the Golf and Cnga2 mutants, but the axon projection is not affected in the two strains. Site mutagenesis M71 mutant co-converges with wildtype M71. In the mutant where M71 is swapped with M72 (M71->M72 mutant), neurons expressing M72 from the swapped allele also co-converge and co-mingle with wildtype M71. Since both the site mutagenesis M71 and M71->M72 mutant co-converge and co-mingle with wildtype M71, they should have the same activity. However, the site mutagenesis M71 mutant doesn't co-mingle with M71->M72 mutant. Second, ligand independent intrinsic activity from OR-Gs coupling has

recently been shown to be involved in the convergence of OSN axons (Nakashima et al., 2013). The intrinsic (Nakashima et al., 2013) and spontaneous (Connelly et al., 2013) activities are correlated to the OR identity as well. Since the ligand independent activities carry the OR identity, they could serve to distinguish the axons during the development of the olfactory map.

Based on the current results, I propose a novel mechanism for the development of olfactory map. First, the development of olfactory map requires a critical period during postnatal development. The neurons generated during critical period are required for the precise map formation. These neurons are defined as settler neurons because of their unique axon guidance properties. Only settler neurons are able to form the map *de novo*, and are eliminated from the epithelia after the critical period. The elimination of settler neurons closes the critical period. Second, both the ligand dependent and independent neural activities are involved during the critical period. These activities must be coupled to additional GPCRs, such as Frizzled receptors, to be distinguishable between OR types. The neurons generated after the critical period do not express the coreceptors to prevent further remodeling of the circuit. This model could reconcile the contradictory results from the previous studies. For example, in the Cnga2 knockout and Golf knockout animals, the ORs are still coupled to Fzds. The signaling through Fzds is sufficient to mediate the sorting of the axons. In the M71 and M72 swapping experiment, the site mutagenesis mutant M71 and the M71->M72 mutant have very small difference in the signaling compared to the wildtype M71. But the difference between the two are enough to be separated with the coupling with Fzds. The receptor coupling could also explain how the ligand independent activity works. Even without the existence of the odors, Fzds can be activated constantly by Wnt. The association of ORs creates a difference in the Fzd signaling and separates the axons, which only requires the ORs to be different, but don't required them to be activated.

5.4.4 Fzd1 and Fzd2 are not redundant in regulating the critical period

The Fzd1 and Fzd2 are very similar in coding sequence. The expression of the two receptors also follows a similar timeline inside mOSN. However, the knockout and overexpression experiment show that they are not redundant in regulating the critical period. Neither the ectopic expression nor knockout of Fzd1 and Fzd2 showed similar phenotypes. They obviously serve distinct functions in the OSN. Because Fzd2 knockout but not Fzd1 knockout is anosmia, it is possible that Fzd2 is coupled to Golf and mediates the sensing of odorant.

6 Chapter VI. Development of the next generation genetic screening methods in mammals.

6.1 Introduction

In my study, I used RNA-seq to identify genes regulating the critical period. RNA-seq is a high-throughput method that gives new opportunities to find genes related to specific phenotypes quickly without bias. However, for mammalian model organisms like mice, traditional genetic interrogation methods and phenotyping methods often fall behind. The traditional process of a genetic study like this study often consists three steps. First, the genes of interest are confirmed with *in situ* hybridization (for transcripts) and immunohistochemistry (for proteins). Second, transgenesis and embryonic stem cell (ESC) genome targeting techniques are used to manipulate the expression of the genes. Third, the phenotype is analyzed using histology that employs tedious sectioning and staining. The caveats of this process lie in the technical challenge, cost and time consumption. For example, a typical ESC targeting experiment takes 1-2 years depending on the target.

During my Ph. D. study, I have been working on developing new methods for the high-throughput screening purpose in mice. Recently, with the advance in the microbiology field, new systems emerge and are harnessed as molecular tools. In this chapter, I will talk about the following perspectives: 1) Introducing these new molecular systems and explain how they can be used as tools to conduct genetic screening in the mouse olfactory system to study the circuit development; 2) Explaining my design and the rationale behind; 3) Demonstrating the proof of principle experiments and analyzing the preliminary results.

6.1.1 Genetic methods to visualize mRNA and proteins *in vivo*.

For high throughput purpose, a genetic method is preferred to visualize the transcripts and proteins of the genes of interest. This is because the genetic tools are reliable and scalable. Protein probes can be introduced into the cell using the DNA constructs. DNA constructs can be mass produced through molecular cloning to speed up the process. Several methods have been developed to visualize single RNA molecule using protein probes *in vivo* (Halstead et al., 2015; Park et al., 2014). The most successful approach is to genetically insert multiple phage MS2 recognition sequences into the genome regions of the target. The MS2 recognition sequences will be subsequently transcribed on the same mRNA. Multiple MS2 proteins fused with fluorescent proteins bind to the mRNA and render the target with fluorescence. This approach requires the generation of transgenic animals for individual target, making it difficult to apply for high throughput.

The recently discovered CRISPR/C2c2 system is suitable for this purpose. Class 2 type VI-A CRISPR-Cas effector C2c2 recognizes RNA instead of DNA (Abudayyeh et al., 2016). This property makes it a potential molecular tool to detect mRNA. Studies from Doudna lab demonstrate the C2c2 can detect RNA *in vitro* (East-Seletsky et al., 2016). The system has not been tested in eukaryotic systems.

For the proteins of interest, SUNtag system developed by Tanenbaum and colleagues is the best candidate. It achieves single molecule resolution through recruiting multiple florescent proteins on one target (Tanenbaum et al., 2014). The system utilizes an antibody against GCN4. The single-chain variable fragment of the GCN4 antibody is fused with sfGFP and GB1 to make it soluble in the cell. Multiple copies of the epitope from GCN4 are fused to the target protein. When expressed together, Multiple sfGFPs will be recruited to the target protein making it visible by traditional light microscopy.

6.1.2 Genomic editing using CRISPR system

After the target gene's expression is confirmed, genetic interrogation is the next step to study the gene's function. Recently, genomic editing technologies using CRISPR/Cas9 have been developed for high throughput use and gaining great popularity over time because of its high efficiency. Many reviews have been written (Doudna and Charpentier, 2014; Hsu et al., 2014; Sander and Joung, 2014). The most common version for use *in vivo* is a two component system consists of Cas9 and its guide RNA. The guide RNA is a 20-25 nt RNA recognizing its reverse complimentary sequence in the genome. The target in the genome has to have a "NGG" sequence at the end of the guide RNA binding site, called protospacer adjacent motif (PAM). Cas9 binds to the RNA-DNA duplex at the target site and generates double strand break on the DNA. The double strand break is subsequently repaired by DNA repair mechanisms, such as non-homologous end joining (NHEJ) and homology directed repair (HDR). The repair normally generates errors and disrupts the gene's coding sequence if the target is inside the open reading frame.

The system can be harnessed for other purposes other than genome editing. One example is the CRISPR/Cas9 Synergistic Activation Mediator (CRISPR-SAM) system developed by Kornerman and colleagues (Konermann et al., 2014). The CRISPR-SAM system is composed of two modified transcription activator proteins and a modified guide RNA. One of the activators is made by fusing catalytic dead Cas9 (dCas9) with VP64, a transcription activator. The other is a fusion protein formed by two transcription activators, HSF1 and P65, with the phage MS2 protein. Two MS2 recognition sequences are added on the stem loops of the guide RNA. When all the components are expressed in the cell, the guide RNA-dCas9-transcription activator complex recruits the transcription machinery to the target locus to initiate transcription (Abudayyeh et al., 2016; East-Seletsky et al., 2016).

6.1.3 Brain clearing and imaging techniques

Neurons form very complex connectivity. The traditional histology is done by sectioning the brain into thin slices to see the inside of the tissue, as well as to allow the antibodies or other staining agents to contact the targets. The tedious sectioning and staining limit the study of the connectivity. The alternative approach is tissue clearing, which was proposed more than a century ago, but did not become a widespread practice until recently. A comprehensive review of the recent advancements in the tissue clearing has been written by Richardson and Lichtman (Richardson and Lichtman, 2015). Briefly, there are three types of clearings: refractive index matching, hyperhydration, and lipid removal. Some protocols may involve more than one mechanism. The earliest experiment of this kind was done in 1914. Spalteholz described a method for clearing large organs using organic solvents (Spalteholz, 1902, 1914). The principle of this method is simple. The lipid in the cell membrane scatters light. Partially removing lipid helps improve transparency. But this method doesn't meet the needs of fluorescent microscopy. Many new methods are invented to improve the preservation of fluorescence and transparency. BABB and 3DISCO are developed following the same principle (Ertürk et al., 2012). The heterogeneity of the tissue is another factor that scatters the light. Focus clear (CelExplorer Labs Co.), Scale (Hama et al., 2011), ClearT (Kuwajima et al., 2013), SeeDB (Ke et al., 2013), and FRUIT (Hou et al., 2015) are developed to homogenize the refractive index of the tissue by immersing the tissue into a high refractive index solution. However, simply removing the lipid also removes the membrane proteins and destroys the cell's morphology. The effect of refractive index matching is limited without changing the composition of the tissue. A revolutionary approach is CLARITY (Chung et al., 2013). CLARITY fixes the proteins in the tissue onto a hydrogel. It then uses electrophoresis to remove the lipid. This approach drastically decreases the refractive index and renders the tissue transparent. Another way to alter the refractive index is to permanently denature the proteins with urea or other similar chemicals. CUBIC is developed by screening a series of chemicals that could denature and hyperhydrate the proteins (Susaki et al., 2014). These new techniques could be used in the olfactory system to shorten the time of histology and provide an intact view of the samples.

6.2 Material and method

6.2.1 Animals

tetO-GCaMP2, Thy1-eYFP-H, M72-IRES-tauGFP and OMP-IRES-tTA animals (the Jackson laboratory, stock number 017755, 003782, 006676 and 017754 respectively) were described previously. All animals were maintained in Lab Animal Services Facility of Stowers Institute with a 14:10 light cycle, and provided with food and water *ad libitum*. Experimental protocols were approved by the Institutional Animal Care and Use Committee at Stowers Institute and in compliance with the NIH Guide for Care and Use of Animals.

6.2.2 Transgenesis

The tetO-SAM plasmid was purified using BenchPro 2100 (ThermoFisher). The purified plasmid was linearized using AscI and FseI (NEB) and further purified using gel extraction kit (Zymo Research). The linearized DNA was injected to the FVB strain mouse embryo. The potential founders were screened through Transnytex using PCR against Tdtomato. The positive founders were bred with OMP-IRES-tTA and M72-IRES-tauGFP animals.

6.2.3 Adenovirus production

The adenoviruses were produced with the same protocol as in chapter 4. In this case, the pShuttle vectors containing CRISPR systems were used instead of GFP or RFP.

6.2.4 Cloning

All the vectors were constructed by Gibson using Q5 polymerase (NEB). The sgRNA cloning was conducted according to the published protocol (Cong et al., 2013).

6.2.5 CUBIC

CUBIC imaging and staining were conducted according to the published protocol (Susaki et al., 2014). The antibodies used were Rabbit anti-phosphorylated ribosomal protein S6 (Invitrogen 44-923G), mouse anti-Ncam (Sigma C9672), Goat anti-Ocam (R&D systems AF778) donkey anti-rabbit Alexa 488 (Invitrogen), donkey anti-mouse Alexa 488 (Invitrogen), and donkey anti-goat Alexa594 (Invitrogen). The samples were imaged using spinning disk confocal microscope (PerkinElmer)

6.2.6 SeeDB

SeeDB brain clearance was conducted according to the published protocol (Ke et al., 2013). After the treatment, the samples were imaged using LSM 700 confocal microscope (Zeiss).

6.2.7 DiI tracing

Mice were perfused and postfixed overnight with 4% PFA and embedded in 4% low melting point agarose for DiI (Invitrogen) injection. DiI crystals were placed at indicated positions and covered with agarose. The samples were then placed under 37C in 4% PFA without light exposure until imaging. Images were taken using LSM 700 confocal microscope (Zeiss).

6.3 Results

6.3.1 High throughput knockout using adenovirus carrying CRISPR/Cas9

There are several challenges adapting the CRISPR/Cas9 system to the olfactory sensory system. First, Cas9 and the single guide RNA must be introduced into the OSNs *in vivo*. Second, the vector carrying the two components should be made by simple means and be compatible for high throughput production. Third, because Cas9 is a long gene with a length of 4000 bp, the vector must have the packaging capacity to carry the components. Last, the vector should allow the visualization of the phenotype directly.

To achieve these goals, I decided to use adenovirus vector. Compared to making transgenic mice, virus vectors are fast and scalable. Electroporation and in vivo transfection are two faster methods than viruses. But both methods perform poorly in OSNs (Marcucci, 2011). For example, electroporation can only label the cells from embryonic stage to P3. Even when it works, the labeling efficiency is very low. There are several viruses that can infect OSNs, including lentivirus, rabies virus, adenovirus associated virus (AAV), and human simplex virus (HSV). Lentivirus, rabies virus and AAV have very limited packaging capacity (about 3 kb), making it difficult to carry the long Cas9 gene. HSV has a very large packaging capacity. But its production is complex and lengthy. Adenovirus is the most used virus in the OSNs. It has a packaging capacity of 10kb, which is enough for Cas9 together with fluorescent markers. I chose the human adenovirus 5 as the final vector, because it has a well-established production protocol (Luo et al., 2007), and can be produced with very high titer (10^{13} particles/mL).

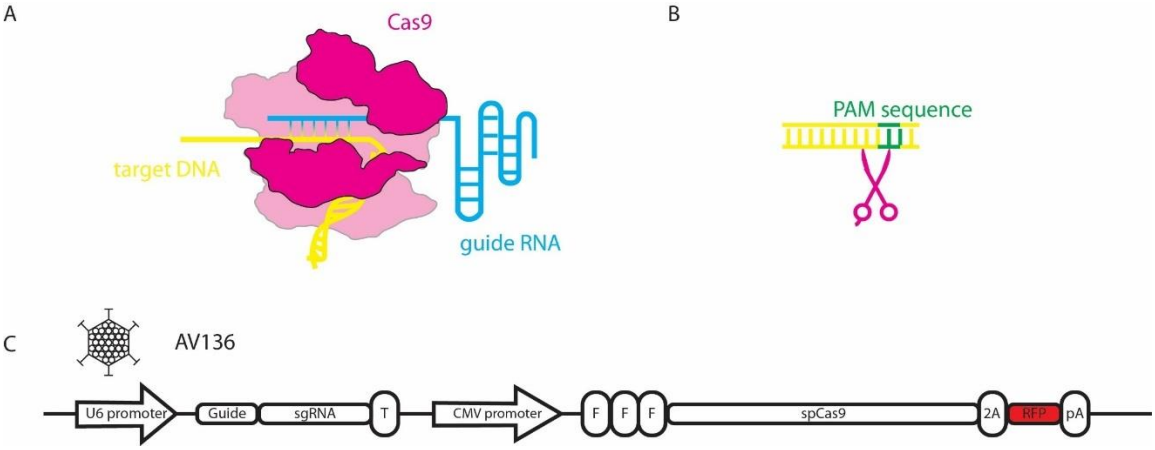

Figure 6.3.1-1 Design of the high throughput knockout vector AV136.

(A) Illustration of Cas9 in association with target DNA and the guide RNA.

(B) Illustration of the Cas9 cleavage site.

(C) Illustration of AV136.

I designed a vector (AV136) that expressed nuclear localized Cas9 under the control of CMV promoter. RFP was express together with Cas9 to visualize the axon morphology. RFP and Cas9 were separated by a 2A self-cleaving peptide to be translated into independent proteins. The guide RNA was expressed on the same vector under a human U6 polymerase III promoter to ensure the precise transcription (Figure 6.3.1-1).

To test the efficiency of the adenovirus mediated genomic editing, I cloned guide RNA against human DNA Ligase IV (also known as Lig4), and guide RNA against eGFP into AV136 (AV136-Lig4 and AV136-GFP). I applied AV136-GFP to the HEK293 cells together with an adenovirus expressing eGFP. None of the cells infected with AV136-GFP showed detectable green fluorescence (Figure 6.3.1-2). In the control vial, both GFP and RFP were expressed in the same cells. The quantification showed that the GFP and RFP fluorescent signals in the AV136-GFP vial were negatively correlated. This result indicates a strong disruption of the eGFP coding sequence. Since multiple viruses could get into one cell, this result also shows AV136 is capable of editing multiple copies of the target sequence.

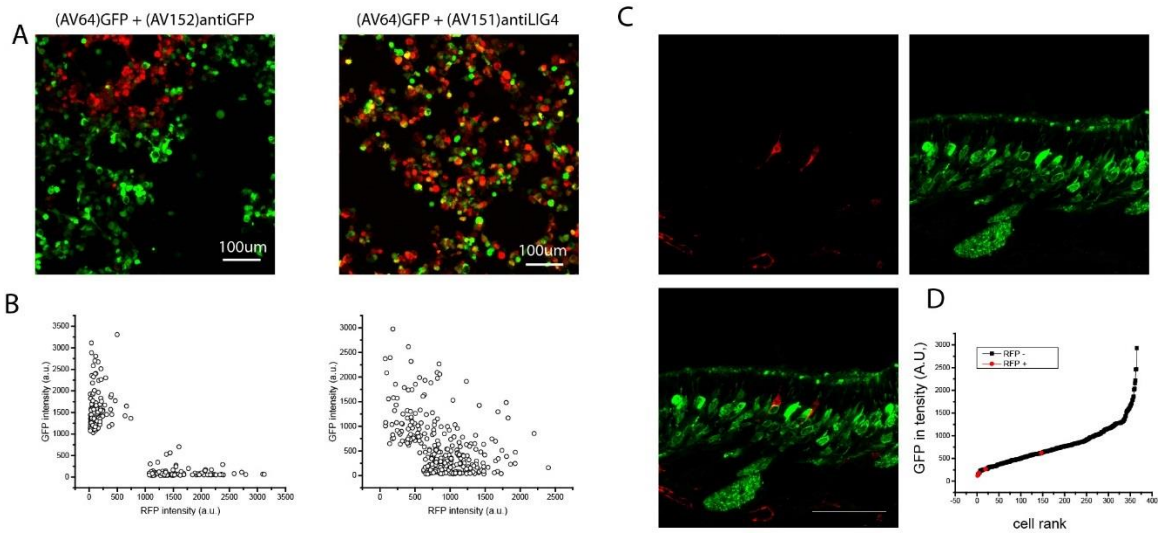

Figure 6.3.1-2 Validation of the adenovirus mediated genome editing *in vitro* and *in vivo*.

(A) Representative images showing HEK293 cells transduced with AV64, AV152 and AV151.

(B) Quantification of the RFP (x axis) and GFP (y axis) intensities in the cells from (A).

(C) Olfactory epithelium sections from the tet-GCaMP2 animal transduced with AV152. The green fluorescence from GCaMP2 in the two cells infected with AV152 (red) are diminished.

(D) Quantification of the green fluorescence in (C). The fluorescence from all cells are shown in black dots. The AV152 infected cells are shown in red.

To test whether AV136 can perform genome editing *in vivo*, I applied AV136-GFP viruses to GCaMP2 animals. GCaMP2 is a modified version of GFP, which contains the targeting site of AV136-GFP. In animals infected with AV136-GFP, GFP fluorescence is eliminated from the virus infected cells (Figure 6.3.1-2). The distribution of GFP fluorescence in this experiment was quantified in Figure 6.3.1-2. Among the RFP positive cells (n=25), only one cell showed noticeable GFP fluorescence (Figure 6.3.1-2). This result showed AV136 could edit genome sequence *in vivo*.

The GFP knockout experiment was tested using an ectopically expressed gene. To test whether AV136 was able to edit the endogenous genomic locus. I applied the AV136-Lig4 viruses to the HEK293 cells. Genome editing is stochastic among cells. PCR cannot reliably detect the genome editing from a single cell. To acquire enough samples for PCR, I isolated single cells and expanded them into colonies. The genomes of the cells in each colony represented the genome of the initial cell. I then did PCR from the single cell derived colonies to detect the genome editing. Multiple PCR bands of different length appeared in the edited cells. Conversely, only one band appeared in the control cells (Figure 6.3.1-3). To confirm these extra bands were actual mutations in Lig4 locus, I cloned and sequenced these bands. The sequencing results confirmed they were mutations from the Lig4 locus (Figure 6.3.1-3). In summary, These results showed that AV136 could edit endogenous locus and could mutate both alleles.

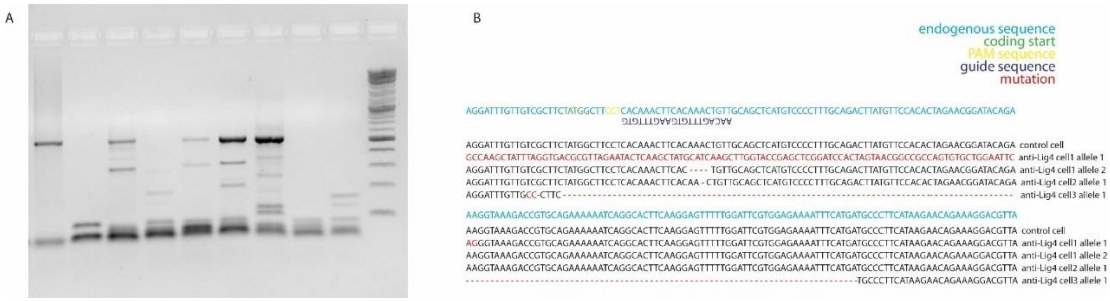

Figure 6.3.1-3 Genomic editing of endogenous locus using adenovirus mediated CRISPR.

(A) PCR products of Lig4 gene from the cells transduced with AV151. PCR products in each lane are from a single cell expanded colony. The first lane is from a colony not transduced by AV151.

(B) Sanger sequencing results of the PCR products. Red color indicates the mutated sequence.

6.3.2 High through-put connectivity profiling using next generation brain imaging techniques

I compared three methods, CLARITY, CUBIC and SeeDB for use in the olfactory system. CLARITY did not work in my test because the brain samples experienced dramatic distortion and even burning during the electrophoresis process. The SeeDB worked very well for the neonatal animals (Figure 6.3.2-4) but did not work well with adult samples. I was able to acquire cleared adult brain samples from the CUBIC (Figure 6.3.2-1) With a regular spinning disc confocal microscope and a 5X lens, I was able to image 2000 um from each sides of the brain. Because of its consistency, I chose the CUBIC for further test.

I tested whether the CUBIC is suitable for immunohistochemistry. Ncam and Ocam are two axon guidance molecules expressed specifically in the OSNs. There are established antibodies and staining protocols to detect them, making them good controls. I performed double immunostainings against Ncam and Ocam using the CUBIC method. The Ncam and Ocam antibodies worked well in the CUBIC processed samples (Figure 6.3.2-2). I was able to obtain the whole bulb distribution of the two molecules. There were some new observations from the whole bulb distribution. First, the necklace glomeruli retained strong staining for Ocam, but not Ncam. Second, the staining intensity of the two molecules in the AOB were different. Ocam stained the entire AOB. But Ncam preferentially stained the anterior axons. Third, the axons of type 1 and type 2 vomeronasal receptors were clearly separated before entering the glomeruli, indicating a pre-target sorting mechanism. Fourth, a small population of anterior glomeruli was also labeled with Ocam, which was easily dismissed in the sectioning.

The major advantage of the whole brain clearing and imaging techniques is the ability to visualize the entire olfactory circuit from an intact brain. Mapping the circuit has been a long-term interest in the olfactory field, because it provides structure information about how the sensory stimulus is represented in the brain. One example is phenethylamine (PEA), a chemical from fox feces that serves as an alarm pheromone for the mice and causes freezing behavior in the mice (Dewan et al., 2013; Liberles and

Buck, 2006). Previous studies showed that only the TAAR4 receptor was specifically activated at a defined concentration. But the downstream olfactory circuit has not been mapped. I took advantage of the staining capacity of the CUBIC, and conducted whole brain olfactory activity mapping using phosphorylated ribosomal protein S6 (pS6) staining. pS6 is an activity marker that can be used to label the neurons responding to a specific external stimulus (Knight et al., 2012). I stimulated the animals with PEA and used mineral oil as a control. Compared to the control animal, PEA activated a very large population of neurons spanning a large area in the piriform cortex. Outside the piriform cortex, some other brain areas were also activated. Among them, the most significant activation was seen in anterior olfactory nucleus (AON). AON could be an important nucleus detecting danger in the environment through olfactory pathway.

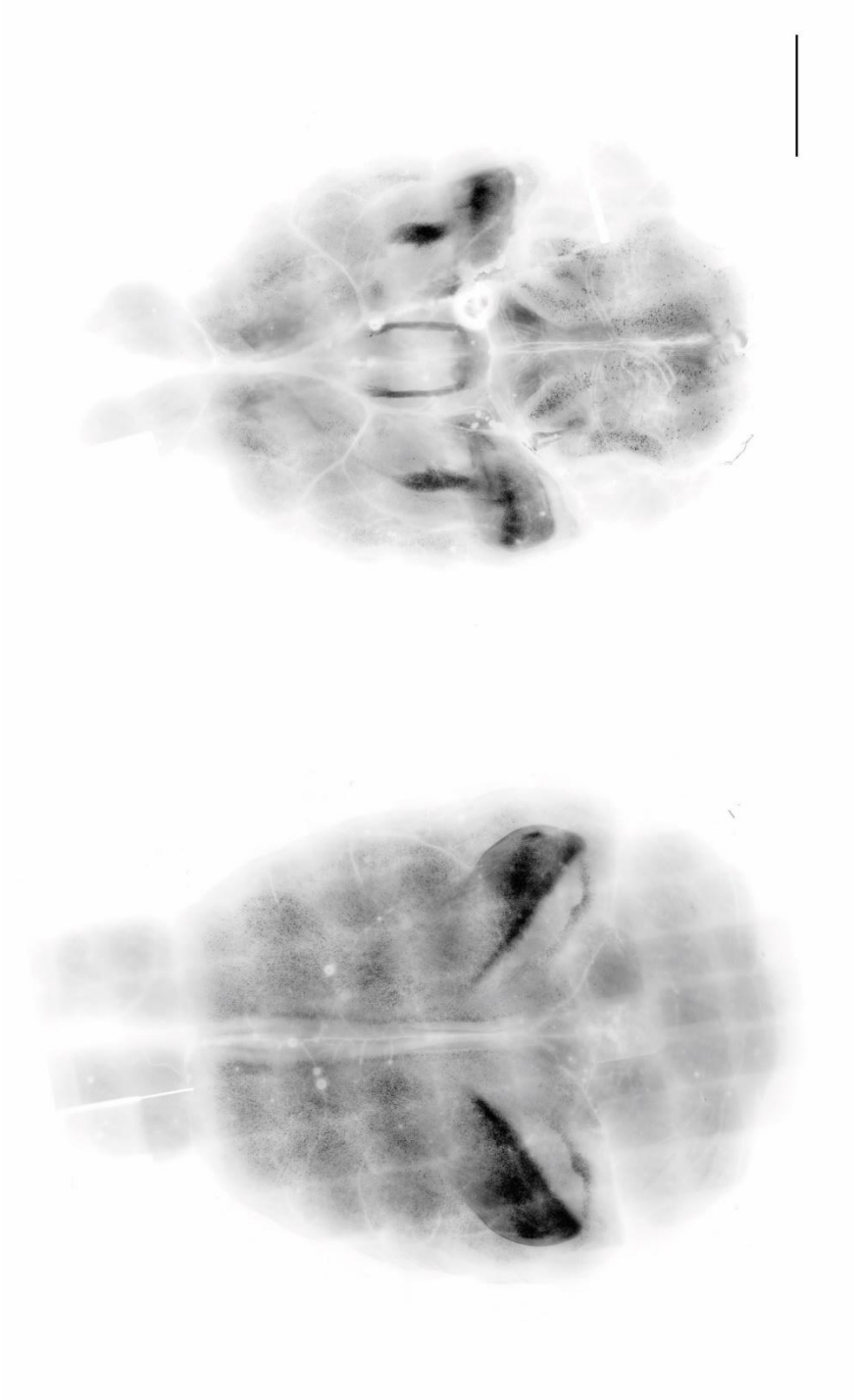

Figure 6.3.2-1 The Thy1-eYFP-H line mouse cleared by CUBIC.

A Thy1-eYFP-H mouse cleared according to the CUBIC method. The image is taken using spinning disk confocal microscope from dorsal (A) and ventral (B) side of the brain. The YFP signal is shown in gray scale.

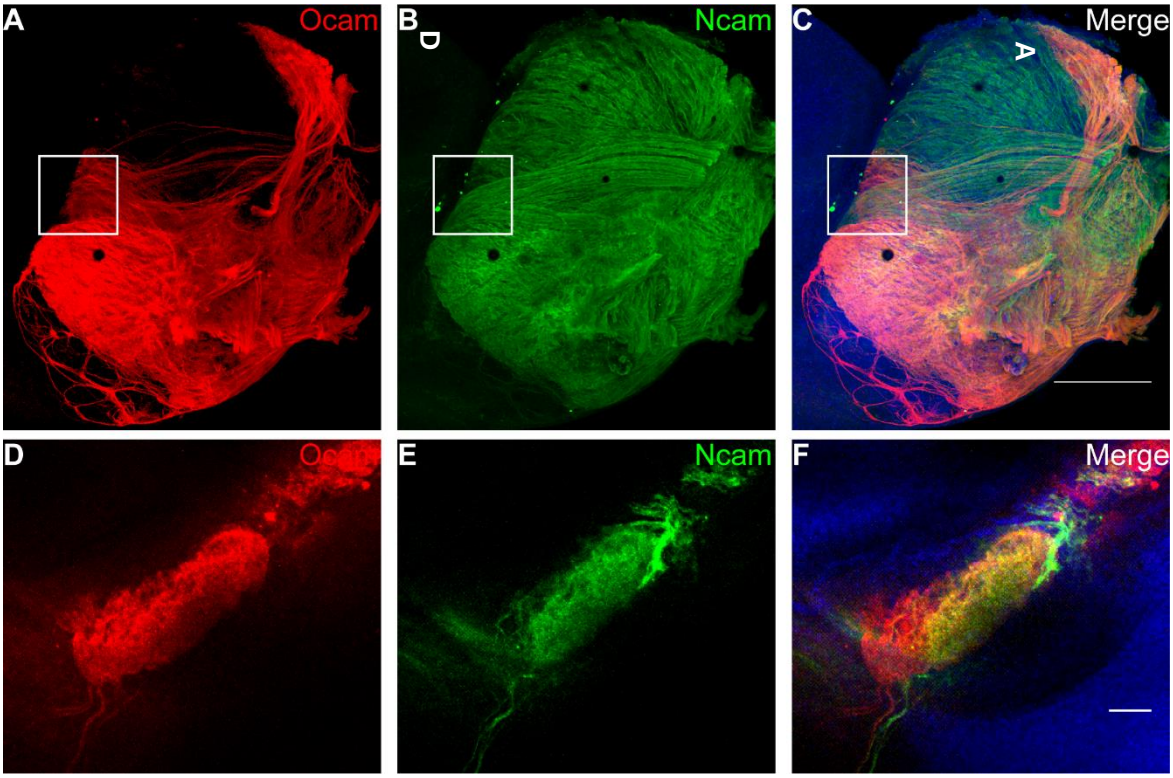

Figure 6.3.2-2 Visualization of axon guidance molecules over the whole olfactory bulb using CUBIC.

The olfactory bulb is processed with CUBIC and stained with antibodies against Ocam (red, A, D) and Ncam (green, B, E). Magnified images of AOB (white box) are shown in D, E, F. The axons expressing Ocam and Ncam enter AOB through different routes.

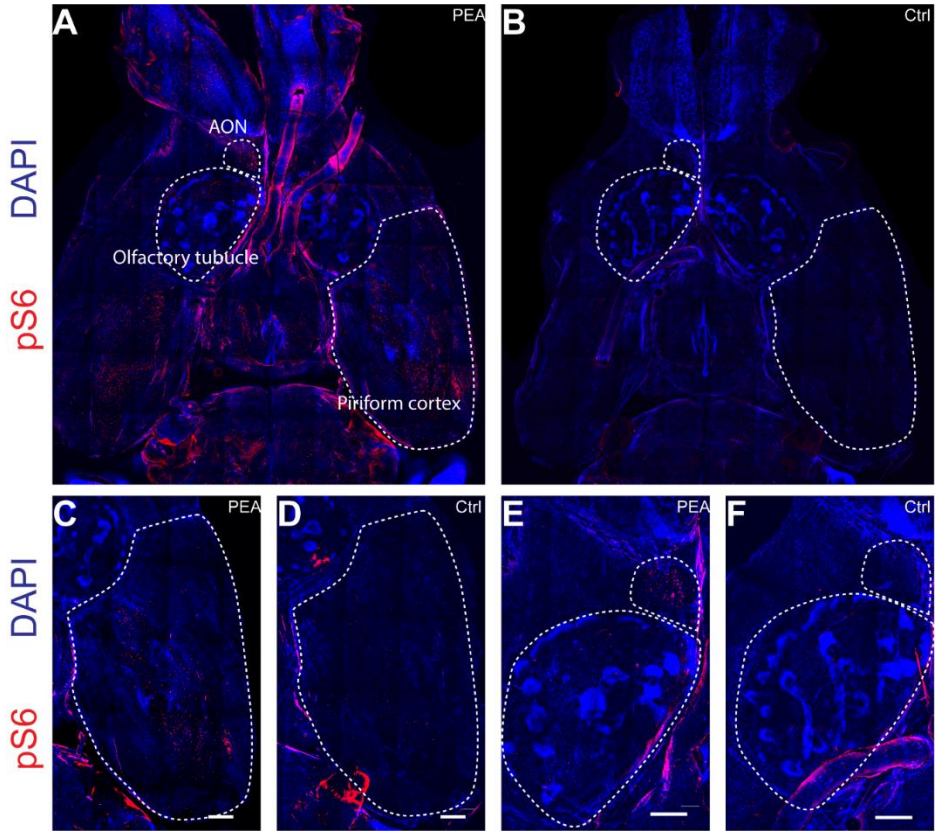

Figure 6.3.2-3 Visualizing the entire olfactory pathway using CUBIC immunohistochemistry

Animals were stimulated with PEA and mineral oil (control). The brains are processed with CUBIC and stained against pS6 (red).

(A) The ventral view of the PEA stimulated brain. Dashed lines indicate anterior olfactory nucleus (AON, E and F upper), olfactory tubucle (OT, E and F bottom), and piriform cortex (C and D).

(B) The ventral view of the control brain.

(C) Magnified image of the piriform cortex from (A).

(D) Magnified image of the piriform cortex from (B).

(E) Magnified image of AON and OT from (A).

(F) Magnified image of AON and OT from (B).

Scale bar: 100 μm. Tissues are counter stained with DAPI (blue).

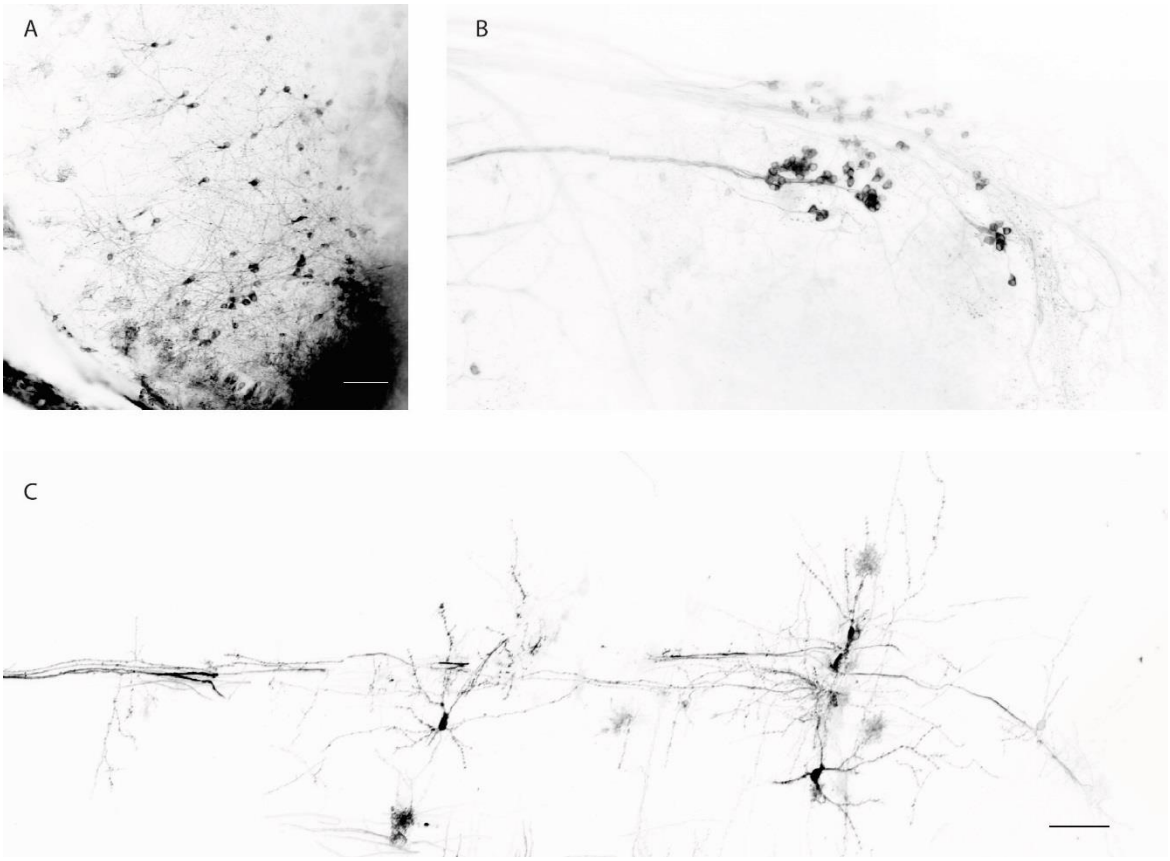

Figure 6.3.2-4 Neurons visualized by SeeDB.

(A) Representative images of mitral cells labeled with DiI and processed with SeeDB.

(B) Representative images of Gruenenburg ganglion labeled with DiI and processed with SeeDB.

(C) Representative images of three cortical neurons labeled with DiI and processed with SeeDB.

Scale bar: 100 μm.

6.3.3 High throughput RNA detection using CRISPR/C2c2 system

To adopt the CRISPR/C2c2 system as a RNA visualization tool *in vivo*, I designed a two-vector virus system. The catalytic dead C2c2 (dC2c2) is expressed from one vector driven by CMV promoter. dC2c2 is tagged with the SUNtag antigens (multiple SUNtags, MS for short) to be amplified in the following steps. The SUNtag recognition antibody, SvFc-sfGFP-GB1 (GFP antibody complex, GC for short) is expressed in another vector together with the guide RNA for dC2c2 (Figure 6.3.3-1). When both vectors are expressed in the cell, dC2c2 will bind to the target mRNA specified by the guide RNA. The GC will recognize the MS fused to dC2c2 and form fluorescent protein aggregations on the target. I named this system CRISPR/C2c2 labeled and amplified RNA tracking (CLARNT).

To test this system, I transfected Neuro2A cells with the CLARNT plasmids. When GC alone was expressed, the sfGFP signal was only seen in the nucleus (Figure 6.3.3-1). When both dC2c2 and GC were expressed, sfGFP was seen both in the nucleus and cytosol, indicating the binding between GC and dC2c2 was pulling the nuclear GFP outside (Figure 6.3.3-1). After the guide RNA against GFP was added, the sfGFP signals formed aggregates in the cytosol. These aggregates were potential GFP mRNAs (Figure 6.3.3-1). I also tested the guide RNA against beta actin (Actb). The sfGFP aggregated into several bright spots in the cytosol too (Figure 6.3.3-1), indicating the successful detection of Actb mRNAs.

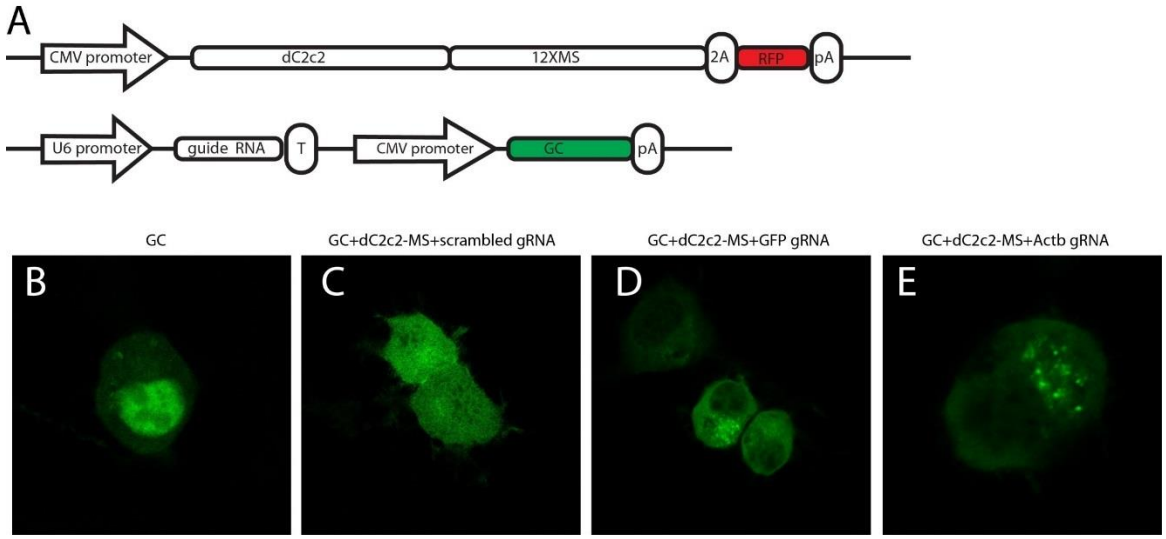

Figure 6.3.3-1 CRISPR/C2c2 labeled and amplified RNA tracking (CLARNT).

(A) Schematic illustration of the experiment design.

(B) – (E) Representative images of Neuro2A cells transfected with different constructs. (B) GC is expressed alone in the cell. (C) GC, dC2c2-MS are expressed with a scrambled guide RNA that doesn't target any transcript. (D) GC, dC2c2-MS are expressed with a guide RNA targeting GFP as a positive control. (E) GC, dC2c2-MS are expressed with a guide RNA targeting beta-actin transcripts.

6.3.4 High through-put ectopic gene activation using CRISPR/SAM

The CRISPR/SAM system has been reported to activate gene expression from silence locus in the genome *in vitro* (Konermann et al., 2014). The system has not been tested in vivo. The SAM system has multiple components. Its long size makes it a challenge to package the entire system in a virus vector. I took an alternative approach. I made a transgenic animal to express the invariant components in the SAM system, including dCas9-VP64, MS2-HSF1-P65, together with a marker Tdtomato. Then the guide RNA for targeting was supplied through adenvirus (AV160) together with a marker BFP (Figure 6.3.4-1). The preliminary results showed successful expression of Tdtomato and BFP. But whether the gene activation works was not tested by the time this thesis was written.

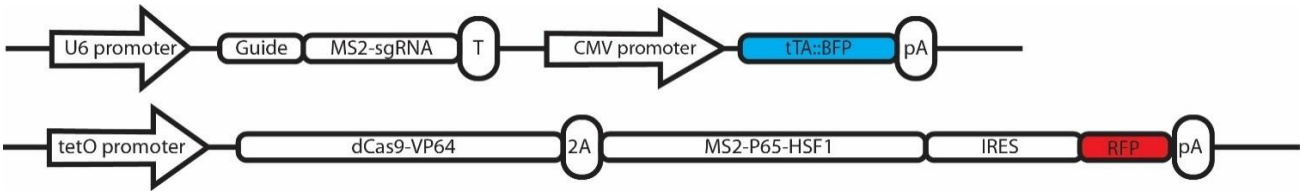

Figure 6.3.4-1 Schematic illustration of the adenovirus mediated CRISPR/SAM system.

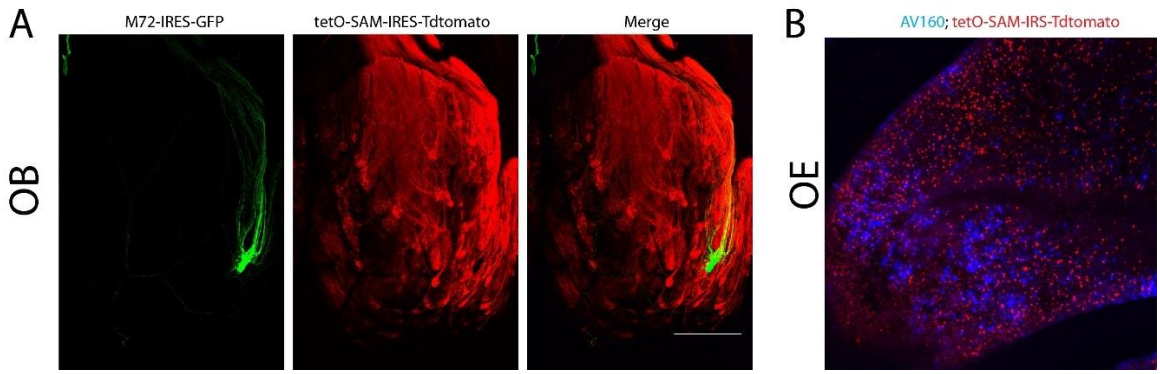

Figure 6.3.4-2 tet-SAM animal and AV160.

(A) Representative image of the M72 glomeruli in the tet-SAM animal.

(B) Olfactory epithelium of tet-SAM animal infected with AV160 (blue). The cells expressing tdTomato are labeled red.

6.4 Discussion.

In this chapter, I have demonstrated a series of proof of principle experiments for the adaptation of the high throughput approach to study the circuit development in the olfactory system. With the successful of these experiment, we can envision a new workflow for a developmental event such as the critical period. In this new scenario, the genes potentially associated with the event can be first screened through RNA-seq by the correlation of timing. The candidate genes are then visualized through CLARNT system. This step can screen for the genes with spatial expression within the cell population of interest. Next, the genes can be knocked out at specific developmental stages using AV136, or ectopically expressed using AV160. The phenotype can be visualized by CUBIC. With this approach, the entire genome, including the non-coding genes could be screened efficiently without bias.

Abbreviations

abbreviation	full name
3DISCO	3D imaging of solvent cleared organs
5-HT	5-hydroxytryptamine, also known as serotonin
AAV	adeno-associated virus
ACIII	adenylate cyclase 3
AdV	adenovirus
ANOVA	analysis of variance
AOB	accessory olfactory bulb
A-P	anterior-posterior axis
Arx	Aristaless Related Homeobox
Ascl	Achaete-Scute Family BHLH Transcription Factor, used in gene names.
ATF5	Activating Transcription Factor 5
AV	adenovirus
BABB	one part benzyl alcohol and two parts benzyl benzoate
BPTF	bromo and PDH-finger transcription factor
BrdU	5-bromo-2'-deoxyuridine
C/EBP	CCAAT enhancer binding protein
CLARITY	Clear Lipid-exchanged Acrylamide-hybridized Rigid Imaging/Immunostaining/In situ hybridization-compatible Tissue-hYdrogel
CNG	cyclic nucleotide gated channel
CREB	cAMP response element-binding protein

CRISPR	Clustered Regularly Interspaced Short Palindromic Repeats
CTX	cortex
CUBIC	Clear, unobstructed brain imaging cocktails and computational analysis
CUBIC	Clear, Unobstructed Brain/Body ImagingCocktails and Computational analysis
DAPI	4',6-diamidino-2-phenylindole, a nuclear staining dye
DIG	Digoxigenin
DiI	a common name for lipophilc tracer 1,1'-Dioctadecyl-3,3,3',3'-Tetramethylindocarbocyanine Perchlorate
Dlx	Distal-Less Homeobox, used in gene names.
DNA	deoxyribonucleic acid
DOX	doxycycline
DTA	diphtheria virus toxin A
D-V	dorsal-ventral axis
EDTA	Ethylenediaminetetraacetic acid
Emx	Empty Spiracles Homeobox
EPL	external plexiform layer
ER	endoplasmic reticulum
ESC	embryonic stem cell
FACS	fluorescence activated cell sorting
FDR	false discovery rate
Fez	Fasciculation And Elongation Protein Zeta
Fgf	Fibroblast growth factor
FRET	Förster resonance energy transfer
Fzd	Frizzled receptor

GABA	gamma-Aminobutyric acid
GAP43	growthcorn associated protein 43
GBC	globose basal cell
GC-D	Guanylyl cyclase-D
GG	Gruenenberg ganglion
Gli	Glioma-Associated Oncogene Family Zinc Finger
Glo	glomerulus
GnRH	Gonadotropin-releasing hormone
Go	Guanine Nucleotide Binding Protein (G Protein), Alpha Activating Activity Polypeptide O
GO	gene ontology
Golf	Guanine Nucleotide Binding Protein (G Protein), Alpha Activating Activity Polypeptide, Olfactory Type
GPCR	G protein coupled receptor
Gs	Guanine Nucleotide Binding Protein (G Protein), Alpha Stimulating Activity Polypeptide
HBC	horizontal basal cell
HDB	horizontal diagnol band
HNPP	2-hydroxy-3-naphtoic acid-2`-phenylanilide phosphate
I7	a common name for olfactory receptor gene Olfr2
IAA	isoamyl alcohol
Igf	Insulin-like growth factor
INP	intermediate progenitor cell
iOSN	immature olfactory sensory neuron

IRES	internal ribosome entry site
Kir	potassium inward rectifier channel
Klf	Krueppel-like factor
LBR	lamin B receptor
LGN	lateral geniculate nucleus
LOT	lateral olfactory tract
LSD1	lysine (K)-specific demethylase 1A
M71	a common name for olfactory receptor gene Olfr151
M72	a common name for olfactory receptor gene Olfr160
MHC	major histocompatibility complex
MOB	main olfactory bulb
MOE	main olfactory epithelium
MOR28	a common name for olfactory receptor gene Olfr1507
mOSN	mature olfactory sensory neuron
MT	mutant
NBT/BCIP	nitro-blue tetrazolium chloride/5-bromo-4-chloro-3'-indolyphosphate p-toluidine salt
Ncam	neural cell adhesion molecule
Next-gen	next generation
Nrp	Neuropilin
OB	olfactory bulb
Ocam	olfactory cell adhesion molecule
OE	olfactory epithelium
OMP	olfactory marker protein

OMP-TetTag	OMP-IRES-tTA;tetZ-tTA
ONL	olfactory nerve layer
OR	olfactory receptor
OSN	Olfactory sensory neuron
P2	a common name for olfactory receptor gene Olfr17
PAM	Protospacer adjacent motif
Pavlb	parvalbumin
PAX	Paired box protein, used in gene names.
PBS	phosphate buffered saline
PBST	phosphate buffered saline with TritionX-100
PCA	principle component analysis
PCR	Polymerase chain reaction
PERK	PKR-like ER kinase
PG	periglomerulus
PKA	protein kinase A
PKC	protein kinase C
Plxn	Plexin
RE	respiratory epithelium
RNA	ribonucleic acid
RNA-seq	RNA sequencing
RTP	receptor transpoter protein
SAM	Synergistic Activation Mediator
SeeDB	see deep brain
Sema	Semaphorin

Six	Sine Oculis Homeobox Homolog
Smo	smoothened
SO	septal organ of Masera
Sox	(sex determining region Y)-box, used in gene names.
sPH	synapto-PHluorin
SVZ	subventricular zone
TAC	transient amplifying cell
TPM	transcript per million reads
tTA	tetracycline trans-activator
UNO	unilateral naris occlusion
VNO	vomeronasal organ
WT	wildtype

7 Reference

Abudayyeh, O.O., Gootenberg, J.S., Konermann, S., Joung, J., Slaymaker, I.M., Cox, D.B., Shmakov, S., Makarova, K.S., Semenova, E., and Minakhin, L. (2016). C2c2 is a single-component programmable RNA-guided RNA-targeting CRISPR effector. Science *353*, aaf5573.

Alvarez-Buylla, A., and Garcıa-Verdugo, J.M. (2002). Neurogenesis in adult subventricular zone. Journal of Neuroscience *22*, 629-634.

Bailey, T.L., and Elkan, C. (1994). Fitting a mixture model by expectation maximization to discover motifs in biopolymers. Proc Int Conf Intell Syst Mol Biol *2*, 28-36.

Barnea, G., O'Donnell, S., Mancia, F., Sun, X., Nemes, A., Mendelsohn, M., and Axel, R. (2004). Odorant receptors on axon termini in the brain. Science *304*, 1468-1468.

Beites, C.L., Kawauchi, S., Crocker, C.E., and Calof, A.L. (2005). Identification and molecular regulation of neural stem cells in the olfactory epithelium. Experimental cell research *306*, 309-316.

Belluscio, L., Gold, G.H., Nemes, A., and Axel, R. (1998). Mice deficient in G olf are anosmic. Neuron *20*, 69-81.

Benjamini, Y., and Hochberg, Y. (1995). Controlling the false discovery rate: a practical and powerful approach to multiple testing. Journal of the royal statistical society Series B (Methodological), 289-300.

Borroto-Escuela, D.O., Tarakanov, A.O., and Fuxe, K. (2016). FGFR1–5-HT1A Heteroreceptor Complexes: Implications for Understanding and Treating Major Depression. Trends in neurosciences *39*, 5-15.

Bozza, T., McGann, J.P., Mombaerts, P., and Wachowiak, M. (2004). In vivo imaging of neuronal activity by targeted expression of a genetically encoded probe in the mouse. Neuron *42*, 9-21.

Brann, J.H., Ellis, D.P., Ku, B.S., Spinazzi, E.F., and Firestein, S. (2015). Injury in aged animals robustly activates quiescent olfactory neural stem cells. Frontiers in neuroscience *9*.

Breer, H., and Fleischer, J. (2010). The Grueneberg ganglion, a novel sensory system in the nose. Histology and histopathology.

Brunet, L.J., Gold, G.H., and Ngai, J. (1996). General anosmia caused by a targeted disruption of the mouse olfactory cyclic nucleotide–gated cation channel. Neuron *17*, 681-693.

Brunjes, P.C. (1994). Unilateral naris closure and olfactory system development. Brain Research Reviews *19*, 146-160.

Buck, L., and Axel, R. (1991). A novel multigene family may encode odorant receptors: a molecular basis for odor recognition. Cell *65*, 175-187.

Bulfone, A., Wang, F., Hevner, R., Anderson, S., Cutforth, T., Chen, S., Meneses, J., Pedersen, R., Axel, R., and Rubenstein, J.L. (1998). An olfactory sensory map develops in the absence of normal projection neurons or GABAergic interneurons. Neuron *21*, 1273-1282.

Carron, C., Pascal, A., Djiane, A., Boucaut, J.-C., Shi, D.-L., and Umbhauer, M. (2003). Frizzled receptor dimerization is sufficient to activate the Wnt/β-catenin pathway. Journal of cell science *116*, 2541-2550.

Cau, E., Casarosa, S., and Guillemot, F. (2002). Mash1 and Ngn1 control distinct steps of determination and differentiation in the olfactory sensory neuron lineage. Development *129*, 1871-1880.

Chen, M., Tian, S., Yang, X., Lane, A.P., Reed, R.R., and Liu, H. (2014). Wnt-responsive Lgr5+ globose basal cells function as multipotent olfactory epithelium progenitor cells. Journal of Neuroscience *34*, 8268-8276.

Cho, J.H., Lépine, M., Andrews, W., Parnavelas, J., and Cloutier, J.-F. (2007). Requirement for Slit-1 and Robo-2 in zonal segregation of olfactory sensory neuron axons in the main olfactory bulb. Journal of Neuroscience *27*, 9094-9104.

Chung, K., Wallace, J., Kim, S.-Y., Kalyanasundaram, S., Andalman, A.S., Davidson, T.J., Mirzabekov, J.J., Zalocusky, K.A., Mattis, J., and Denisin, A.K. (2013). Structural and molecular interrogation of intact biological systems. Nature *497*, 332-337.

Clevers, H. (2006). Wnt/β-catenin signaling in development and disease. Cell *127*, 469-480.

Clowney, E.J., LeGros, M.A., Mosley, C.P., Clowney, F.G., Markenskoff-Papadimitriou, E.C., Myllys, M., Barnea, G., Larabell, C.A., and Lomvardas, S. (2012). Nuclear aggregation of olfactory receptor genes governs their monogenic expression. Cell *151*, 724-737.

Cong, L., Ran, F.A., Cox, D., Lin, S., Barretto, R., Habib, N., Hsu, P.D., Wu, X., Jiang, W., and Marraffini, L.A. (2013). Multiplex genome engineering using CRISPR/Cas systems. Science *339*, 819-823.

Connelly, T., Savigner, A., and Ma, M. (2013). Spontaneous and sensory-evoked activity in mouse olfactory sensory neurons with defined odorant receptors. J Neurophysiol *110*, 55-62.

Conzelmann, S., Levai, O., Breer, H., and Strotmann, J. (2002). Extraepithelial cells expressing distinct olfactory receptors are associated with axons of sensory cells with the same receptor type. Cell and tissue research *307*, 293-301.

Costanzo, R.M. (2000). Rewiring the olfactory bulb: changes in odor maps following recovery from nerve transection. Chemical senses *25*, 199-205.

Cummings, D.M., and Belluscio, L. (2010). Continuous neural plasticity in the olfactory intrabulbar circuitry. Journal of Neuroscience *30*, 9172-9180.

Dalton, R.P., and Lomvardas, S. (2015). Chemosensory receptor specificity and regulation. Annual review of neuroscience *38*, 331-349.

Dalton, R.P., Lyons, D.B., and Lomvardas, S. (2013). Co-opting the unfolded protein response to elicit olfactory receptor feedback. Cell *155*, 321-332.

Dewan, A., Pacifico, R., Zhan, R., Rinberg, D., and Bozza, T. (2013). Non-redundant coding of aversive odours in the main olfactory pathway. Nature *497*, 486-489.

Doudna, J.A., and Charpentier, E. (2014). The new frontier of genome engineering with CRISPR-Cas9. Science *346*, 1258096.

East-Seletsky, A., O'Connell, M.R., Knight, S.C., Burstein, D., Cate, J.H., Tjian, R., and Doudna, J.A. (2016). Two distinct RNase activities of CRISPR-C2c2 enable guide-RNA processing and RNA detection. Nature *538*, 270-273.

Ertürk, A., Becker, K., Jährling, N., Mauch, C.P., Hojer, C.D., Egen, J.G., Hellal, F., Bradke, F., Sheng, M., and Dodt, H.-U. (2012). Three-dimensional imaging of solvent-cleared organs using 3DISCO. Nature protocols *7*, 1983-1995.

Erzurumlu, R.S., and Gaspar, P. (2012). Development and critical period plasticity of the barrel cortex. European Journal of Neuroscience *35*, 1540-1553.

Feinstein, P., and Mombaerts, P. (2004). A contextual model for axonal sorting into glomeruli in the mouse olfactory system. Cell *117*, 817-831.

Filiano, A.J., Xu, Y., Tustison, N.J., Marsh, R.L., Baker, W., Smirnov, I., Overall, C.C., Gadani, S.P., Turner, S.D., and Weng, Z. (2016). Unexpected role of interferon-γ in regulating neuronal connectivity and social behaviour. Nature *535*, 425-429.

Fleischmann, A., Shykind, B.M., Sosulski, D.L., Franks, K.M., Glinka, M.E., Mei, D.F., Sun, Y., Kirkland, J., Mendelsohn, M., and Albers, M.W. (2008). Mice with a "monoclonal nose": perturbations in an olfactory map impair odor discrimination. Neuron *60*, 1068-1081.

Gogos, J.A., Osborne, J., Nemes, A., Mendelsohn, M., and Axel, R. (2000). Genetic ablation and restoration of the olfactory topographic map. Cell *103*, 609-620.

Gong, Q., and Shipley, M.T. (1995). Evidence that pioneer olfactory axons regulate telencephalon cell cycle kinetics to induce the formation of the olfactory bulb. Neuron *14*, 91-101.

Gordon, M.D., and Nusse, R. (2006). Wnt signaling: multiple pathways, multiple receptors, and multiple transcription factors. Journal of Biological Chemistry *281*, 22429-22433.

Graziadei, P.P., Levine, R.R., and Graziadei, G.A. (1978). Regeneration of olfactory axons and synapse formation in the forebrain after bulbectomy in neonatal mice. Proceedings of the National Academy of Sciences of the United States of America *75*, 5230-5234.

Greer, P.L., Bear, D.M., Lassance, J.M., Bloom, M.L., Tsukahara, T., Pashkovski, S.L., Masuda, F.K., Nowlan, A.C., Kirchner, R., Hoekstra, H.E., *et al.* (2016). A Family of non-GPCR Chemosensors Defines an Alternative Logic for Mammalian Olfaction. Cell *165*, 1734-1748.

Guillemot, F., Lo, L.-C., Johnson, J.E., Auerbach, A., Anderson, D.J., and Joyner, A.L. (1993). Mammalian achaete-scute homolog 1 is required for the early development of olfactory and autonomic neurons. Cell *75*, 463-476.

Haga-Yamanaka, S., Ma, L., He, J., Qiu, Q., Lavis, L.D., Looger, L.L., and Yu, C.R. (2014). Integrated action of pheromone signals in promoting courtship behavior in male mice. Elife *3*, e03025.

Hall, S.E., Floriano, W.B., Vaidehi, N., and Goddard, W.A. (2004). Predicted 3-D structures for mouse I7 and rat I7 olfactory receptors and comparison of predicted odor recognition profiles with experiment. Chemical senses *29*, 595-616.

Halstead, J.M., Lionnet, T., Wilbertz, J.H., Wippich, F., Ephrussi, A., Singer, R.H., and Chao, J.A. (2015). An RNA biosensor for imaging the first round of translation from single cells to living animals. Science *347*, 1367-1671.

Hama, H., Kurokawa, H., Kawano, H., Ando, R., Shimogori, T., Noda, H., Fukami, K., Sakaue-Sawano, A., and Miyawaki, A. (2011). Scale: a chemical approach for fluorescence imaging and reconstruction of transparent mouse brain. Nature neuroscience *14*, 1481-1488.

Hanchate, N.K., Kondoh, K., Lu, Z., Kuang, D., Ye, X., Qiu, X., Pachter, L., Trapnell, C., and Buck, L.B. (2015). Single-cell transcriptomics reveals receptor transformations during olfactory neurogenesis. Science *350*, 1251-1255.

He, J., Ma, L., Kim, S., Nakai, J., and Yu, C.R. (2008). Encoding gender and individual information in the mouse vomeronasal organ. Science *320*, 535-538.

Hedgecock, E.M., Culotti, J.G., and Hall, D.H. (1990). The unc-5, unc-6, and unc-40 genes guide circumferential migrations of pioneer axons and mesodermal cells on the epidermis in C. elegans. Neuron *4*, 61-85.

Hensch, T.K. (2004). Critical period regulation. Annu Rev Neurosci *27*, 549-579.

Hensch, T.K. (2005). Critical period plasticity in local cortical circuits. Nature Reviews Neuroscience *6*, 877-888.

Hou, B., Zhang, D., Zhao, S., Wei, M., Yang, Z., Wang, S., Wang, J., Zhang, X., Liu, B., and Fan, L. (2015). Scalable and DiI-compatible optical clearance of the mammalian brain. Frontiers in neuroanatomy *9*, 19.

Hsu, P.D., Lander, E.S., and Zhang, F. (2014). Development and applications of CRISPR-Cas9 for genome engineering. Cell *157*, 1262-1278.

Huard, J.M., and Schwob, J.E. (1995). Cell cycle of globose basal cells in rat olfactory epithelium. Developmental dynamics *203*, 17-26.

Hubel, D.H., and Wiesel, T.N. (1959). Receptive fields of single neurones in the cat's striate cortex. The Journal of physiology *148*, 574-591.

Hubel, D.H., and Wiesel, T.N. (1962). Receptive fields, binocular interaction and functional architecture in the cat's visual cortex. The Journal of physiology *160*, 106-154.

Hubel, D.H., and Wiesel, T.N. (1970). The period of susceptibility to the physiological effects of unilateral eye closure in kittens. The Journal of physiology *206*, 419.

Igarashi, K.M., Ieki, N., An, M., Yamaguchi, Y., Nagayama, S., Kobayakawa, K., Kobayakawa, R., Tanifuji, M., Sakano, H., and Chen, W.R. (2012). Parallel mitral and tufted cell pathways route distinct odor information to different targets in the olfactory cortex. Journal of Neuroscience *32*, 7970-7985.

Imai, T., Yamazaki, T., Kobayakawa, R., Kobayakawa, K., Abe, T., Suzuki, M., and Sakano, H. (2009). Pre-target axon sorting establishes the neural map topography. Science *325*, 585-590.

Ishii, T., Omura, M., and Mombaerts, P. (2004). Protocols for two-and three-color fluorescent RNA in situ hybridization of the main and accessory olfactory epithelia in mouse. Journal of neurocytology *33*, 657-669.

Jang, W., Chen, X., Flis, D., Harris, M., and Schwob, J.E. (2014). Label‐retaining, quiescent globose basal cells are found in the olfactory epithelium. Journal of Comparative Neurology *522*, 731-749.

Jerison, H. (2012). Evolution of the Brain and Intelligence (Elsevier).

Johnson, J.S., and Newport, E.L. (1989). Critical period effects in second language learning: The influence of maturational state on the acquisition of English as a second language. Cognitive psychology *21*, 60-99.

Jones, D.T., Masters, S.B., Bourne, H.R., and Reed, R.R. (1990). Biochemical characterization of three stimulatory GTP-binding proteins. The large and small forms of Gs and the olfactory-specific G-protein, Golf. Journal of Biological Chemistry *265*, 2671-2676.

Katada, S., Hirokawa, T., Oka, Y., Suwa, M., and Touhara, K. (2005). Structural basis for a broad but selective ligand spectrum of a mouse olfactory receptor: mapping the odorant-binding site. Journal of Neuroscience *25*, 1806-1815.

Ke, M.-T., Fujimoto, S., and Imai, T. (2013). SeeDB: a simple and morphology-preserving optical clearing agent for neuronal circuit reconstruction. Nature neuroscience *16*, 1154-1161.

Khan, M., Vaes, E., and Mombaerts, P. (2011). Regulation of the probability of mouse odorant receptor gene choice. Cell *147*, 907-921.

Knight, Z.A., Tan, K., Birsoy, K., Schmidt, S., Garrison, J.L., Wysocki, R.W., Emiliano, A., Ekstrand, M.I., and Friedman, J.M. (2012). Molecular profiling of activated neurons by phosphorylated ribosome capture. Cell *151*, 1126-1137.

Konermann, S., Brigham, M.D., Trevino, A.E., Joung, J., Abudayyeh, O.O., Barcena, C., Hsu, P.D., Habib, N., Gootenberg, J.S., and Nishimasu, H. (2014). Genome-scale transcriptional activation by an engineered CRISPR-Cas9 complex. Nature.

Kral, A. (2013). Auditory critical periods: a review from system's perspective. Neuroscience *247*, 117-133.

Kuwajima, T., Sitko, A.A., Bhansali, P., Jurgens, C., Guido, W., and Mason, C. (2013). ClearT: a detergent- and solvent-free clearing method for neuronal and non-neuronal tissue. Development *140*, 1364-1368.

Lee, S.Y., and Soltesz, I. (2011). Cholecystokinin: A multi‐functional molecular switch of neuronal circuits. Developmental neurobiology *71*, 83-91.

Lewis, T.L., and Maurer, D. (2005). Multiple sensitive periods in human visual development: evidence from visually deprived children. Developmental psychobiology *46*, 163-183.

Liberles, S.D., and Buck, L.B. (2006). A second class of chemosensory receptors in the olfactory epithelium. Nature *442*, 645-650.

Lin, D.M., Wang, F., Lowe, G., Gold, G.H., Axel, R., Ngai, J., and Brunet, L. (2000). Formation of precise connections in the olfactory bulb occurs in the absence of odorant-evoked neuronal activity. Neuron *26*, 69-80.

Liu, Y., Wang, X., Lu, C.-C., Sherman-Kermen, R., Steward, O., Xu, X.-M., and Zou, Y. (2008). Repulsive Wnt signaling inhibits axon regeneration after CNS injury. Journal of Neuroscience *28*, 8376-8382.

Luo, J., Deng, Z.-L., Luo, X., Tang, N., Song, W.-X., Chen, J., Sharff, K.A., Luu, H.H., Haydon, R.C., and Kinzler, K.W. (2007). A protocol for rapid generation of recombinant adenoviruses using the AdEasy system. Nature protocols *2*, 1236-1247.

Lyons, D.B., Allen, W.E., Goh, T., Tsai, L., Barnea, G., and Lomvardas, S. (2013). An epigenetic trap stabilizes singular olfactory receptor expression. Cell *154*, 325-336.

Lyuksyutova, A.I., Lu, C.-C., Milanesio, N., King, L.A., Guo, N., Wang, Y., Nathans, J., Tessier-Lavigne, M., and Zou, Y. (2003). Anterior-posterior guidance of commissural axons by Wnt-frizzled signaling. Science *302*, 1984-1988.

Ma, L., Wu, Y., Qiu, Q., Scheerer, H., Moran, A., and Yu, C.R. (2014). A developmental switch of axon targeting in the continuously regenerating mouse olfactory system. Science *344*, 194-197.

Magklara, A., Yen, A., Colquitt, B.M., Clowney, E.J., Allen, W., Markenscoff-Papadimitriou, E., Evans, Z.A., Kheradpour, P., Mountoufaris, G., and Carey, C. (2011). An epigenetic signature for monoallelic olfactory receptor expression. Cell *145*, 555-570.

Malnic, B., Hirono, J., Sato, T., and Buck, L.B. (1999). Combinatorial receptor codes for odors. Cell *96*, 713-723.

Marcucci, F. (2011). Axon Development and Synapse Formation in Olfactory Sensory Neurons (Columbia University).

Markenscoff-Papadimitriou, E., Allen, W.E., Colquitt, B.M., Goh, T., Murphy, K.K., Monahan, K., Mosley, C.P., Ahituv, N., and Lomvardas, S. (2014). Enhancer interaction networks as a means for singular olfactory receptor expression. Cell *159*, 543-557.

McIntyre, J.C., Titlow, W.B., and McClintock, T.S. (2010). Axon growth and guidance genes identify nascent, immature, and mature olfactory sensory neurons. Journal of neuroscience research *88*, 3243-3256.

Mitsui, S., Igarashi, K.M., Mori, K., and Yoshihara, Y. (2011). Genetic visualization of the secondary olfactory pathway in Tbx21 transgenic mice. Neural systems & circuits *1*, 5.

Miyamichi, K., Amat, F., Moussavi, F., Wang, C., Wickersham, I., Wall, N.R., Taniguchi, H., Tasic, B., Huang, Z.J., and He, Z. (2011). Cortical representations of olfactory input by trans-synaptic tracing. Nature *472*, 191-196.

Mombaerts, P., Wang, F., Dulac, C., Chao, S.K., Nemes, A., Mendelsohn, M., Edmondson, J., and Axel, R. (1996). Visualizing an olfactory sensory map. Cell *87*, 675-686.

Mori, K., and Sakano, H. (2011). How is the olfactory map formed and interpreted in the mammalian brain? Annu Rev Neurosci *34*, 467-499.

Mori, K., Takahashi, Y.K., Igarashi, K.M., and Yamaguchi, M. (2006). Maps of odorant molecular features in the mammalian olfactory bulb. Physiological reviews *86*, 409-433.

Movahedi, K., Grosmaitre, X., and Feinstein, P. (2016). Odorant receptors can mediate axonal identity and gene choice via cAMP-independent mechanisms. Open biology *6*.

Murdoch, B., and Roskams, A.J. (2008). A novel embryonic nestin-expressing radial glia-like progenitor gives rise to zonally restricted olfactory and vomeronasal neurons. Journal of Neuroscience *28*, 4271-4282.

Nagai, Y., Sano, H., and Yokoi, M. (2005). Transgenic expression of Cre recombinase in mitral/tufted cells of the olfactory bulb. Genesis *43*, 12-16.

Nakashima, A., Takeuchi, H., Imai, T., Saito, H., Kiyonari, H., Abe, T., Chen, M., Weinstein, L.S., Yu, C.R., and Storm, D.R. (2013). Agonist-independent GPCR activity regulates anterior-posterior targeting of olfactory sensory neurons. Cell *154*, 1314-1325.

Nguyen-Ba-Charvet, K.T., Di Meglio, T., Fouquet, C., and Chédotal, A. (2008). Robos and slits control the pathfinding and targeting of mouse olfactory sensory axons. Journal of Neuroscience *28*, 4244-4249.

Nguyen, M.Q., Zhou, Z., Marks, C.A., Ryba, N.J., and Belluscio, L. (2007). Prominent roles for odorant receptor coding sequences in allelic exclusion. Cell *131*, 1009-1017.

Nishimura, S., Bilgüvar, K., Ishigame, K., Sestan, N., Günel, M., and Louvi, A. (2015). Functional synergy between cholecystokinin receptors CCKAR and CCKBR in mammalian brain development. PloS one *10*, e0124295.

Norlin, E.M., Alenius, M., Gussing, F., Hägglund, M., Vedin, V., and Bohm, S. (2001). Evidence for gradients of gene expression correlating with zonal topography of the olfactory sensory map. Molecular and Cellular Neuroscience *18*, 283-295.

Nusse, R. (2005). Wnt signaling in disease and in development. Cell research *15*, 28-32.

Nusse, R., Brown, A., Papkoff, J., Scambler, P., Shackleford, G., McMahon, A., Moon, R., and Varmu, H. (1991). A New Nomenclature for in&l and Related Genes: The Writ Gene Family. Cell *64*, 231-232.

Nusse, R., van Ooyen, A., Cox, D., Fung, Y.K.T., and Varmus, H. (1984). Mode of proviral activation of a putative mammary oncogene (int-1) on mouse chromosome 15. Nature *307*, 131-136.

Packard, A., Giel‐Moloney, M., Leiter, A., and Schwob, J.E. (2011). Progenitor cell capacity of NeuroD1‐expressing globose basal cells in the mouse olfactory epithelium. Journal of Comparative Neurology *519*, 3580-3596.

Packard, M., Mathew, D., and Budnik, V. (2003). Wnts and TGFβ in synaptogenesis: old friends signalling at new places. Nature Reviews Neuroscience *4*, 113-120.

Park, H.Y., Lim, H., Yoon, Y.J., Follenzi, A., Nwokafor, C., Lopez-Jones, M., Meng, X., and Singer, R.H. (2014). Visualization of dynamics of single endogenous mRNA labeled in live mouse. Science *343*, 422-424.

Parmentier, M. (2015). GPCRs: Heterodimer-specific signaling. Nature chemical biology *11*, 244-245.

Paschaki, M., Cammas, L., Muta, Y., Matsuoka, Y., Mak, S.-S., Rataj-Baniowska, M., Fraulob, V., Dollé, P., and Ladher, R.K. (2013). Retinoic acid regulates olfactory progenitor cell fate and differentiation. Neural development *8*, 13.

Potter, S.M., Zheng, C., Koos, D.S., Feinstein, P., Fraser, S.E., and Mombaerts, P. (2001). Structure and emergence of specific olfactory glomeruli in the mouse. Journal of Neuroscience *21*, 9713-9723.

Qiu, Q., Scott, A., Scheerer, H., Sapkota, N., Lee, D.K., Ma, L., and Yu, C.R. (2014). Automated analyses of innate olfactory behaviors in rodents. PloS one *9*, e93468.

Reed, R.R. (1992). Signaling pathways in odorant detection. Neuron *8*, 205-209.

Reijmers, L.G., Perkins, B.L., Matsuo, N., and Mayford, M. (2007). Localization of a stable neural correlate of associative memory. Science *317*, 1230-1233.

Ressler, K.J., Sullivan, S.L., and Buck, L.B. (1993). A zonal organization of odorant receptor gene expression in the olfactory epithelium. Cell *73*, 597-609.

Richard, M.B., Taylor, S.R., and Greer, C.A. (2010). Age-induced disruption of selective olfactory bulb synaptic circuits. Proceedings of the National Academy of Sciences *107*, 15613-15618.

Richardson, D.S., and Lichtman, J.W. (2015). Clarifying tissue clearing. Cell *162*, 246-257.

Rodolfo-Masera, T. (1943). Su l'esistenza di un particolare organo olfacttivo nel setto nasale della cavia e di altri roditori. Arch Ital Anat Embryol *48*, 157–212.

Rodriguez‐Gil, D.J., and Greer, C.A. (2008). Wnt/Frizzled family members mediate olfactory sensory neuron axon extension. Journal of Comparative Neurology *511*, 301-317.

Rodriguez, J., Esteve, P., Weinl, C., Ruiz, J.M., Fermin, Y., Trousse, F., Dwivedy, A., Holt, C., and Bovolenta, P. (2005). SFRP1 regulates the growth of retinal ganglion cell axons through the Fz2 receptor. Nature neuroscience *8*, 1301-1309.

Rosso, S.B., Sussman, D., Wynshaw-Boris, A., and Salinas, P.C. (2005). Wnt signaling through Dishevelled, Rac and JNK regulates dendritic development. Nature neuroscience *8*, 34-42.

Royal, S.J., and Key, B. (1999). Development of P2 olfactory glomeruli in P2-internal ribosome entry site-tau-LacZ transgenic mice. Journal of Neuroscience *19*, 9856-9864.

Ryba, N.J., and Tirindelli, R. (1995). A novel GTP-binding protein gamma-subunit, G gamma 8, is expressed during neurogenesis in the olfactory and vomeronasal neuroepithelia. J Biol Chem *270*, 6757-6767.

Saito, H., Kubota, M., Roberts, R.W., Chi, Q., and Matsunami, H. (2004). RTP family members induce functional expression of mammalian odorant receptors. Cell *119*, 679-691.

Sakano, H. (2010). Neural map formation in the mouse olfactory system. Neuron *67*, 530-542.

Sander, J.D., and Joung, J.K. (2014). CRISPR-Cas systems for editing, regulating and targeting genomes. Nature biotechnology *32*, 347-355.

Sathyanesan, A., Feijoo, A., Mehta, S., Nimarko, A., and Lin, W. (2013). Expression profile of G-protein βγ subunit gene transcripts in the mouse olfactory sensory epithelia. Frontiers in Cellular Neuroscience *7*.

Schmitt, A.M., Shi, J., Wolf, A.M., Lu, C.-C., King, L.A., and Zou, Y. (2006). Wnt–Ryk signalling mediates medial–lateral retinotectal topographic mapping. Nature *439*, 31-37.

Schulte, G., and Bryja, V. (2007). The Frizzled family of unconventional G-protein-coupled receptors. Trends in pharmacological sciences *28*, 518-525.

Schwanzel-Fukuda, M., and Pfaff, D.W. (1989). Origin of luteinizing hormone-releasing hormone neurons. Nature *338*, 161-164.

Schwob, J.E., Youngentob, S.L., and Mezza, R.C. (1995). Reconstitution of the rat olfactory epithelium after methyl bromide‐induced lesion. Journal of Comparative Neurology *359*, 15-37.

Scolnick, J.A., Cui, K., Duggan, C.D., Xuan, S., Yuan, X.-b., Efstratiadis, A., and Ngai, J. (2008a). Role of IGF signaling in olfactory sensory map formation and axon guidance. Neuron *57*, 847-857.

Scolnick, J.A., Cui, K., Duggan, C.D., Xuan, S., Yuan, X.B., Efstratiadis, A., and Ngai, J. (2008b). Role of IGF signaling in olfactory sensory map formation and axon guidance. Neuron *57*, 847-857.

Scovel, T. (1988). A time to speak: A psycholinguistic inquiry into the critical period for human speech (Newbury House Publishers).

Serafini, T., Kennedy, T.E., Gaiko, M.J., Mirzayan, C., Jessell, T.M., and Tessier-Lavigne, M. (1994). The netrins define a family of axon outgrowth-promoting proteins homologous to C. elegans UNC-6. Cell *78*, 409-424.

Serizawa, S., Ishii, T., Nakatani, H., Tsuboi, A., Nagawa, F., Asano, M., Sudo, K., Sakagami, J., Sakano, H., and Ijiri, T. (2000). Mutually exclusive expression of odorant receptor transgenes. Nature neuroscience *3*, 687-693.

Serizawa, S., Miyamichi, K., Nakatani, H., Suzuki, M., Saito, M., Yoshihara, Y., and Sakano, H. (2003). Negative feedback regulation ensures the one receptor-one olfactory neuron rule in mouse. Science *302*, 2088-2094.

Serizawa, S., Miyamichi, K., Takeuchi, H., Yamagishi, Y., Suzuki, M., and Sakano, H. (2006). A neuronal identity code for the odorant receptor-specific and activity-dependent axon sorting. Cell *127*, 1057-1069.

Sosulski, D.L., Bloom, M.L., Cutforth, T., Axel, R., and Datta, S.R. (2011). Distinct representations of olfactory information in different cortical centres. Nature *472*, 213-216.

Spalteholz, W. (1902). HAND ATLAS OF HUMAN ANATOMY. The American Journal of the Medical Sciences *123*, 896.

Spalteholz, W. (1914). Über das Durchsichtigmachen von menschlichen und tierischen Präparaten und seine theoretischen Bedingungen, nebst Anhang: Über Knochenfärbung (S. Hirzel).

St John, J.A., Clarris, H.J., McKeown, S., Royal, S., and Key, B. (2003). Sorting and convergence of primary olfactory axons are independent of the olfactory bulb. Journal of Comparative Neurology *464*, 131-140.

Stettler, D.D., and Axel, R. (2009). Representations of odor in the piriform cortex. Neuron *63*, 854-864.

Susaki, E.A., Tainaka, K., Perrin, D., Kishino, F., Tawara, T., Watanabe, T.M., Yokoyama, C., Onoe, H., Eguchi, M., and Yamaguchi, S. (2014). Whole-brain imaging with single-cell resolution using chemical cocktails and computational analysis. Cell *157*, 726-739.

Syken, J., Grandpre, T., Kanold, P.O., and Shatz, C.J. (2006). PirB restricts ocular-dominance plasticity in visual cortex. Science *313*, 1795-1800.

Takeuchi, H., Inokuchi, K., Aoki, M., Suto, F., Tsuboi, A., Matsuda, I., Suzuki, M., Aiba, A., Serizawa, S., and Yoshihara, Y. (2010). Sequential arrival and graded secretion of Sema3F by olfactory neuron axons specify map topography at the bulb. Cell *141*, 1056-1067.

Tan, L., Li, Q., and Xie, X.S. (2015). Olfactory sensory neurons transiently express multiple olfactory receptors during development. Molecular systems biology *11*, 844.

Tanenbaum, M.E., Gilbert, L.A., Qi, L.S., Weissman, J.S., and Vale, R.D. (2014). A protein-tagging system for signal amplification in gene expression and fluorescence imaging. Cell *159*, 635-646.

Tessier-Lavigne, M., and Goodman, C.S. (1996). The molecular biology of axon guidance. Science *274*, 1123.

Toba, Y., Tiong, J.D., Ma, Q., and Wray, S. (2008). CXCR4/SDF‐1 system modulates development of GnRH‐1 neurons and the olfactory system. Developmental neurobiology *68*, 487-503.

Treloar, H.B., Feinstein, P., Mombaerts, P., and Greer, C.A. (2002). Specificity of glomerular targeting by olfactory sensory axons. Journal of Neuroscience *22*, 2469-2477.

Treloar, H.B., Miller, A.M., Ray, A., and Greer, C.A. (2010). Development of the olfactory system.

Valverde, F., Santacana, M., and Heredia, M. (1992). Formation of an olfactory glomerulus: morphological aspects of development and organization. Neuroscience *49*, 255-275.

Walz, A., Mombaerts, P., Greer, C.A., and Treloar, H.B. (2006). Disrupted compartmental organization of axons and dendrites within olfactory glomeruli of mice deficient in the olfactory cell adhesion molecule, OCAM. Mol Cell Neurosci *32*, 1-14.

Wang, F., Nemes, A., Mendelsohn, M., and Axel, R. (1998). Odorant receptors govern the formation of a precise topographic map. Cell *93*, 47-60.

Whitlock, K.E., and Westerfield, M. (1998). A transient population of neurons pioneers the olfactory pathway in the zebrafish. J Neurosci *18*, 8919-8927.

Wong, S.T., Trinh, K., Hacker, B., Chan, G.C., Lowe, G., Gaggar, A., Xia, Z., Gold, G.H., and Storm, D.R. (2000). Disruption of the type III adenylyl cyclase gene leads to peripheral and behavioral anosmia in transgenic mice. Neuron *27*, 487-497.

Wu, Y., Helt, J.-C., Wexler, E., Petrova, I.M., Noordermeer, J.N., Fradkin, L.G., and Hing, H. (2014). Wnt5 and Drl/Ryk gradients pattern the Drosophila olfactory dendritic map. Journal of Neuroscience *34*, 14961-14972.

Yao, Y., Wu, Y., Yin, C., Ozawa, R., Aigaki, T., Wouda, R.R., Noordermeer, J.N., Fradkin, L.G., and Hing, H. (2007). Antagonistic roles of Wnt5 and the Drl receptor in patterning the Drosophila antennal lobe. Nature neuroscience *10*, 1423-1432.

Young, M.D., Wakefield, M.J., Smyth, G.K., and Oshlack, A. (2010). Gene ontology analysis for RNA-seq: accounting for selection bias. Genome Biol *11*, R14.

Young, M.D., Wakefield, M.J., Smyth, G.K., and Oshlack, A. (2012). goseq: Gene Ontology testing for RNA-seq datasets. R Bioconductor.

Yu, C.R., Power, J., Barnea, G., O'Donnell, S., Brown, H.E., Osborne, J., Axel, R., and Gogos, J.A. (2004). Spontaneous neural activity is required for the establishment and maintenance of the olfactory sensory map. Neuron *42*, 553-566.

Yu, C.R., and Wu, Y. (2017). Regeneration and rewiring of rodent olfactory sensory neurons. Experimental neurology *287*, 395-408.

Yu, H., Smallwood, P.M., Wang, Y., Vidaltamayo, R., Reed, R., and Nathans, J. (2010). Frizzled 1 and frizzled 2 genes function in palate, ventricular septum and neural tube closure: general implications for tissue fusion processes. Development *137*, 3707-3717.

Zapiec, B., and Mombaerts, P. (2016). Multiplex assessment of the positions of odorant receptor-specific glomeruli in mouse olfactory bulb by serial two-photon tomography. Paper presented at: CHEMICAL SENSES (OXFORD UNIV PRESS GREAT CLARENDON ST, OXFORD OX2 6DP, ENGLAND).

Zhang, X., Rodriguez, I., Mombaerts, P., and Firestein, S. (2004). Odorant and vomeronasal receptor genes in two mouse genome assemblies. Genomics *83*, 802-811.

Zou, D.-J., Feinstein, P., Rivers, A.L., Mathews, G.A., Kim, A., Greer, C.A., Mombaerts, P., and Firestein, S. (2004). Postnatal refinement of peripheral olfactory projections. Science *304*, 1976-1979.

Zou, Y. (2004). Wnt signaling in axon guidance. Trends in neurosciences *27*, 528-532.